



**THESIS APPROVAL**  
**GRADUATE SCHOOL, KASETSART UNIVERSITY**

Master of Engineering (Chemical Engineering)

**DEGREE**

Chemical Engineering

**FIELD**

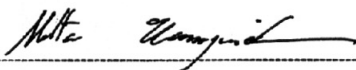
Chemical Engineering

**DEPARTMENT**

**TITLE:** Two-Stage Synthesis of Liquid Fuels from Carbon Dioxide and Methane

**NAME:** Mr. Yuttanawee Koontasang

**THIS THESIS HAS BEEN ACCEPTED BY**



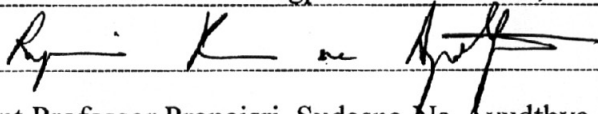
**THESIS ADVISOR**

( Associate Professor Metta Chareonpanich, D.Eng. )



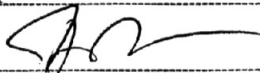
**COMMITTEE MEMBER**

( Associate Professor Phungphai Phanawadee, D.Sc. )



**COMMITTEE MEMBER**

( Assistant Professor Prapaisri Sudasna-Na-Ayudhya, Ph.D. )



**DEPARTMENT HEAD**

( Assistant Professor Thumrongrut Mungcharoen, Ph.D. )

**APPROVED BY THE GRADUATE SCHOOL ON** 31/08/2006



**DEAN**

( Associate Professor Vinai Artkongharn, M.A. )

# **THESIS**

## **TWO-STAGE SYNTHESIS OF LIQUID FUELS FROM CARBON DIOXIDE AND METHANE**

**YUTTANAWEE KOONTASANG**

**A Thesis Submitted in Partial Fulfillment of  
the Requirements for the Degree of  
Master of Engineering (Chemical Engineering)  
Graduate School, Kasetsart University  
2006**

**ISBN 974-16-2623-1**

Yuttanawee Koontasang 2006: Two-Stage Synthesis of Liquid Fuels from Carbon Dioxide and Methane. Master of Engineering (Chemical Engineering), Major Field: Chemical Engineering, Department of Chemical Engineering. Thesis Advisor: Associate Professor Metta Chareonpanich, D.Eng. 117 pages.  
ISBN 974-16-2623-1

In this research, liquid fuels in the range of gasoline to diesel were synthesized from carbon dioxide and methane via reforming reaction and Fischer-Tropsch (FT) synthesis in a two-stage reactor. The influences of catalytic temperature, the amount of cobalt loading and metal promoter types on the synthesis of liquid fuels were investigated. In the first-stage reactor or reforming reactor, carbon dioxide and methane were converted to synthesis gas on 5 wt.% Ni/Al<sub>2</sub>O<sub>3</sub> catalyst at temperatures of 500, 600, 700 and 750 °C with the CH<sub>4</sub>/CO<sub>2</sub> molar ratio of 1, total gas pressure of 10 atm and total flow rate of 50 ml/min (NTP). It was found that the highest CO<sub>2</sub> conversion of 75 % and the highest CH<sub>4</sub> conversion of 76 % are achieved at the temperature of 750 °C. The effluent gas mixtures from the first-stage reactor were directly introduced into the second-stage reactor or FT reactor. Liquid fuels synthesis was performed on Co/SBA-15 catalysts with 10-30 wt.% of cobalt loading and the temperature range of 200-280 °C with the CH<sub>4</sub>/CO<sub>2</sub> molar ratio of 1, total gas pressure of 10 atm and total flow rate of 50 ml/min (NTP). It was found that the appropriate catalyst for liquid fuels synthesis via FT reaction is 30 wt.% Co/SBA-15 catalyst and the optimum temperature of 200 °C. Under this condition, the liquid fuels (C<sub>5</sub>-C<sub>15</sub>) selectivity of 14.1 wt.% is obtained. The effect of promoters including lithium, sodium and potassium on 20Co/SBA-15 catalyst was investigated. It was found that the effect of promoters is not quite satisfied for the promotion of liquid fuels selectivity. Furthermore, it was found that Co/SBA-15 catalyst exhibits a long-lived stability for liquid fuels synthesis during 25 h of catalytic performance test.

Yuttanawee Koontasang  
Student's signature

Metta Chareonpanich  
Thesis Advisor's signature

28 / 08 / 2006

## **ACKNOWLEDGEMENTS**

I would like to express my sincere gratitude to my advisor, Associate Professor Metta Chareonpanich, for her guidance, invaluable suggestion and support throughout this research. I am sincerely grateful to my co-advisor, Associate Professor Phungphai Phanawadee, for his advice in my thesis. I am very thankful to Assistant Professor Prapaisri Sudasna-Na-Ayudhya and Assistant Professor Wirat Vanichsriratana for their kindly giving the time to revise and approve my thesis.

I am grateful to my fellow graduate students at Department of Chemical Engineering, Kasetsart University for assisting me my research and offering valuable suggestion.

The financial supports by the Commission on Higher Education and the Thailand Research Fund (RMU 4880016), the Senior-TRF Scholar (Prof. Jamrus Limtrakul), the Kasetsart University Research and Development Institute (KURDI, MV3.48), the Graduate School and the ADB Program of Department of Chemical Engineering, Kasetsart University are acknowledged.

Finally, I would like to thank my family for their love, support, encouragement, and their understanding during the whole period of my education. My family has been my greatest source of strength and inspiration. My gratefulness devotes to my family who wholeheartedly support me always.

Yuttanawee Koontasang

June 2006

## TABLE OF CONTENTS

	<b>Page</b>
TABLE OF CONTENTS	i
LIST OF TABLES	ii
LIST OF FIGURES	iv
LIST OF ABBREVIATIONS	viii
INTRODUCTION	1
Objectives	2
Benefits	3
LITERATURE REVIEWS	4
Synthesis Gas Production	4
The Conversion of Synthesis Gas to The Hydrocarbon	16
MATERIALS AND METHODS	28
Chemicals and Equipments	28
Experimental Preparation	31
Experimental Procedures	37
RESULTS AND DISCUSSION	44
Catalyst Characterization	44
Thermal Reaction Investigation	54
Catalytic Reaction Investigation	59
CONCLUSION	81
LITERATURE CITED	83
APPENDIX	94
CURRICULUM VITAE	117

## LIST OF TABLES

Table	Page
1 World petroleum consumption	1
2 Variation of equilibrium constant with temperature of methane steam reforming	5
3 History of FT synthesis	19
4 The details of experimental conditions	42
5 The chemical compositions of catalysts	45
6 BET surface areas, pore diameters and total pore volume of catalyst supports, metal-supported catalysts and cobalt-supported catalyst with metal promoters.	49

### Appendix Table

A1 Equation of calibration curves for each standard gas and liquid	103
B1 Calculation of conversion and selectivity	106
B2 Conversion of carbon dioxide and methane to synthesis gas: thermal reaction packed with sand	108
B3 Conversion of synthesis gas to hydrocarbon products: thermal reaction packed with sand	109
B4 Conversion of carbon dioxide and methane to synthesis gas: catalytic reaction on $\text{Al}_2\text{O}_3$ catalyst support	110
B5 Conversion of carbon dioxide and methane to synthesis gas: catalytic reaction on $5\text{Ni}/\text{Al}_2\text{O}_3$ catalyst	110
B6 Conversion of synthesis gas to hydrocarbon products: catalytic reaction on sand catalyst	111
B7 Conversion of synthesis gas to hydrocarbon products: catalytic reaction on SBA-15 catalyst support	112

**LIST OF TABLES (cont'd)**

<b>Appendix Table</b>	<b>Page</b>
B8 Conversion of synthesis gas to hydrocarbon products: catalytic reaction on 10Co/SBA-15 catalyst	113
B9 Conversion of synthesis gas to hydrocarbon products: catalytic reaction on 20Co/SBA-15 catalyst	114
B10 Conversion of synthesis gas to hydrocarbon products: catalytic reaction on 30Co/SBA-15 catalyst	115
B11 Conversion of synthesis gas to hydrocarbon products: catalytic reaction on 20Co/SBA-15 catalyst with metal promoters	116

## LIST OF FIGURES

Figure	Page
1 The proposed reaction mechanism of partial oxidation of methane on yttrium-stabilized zirconia	7
2 Scheme and reaction steps for the reforming of methane with carbon dioxide over the Ru/Al <sub>2</sub> O <sub>3</sub> catalyst	12
3 Scheme of the oxygenate (enol) mechanism	22
4 The insertion of CO into a metal-methyl or metal-methylene carbon bond	23
5 An advanced mechanism for the insertion of CO into a metal-methyl or metal-methylene carbon bond	23
6 An insertion mechanism purposed by Dry (1993)	24
7 The mechanism for the reaction of CO, H <sub>2</sub> and C <sub>2</sub> H <sub>4</sub> on a cobalt catalyst	25
8 The adsorption model has been proposed by Kolbel and Tillmetz (1974)	26
9 Catalytic reaction testing unit: (a) a feed flow measuring and controlling system, (b) a furnace-equipped stainless steel tube reactor and (c) a sampling system	31
10 Aalborg mass flow controller	32
11 (a) The first-stage reforming reactor equipped with the electric heater (b) the second-stage FT reactor equipped with the Carbolite furnace	33
12 Schemes of (a) the first-stage reforming reactor and (b) the second-stage FT reactor	33
13 Heated sampling valve and U-tube cooling trap connecting to quick release valves	34
14 Shimadzu gas chromatograph equipped with thermal conductivity detector and chromatopac data processor	35



## LIST OF FIGURES (cont'd)

Figure	Page
15 Shimadzu gas chromatograph equipped with flame ionization detector and chromatopac data processor	36
16 The setup of equipment for hydrolysis and condensation reactions	38
17 Scheme of mesoporous silica preparation process	39
18 Nitrogen sorption isotherms of $\text{Al}_2\text{O}_3$ support and 5Ni/ $\text{Al}_2\text{O}_3$ catalyst	47
19 Nitrogen sorption isotherms of SBA-15 support, 10Co/SBA-15, 20Co/SBA-15 and 30Co/SBA-15 catalysts	47
20 Nitrogen sorption isotherms of 20Co/SBA-15, 0.1Li-20Co/SBA-15, 0.3Na-20Co/SBA-15 and 0.5K-20Co/SBA-15 catalysts	48
21 TEM images of (a) $\text{Al}_2\text{O}_3$ support (b) 5Ni/ $\text{Al}_2\text{O}_3$ catalyst	51
22 TEM images of (a) SBA-15 support (b) 10Co/SBA-15 catalyst (c) 20Co/SBA-15	52
23 TEM images along the direction perpendicular and parallel to the <i>c</i> axis of (a) and (b) 0.1Li-20Co/SBA-15 catalyst, (c) and (d) 0.3Na-20Co/SBA-15 catalyst and (e) and (f) 0.5K-20Co/SBA-15 catalyst	53
24 Effect of temperature on the $\text{CO}_2$ and $\text{CH}_4$ conversions in the first-stage reforming reactor packed with sand	54
25 Effect of temperature on the effluent compositions in the first-stage reforming reactor packed with sand	55
26 Effect of temperature on the CO conversion and hydrocarbon selectivity in the second-stage FT reactor packed with sand	56
27 Effect of temperature on the effluent composition in the second-stage FT reactor packed with sand	57
28 Effect of temperature on hydrocarbon selectivity in the second-stage FT reactor packed with sand	58

## LIST OF FIGURES (cont'd)

Figure	Page
29     Effect of temperature on CO <sub>2</sub> and CH <sub>4</sub> conversions of Al <sub>2</sub> O <sub>3</sub> and 5Ni/Al <sub>2</sub> O <sub>3</sub> catalyst in the first-stage reforming reactor	60
30     Effect of temperature on CO conversion of SBA-15 support and 10Co/ SBA-15, 20Co/SBA-15 and 30Co/SBA-15 catalysts in the second-stage FT reactor	65
31     Effect of temperature on hydrocarbon selectivity of SBA-15 support in the second-stage FT reactor	66
32     Effect of temperature on hydrocarbon selectivity of 10Co/SBA-15 catalyst in the second-stage FT reactor	66
33     Effect of temperature on hydrocarbon selectivity of 20Co/SBA-15 catalyst in the second-stage FT reactor	67
34     Effect of temperature on hydrocarbon selectivity of 30Co/SBA-15 catalyst in the second-stage FT reactor	67
35     Effect of metal promoter on CO conversion of 0.1Li-20Co/ SBA-15, 0.3Na-20Co/SBA-15 and 0.5K-20Co/SBA-15 catalysts in the second-stage FT reactor	72
36     Effect of metal promoter on hydrocarbon selectivity of 0.1Li-20Co/SBA-15, 0.3Na-20Co/SBA-15 and 0.5K-20Co/SBA-15 catalysts in the second-stage FT reactor	73
37     The alteration of CO conversion as a function of time on stream of 20Co/SBA-15 catalyst in the second-stage FT reactor	76
 <b>Appendix Figure</b>	
A1     Scheme diagram of gas chromatograph	96
A2     CO, CH <sub>4</sub> , CO <sub>2</sub> chromatogram	97

## LIST OF FIGURES (cont'd)

Appendix Figure	Page
A3 (a) C <sub>1</sub> -C <sub>3</sub> hydrocarbons chromatogram (b) C <sub>4</sub> hydrocarbon chromatogram	97
A4 C <sub>5</sub> -C <sub>15</sub> hydrocarbons chromatogram	98
A5 Synthesis gas on 5Ni/Al <sub>2</sub> O <sub>3</sub> at 750 °C from the first-stage reforming reactor	98
A6 Hydrocarbon products (a) C <sub>1</sub> -C <sub>4</sub> (b) C <sub>5+</sub> on 10Co/SBA-15 catalyst at 200 °C from the second-stage FT reactor	99
A7 Hydrocarbon products (a) C <sub>1</sub> -C <sub>4</sub> (b) C <sub>5+</sub> on 20Co/SBA-15 catalyst at 200 °C from the second-stage FT reactor	100
A8 Hydrocarbon products (a) C <sub>1</sub> -C <sub>4</sub> (b) C <sub>5+</sub> on 30Co/SBA-15 catalyst at 200 °C from the second-stage FT reactor	101

## LIST OF ABBREVIATIONS

DRIFT	=	Diffuse Reflectance Infrared Fourier transform
FT	=	Fischer-Tropsch
FTIR	=	Fourier Transform Infrared
FTS	=	Fischer-Tropsch Synthesis
GTL	=	Gas to Liquid
h	=	Hour (s)
LPG	=	Liquefied Petroleum Gas
NTP	=	Normal Temperature and Pressure
POM	=	Partial Oxidation of Methane
TCD	=	Thermal Conductivity Detector
TEM	=	Transmission Electron Microscopy
TPR	=	Temperature-programmed Reduction
XRF	=	X-ray Fluorescence Spectroscopy
YSZ	=	Yttrium-stabilized Zirconia
Zr-MPS	=	Zirconium Silicate Materials

## TWO-STAGE SYNTHESIS OF LIQUID FUELS FROM CARBON DIOXIDE AND METHANE

### INTRODUCTION

The demand of high quality and environmentally friendly liquid fuels, such as diesel fuel, was increasing rapidly with the increasing of world population and transportation. The world petroleum consumption is shown in Table 1.

Table 1 World petroleum consumption (thousand barrels per day).

Region	Years				
	1998	1999	2000	2001	2002
North America	22,820	23,510	23,768	23,690	23,843
Central & South America	5,061	5,156	5,250	5,369	5,238
Western Europe	14,864	14,749	14,668	14,847	14,698
Eastern Europe & Former U.S.S.R.	5,042	5,081	5,052	5,480	5,257
Middle East	4,376	4,481	4,687	4,892	5,044
Africa	2,403	2,434	2,507	2,618	2,675
Asia & Oceania	19,308	20,317	20,897	21,100	21,452
World total	73,875	75,728	76,831	77,997	78,206

Source: International Energy Annual (2002)

Due to the fuel oil crisis, many researchers have tried to find the new energy source or synthesize liquid fuels from other sources instead of the fossil fuels. Natural gas, oil plant or plastic wastes are the alternative sources for liquid fuels synthesis. Among these groups natural gas has attracted much interest to synthesize liquid fuels because of its low cost, availability and enormous amount of reservoirs.

Furthermore, the trend towards increasing regulation of the emission of pollutants leads to higher quality of the liquid fuels with innovations in engines. As is well-known, the natural gas to liquid fuels process, so-called GTL process (Rostrup-

Nielsen, *et al.*, 1994), is composed of two parts. One is the synthesis gas generation from natural gas and the other is synthesis gas conversion to liquid fuels.

Synthesis gas can be produced from methane mainly by steam reforming but this method has some limitations, such as high energy requirements and high  $H_2/CO$  ratio. Synthesis gas is produced by non-catalytic partial oxidation reaction which mildly exothermic but operates at very severe conditions. Recently, the much effort has been devoted to carbon dioxide reforming of methane to produce synthesis gas in the presence of catalysts. Because synthesis gas is produced from carbon dioxide reforming of methane provides the suitable ratio of  $H_2/CO$  for the production of hydrocarbon via Fischer-Tropsch synthesis.

The conversion of synthesis gas to liquid fuels can be accomplished via Fischer-Tropsch synthesis (FTS). Fischer-Tropsch synthesis is a process that uses to convert synthesis gas (mixtures of  $CO$  and  $H_2$ ) to water and hydrocarbons that can be used as liquid fuels or base chemicals. The synthetic fuels produced via Fischer-Tropsch synthesis have high cetane numbers, low contents of sulfur and aromatics. This makes them suitable for diesel engines and friendly with environment (Knottenbelt, 2002).

The aim of this research is to synthesize of liquid fuels from carbon dioxide and methane by the two-stage process. The first stage is the production of synthesis gas from carbon dioxide and methane via reforming process, and the second stage is the conversion of synthesis gas to the hydrocarbon range of liquid fuels using Fischer-Tropsch synthesis.

### **Objectives**

1. To synthesize liquid fuels from carbon dioxide and methane.
2. To investigate the optimum conditions of catalytic temperature, amounts of cobalt loading,  $CO_2/CH_4$  ratio, total flow rate and total pressure to synthesize liquid fuels via carbon dioxide reforming of methane and Fischer-Tropsch synthesis.

### **Benefits**

1. Liquid fuels can be synthesized from carbon dioxide and methane.
2. The optimum conditions of catalytic temperature, amounts of cobalt loading,  $\text{CO}_2/\text{CH}_4$  ratio, total flow rate and total pressure for maximum selectivity of liquid fuels via carbon dioxide reforming of methane and Fischer-Tropsch synthesis are obtained.

## LITERATURE REVIEWS

The increasing demand for high quality and environmentally friendly transportation fuels together with the technological improvements of gas-to-liquid (GTL) processes has renewed the interest of using natural gas as a potential source of hydrocarbons. In particular, liquid fuels in the range of diesel fuel made with GTL technology through the Fischer-Tropsch synthesis (FTS) process (synthesis of hydrocarbons from CO and H<sub>2</sub>) offers significant environmental and efficiency benefits over those derived from crude oil, as they are mainly composed of linear paraffin having high cetane numbers and are free of sulfur and aromatics pollutants (Van der Laan and Beenackers, 1999). Therefore, the synthesis of long chain hydrocarbon has much interest via the two parts. The first part is the production of synthesis gas by using reforming process, and the second part is the conversion of synthesis gas to the liquid fuels ranges of clean diesel fuel.

### Synthesis Gas Production

#### **1. Steam Reforming**

Steam reforming is a highly endothermic process carried out by passing a mixture of steam and natural gas over a catalyst packed into the tubes of high temperature alloys of small diameter in order to facilitate heat transfer. Because the steam reforming reaction is equilibrium limited and endothermic, both heat and catalyst are applied to enhance the conversion. Table 2 shows the effect of temperature on the equilibrium constant for the methane steam reforming reaction (Rostrup-Nielsen, 1973). Temperatures up to 850 °C are commonly used for the reaction with steam-to-methane ratios ranging of 2.5:1 to 4.1:1 and pressures ranging from 10-40 atm. The use of elevated pressure enables the energy efficiency of the process to be improved. Under these conditions the conversion of methane is 80%, the limitation being a result of the equilibrium constraint (Oklany *et al.*, 1998).



Methane steam reforming involves two reversible reactions, which were studied thoroughly by Xu and Froment (1989).



**Table 2** Variation of equilibrium constant with temperature of methane steam reforming.

Temperature (°C)	Equilibrium constant, <i>K</i>
0	$6.00 \times 10^{-31}$
100	$2.70 \times 10^{-20}$
200	$4.90 \times 10^{-14}$
300	$6.80 \times 10^{-10}$
400	$6.20 \times 10^{-7}$
500	$1.02 \times 10^{-4}$
600	$5.40 \times 10^{-3}$
700	$1.30 \times 10^{-1}$
800	1.76
900	15.33
1000	95.5

Source: Rostrup-Nielsen (1984)

For the catalyst type, it was found that elements of group VIII (Fe, Co, Ni, Rd, Ru, Pd, OS, Ir and Pt) were active for the steam reforming reaction (Grenoble, 1978). Nickel is the major metal used as the steam reforming catalyst. Large catalyst size is preferred due to the high flow rate in the normal application. The catalyst support should be strong enough to withstand the operating conditions. Also, the support must be able to disperse the metal catalyst and to allow an access for the species to

approach the surface. Therefore, the support could enhance the adsorption of steam and influence the reaction order (Rostrup-Nielsen, 1973).

## **2. Partial Oxidation**

Partial oxidation of methane (POM) to synthesis gas is slightly exothermic and more energy efficient than steam reforming of CH<sub>4</sub>. Furthermore, POM is mechanically simpler than the steam reforming, since it is completed in a single reactor, without external heating. However, several problems must be solved before using POM in an industrial scale. These include the cofeeding of CH<sub>4</sub>/O<sub>2</sub> under explosive conditions (Ruckenstein and Hu, 1998), and the formation of local hot spots within catalyst beds that can irreversibly damage both the catalyst and the reactor (Drago *et al.*, 1998). Carbon deposition may also deactivate the catalysts (Yan *et al.*, 2000). Therefore, understanding the reaction mechanism and the nature of the active catalytic sites is very important. Thus, a better understanding of mechanisms and kinetics is required. Zhu *et al.* (2004) studied the partial oxidation of methane to synthesis gas over yttrium-stabilized zirconia (YSZ) with in-situ FTIR, and both steady state and transient experiments. The reaction scheme was proposed as shown in Figure 1.

Partial oxidation of methane has constituted the dominant commercial process employed to produce synthesis gas from methane over the past several decades (Tsipouriari *et al.*, 1998):



Supported noble metal catalysts are mainly used for the POM reaction, including Rh (Bradford and Vannice, 1999), Ru (Buyevskaya *et al.*, 1994), Pd (Witt and Schmidt, 1996), and Pt (Torniainen *et al.*, 1994), and supported Ni catalysts (Dissanayake *et al.*, 1993). The type of catalyst employed may strongly influence the reaction steps of catalytic POM. Elmasides and Verykios (2001) investigated the partial oxidation of methane to synthesis gas over Ru/TiO<sub>2</sub> catalyst in both non-steady

state and steady state isotopic transient experiments, combined with in-situ DRIFT spectroscopy. Gas-phase  $\text{CH}_4$  interacted with the catalyst surface, producing  $\text{CH}_x$  surface species. They found that CO was the primary product, resulting from a surface reaction between carbon and adsorbed atomic oxygen on metallic Ru sites, while  $\text{CO}_2$  formed from CO oxidation on oxidized Ru sites.

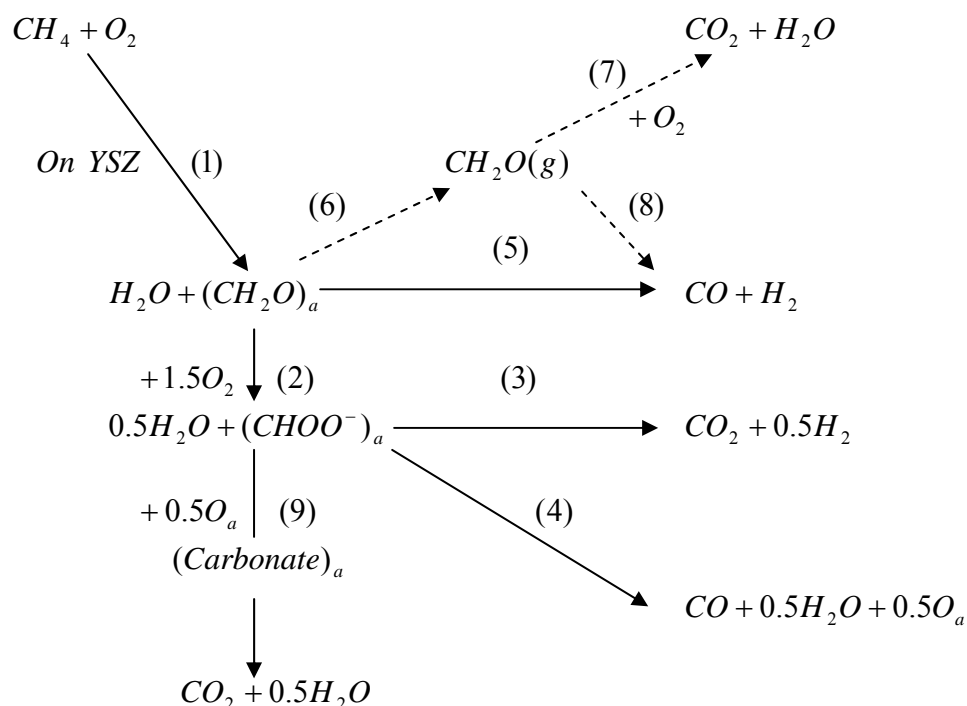


**Figure 1** The proposed reaction mechanism of partial oxidation of methane on yttrium-stabilized zirconia.

Mallens *et al.* (1997) used Rh and Pt catalysts, in the selectivity toward CO and  $\text{H}_2$  during POM. The lower activation energy for methane decomposition on Rh when compared with that of Pt was found. They suggested that the ability of catalyst to activate methane can be considered from the product distribution and the concentration of active surface species of oxygen, carbon, and hydrogen. Fathi *et al.* (2000) studied the partial oxidation of methane to synthesis gas over platinum catalysts and proposed the product distribution was considered by both the concentrations and the types of surface oxygen species present at the catalyst surface. Qin *et al.* (1996) suggested that the support might also influence the concentration of adsorbed oxygen and, as a consequence, the activation of methane and the product

distribution. Li *et al.* (2000) studied the effect of gas-phase O<sub>2</sub>, reversibly adsorbed oxygen, and oxidation state of the nickel in the Ni/Al<sub>2</sub>O<sub>3</sub> catalyst on CH<sub>4</sub> decomposition and partial oxidation using transient response techniques at 700 °C. They concluded that the surface oxidation state of the catalyst affected the reaction mechanism and played an important role in POM conversion and selectivity. They also mentioned that the direct oxidation was the major POM route, and that the indirect oxidation mechanism could not become dominant under their experimental conditions.

### 3. Dry Reforming

The reforming reaction of methane with carbon dioxide to synthesis gas has received significant attention in the last few years as it constitutes a promising alternative route for the production of synthesis gas. This reaction offers important advantages over the process of steam reforming of methane consisting (a) the formation of a suitable H<sub>2</sub>/CO ratio for use in Fischer–Tropsch synthesis to liquid hydrocarbons, (b) utilization of CO<sub>2</sub>, which is a greenhouse gas, and (c) better use in chemical energy transmission systems. CH<sub>4</sub>/CO<sub>2</sub> reforming is strongly endothermic. So, high temperatures (800–1,000 °C) are required. Unfortunately, these extreme temperatures promote carbon deposition of which deactivate the catalyst, and sinter the supported metals (Erdohelyi *et al.*, 1993).

The reforming of methane with carbon dioxide has also been proposed as a means of storing and transporting solar and atomic energy (Richardson and Paripatyadar, 1990). CO<sub>2</sub> reforming of methane has the potential to reduce the cost of synthesis gas and can be applied in solar energy storage (Kodama *et al.*, 2001) and/or CO<sub>2</sub> utilization technologies:



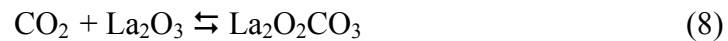
### 3.1 Reaction Mechanism

There has been various reaction mechanisms proposed for methane reforming with carbon dioxide reaction. According to the reaction mechanics, Tsipouriari and Verykios (2001) studied the kinetic behavior of the Ni/La<sub>2</sub>O<sub>3</sub> catalyst in the reforming reaction of methane with carbon dioxide as a function of temperature and partial pressures of CH<sub>4</sub> and CO<sub>2</sub>. It was found that the increase of H<sub>2</sub> partial pressure led to a continuous enhancement of the CO formation rate, due to the simultaneous occurrence of the water-gas shift reaction. The mechanism of CH<sub>4</sub>/CO<sub>2</sub> reaction has been investigated using steady-state isotopic tracing and transient experiments. Based on these observations, the following mechanistic steps, which led to the production of CO and H<sub>2</sub> were proposed:

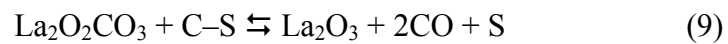
1. Reversible adsorption of methane on the surface of Ni:



2. A strong interaction between CO<sub>2</sub> and La<sub>2</sub>O<sub>3</sub>:



3. La<sub>2</sub>O<sub>2</sub>CO<sub>3</sub> species react with carbon deposited onto Ni particles at the interface between Ni and La<sub>2</sub>O<sub>2</sub>CO<sub>3</sub>:



4. Adsorbed hydrogen interacts with other surface species.



5. Simultaneously, the inverse water-gas shift reaction takes place, which may be described by the following sequence of reaction steps:



Carbon dioxide reforming of methane was studied over two ruthenium catalysts supported on silica and on  $\gamma$ -alumina by Ferreira-Aparicio *et al.* (2000). A different pathway for  $\text{CH}_4$  and  $\text{CO}_2$  reaction over the alumina supported catalyst was proposed as shown in Figure 2. The reaction mechanisms of carbon monoxide and hydrogen formation as shown in Figure 2 were proposed as follows:

1. The possible mechanisms were started with methane activation process over the surface of metal catalyst and generated the intermediate species such as  $\text{CH}_{x(Ru-ads)}$  and  $\text{H}_{x(Ru-ads)}$ .

2. Hydrogen gas was occurred from desorption of the  $\text{H}_{x(Ru-ads)}$  species while  $\text{OH}_{(Ru-ads)}$ ,  $\text{O}_{(Ru-ads)}$  and  $\text{H}_{(Ru-ads)}$  species were occurred from the transfer of OH between  $\text{Al}_2\text{O}_3$  support and Ru metal surface.

3. The interaction between  $\text{CH}_{x(Ru-ads)}$  and  $\text{O}_{(Ru-ads)}$  to form the species of CO and H on the metal site,  $\text{CO}_{(Ru-ads)}$  and  $\text{H}_{(Ru-ads)}$ , followed by desorption of CO.

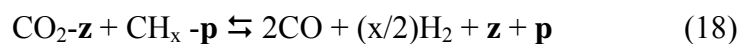
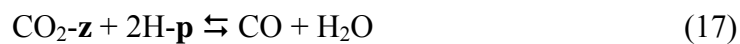
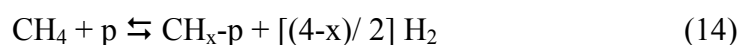
4. Carbon dioxide activation was occurred over the  $\text{Al}_2\text{O}_3$  support and then the surface of carbonate was formed.

5. Hydrogen diffused from the metal surface to the support surface and formed adsorbed species  $H_{(Al_2O_3-ads)}$ .

6.  $H_{(Al_2O_3-ads)}$  species reacted with carbonate surface and  $HCO_2^-_{(Al_2O_3-ads)}$ ,  $OH^-_{(Al_2O_3-ads)}$  and  $H_2O_{(Al_2O_3-ads)}$  species were occurred. Then CO was desorbed from the decomposition of  $HCO_2^-_{(Al_2O_3-ads)}$  over support.

7. In addition to  $CO_{(Al_2O_3-ads)}$ ,  $OH^-_{(Al_2O_3-ads)}$  was occurred from the decomposition of  $HCO_2^-_{(Al_2O_3-ads)}$  and yielded water.

Souza *et al.*, (2001) studied the kinetics of CO<sub>2</sub> reforming of methane over Pt supported on Al<sub>2</sub>O<sub>3</sub>, ZrO<sub>2</sub>, and x%ZrO<sub>2</sub>/Al<sub>2</sub>O<sub>3</sub> (1 ≤ x ≤ 20 wt.%), and the catalysts were characterized using nitrogen adsorption analysis, temperature-programmed reduction (TPR) and H<sub>2</sub> and CO chemisorption analysis. After analyzing the data available in the literature and the results obtained, the following bifunctional mechanism (where **p** is a platinum site and **z** a support site) was proposed for CH<sub>4</sub>–CO<sub>2</sub> reforming:



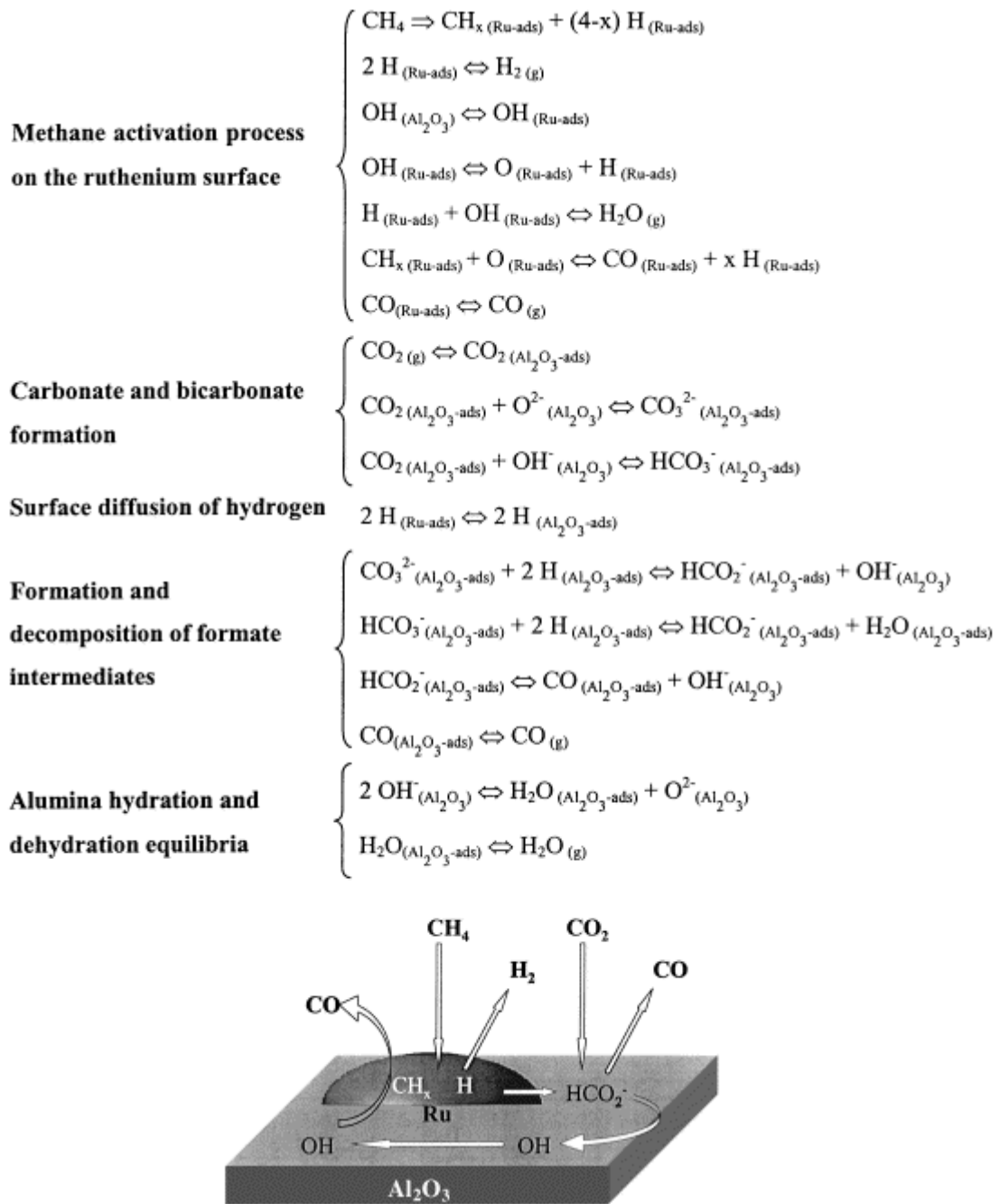


**Figure 2** Scheme and reaction steps for the reforming of methane with carbon dioxide over the Ru/Al<sub>2</sub>O<sub>3</sub> catalyst.

Coke formation in the reforming of hydrocarbons was known to cause the catalyst deactivation (Vernon *et al.*, 1992). According to thermodynamics, coke is expected to be formed mainly via the Boudouard reaction as shown in Equation 19



and methane decomposition as shown in Equation 20, which is favorable under CO<sub>2</sub>-reforming conditions:



### 3.2 Catalyst

Fe supported catalysts (Asami *et al.*, 2003) had much utilized for carbon dioxide reforming with methane because of their inexpensive and availability. However, the disadvantages of Fe were that it could easily be deactivated during reaction due to the coke formation. Co-based catalysts also gave the same result as Fe-based catalyst, when the conventional supports, such as Al<sub>2</sub>O<sub>3</sub> and SiO<sub>2</sub>, were employed. Exceptions were the cases in which MgO was used as support (Ruckenstein and Hu, 1995; Wang and Ruckenstein, 2000).

Nickel and noble metals supported catalysts are found to be the most active catalysts and one of the most important problems in carrying out this reaction is coke deposition which deactivates the catalyst. Even though the noble metal-based catalysts (such as Rh, Ru, Pd, and Pt) can provide high activity and selectivity with little or no carbon deposition, they are unsuitable for large-scale commercial use because of their limited availability makes the development of active and stable nickel catalysts a challenge to the catalytic scientific community.

Some supported Ni catalysts particularly the SiO<sub>2</sub> supported catalysts have been reported to be used in carbon dioxide reforming with methane as follows:

Wang and Au (1997) studied carbon dioxide reforming of methane to produce synthesis gas over SiO<sub>2</sub>-supported rhodium catalysts and investigated the decomposition of CH<sub>4</sub> and CO<sub>2</sub> as well as the reaction between CH<sub>4</sub> and CO<sub>2</sub> over SiO<sub>2</sub>-supported rhodium catalysts in the temperature range of 600-800°C. The initial

activities for methane and CO<sub>2</sub> decompositions increased with the increase of rhodium loading whereas the activity for CO formation from the CH<sub>4</sub> and CO<sub>2</sub> reaction was almost unaffected by the rhodium loading. The different reaction behaviors of methane reforming with CO<sub>2</sub> were observed. At 700°C, CO<sub>2</sub> conversion was higher than CH<sub>4</sub> conversion whereas at 800°C, CH<sub>4</sub> conversion was higher than CO<sub>2</sub> conversion.

The CO<sub>2</sub> reforming of CH<sub>4</sub> over Co supported on an alkaline earth metal oxides (MgO, CaO, SrO, or BaO) as well as on Al<sub>2</sub>O<sub>3</sub> and on SiO<sub>2</sub> were investigated by Ruckenstein and Wang (2000). Among these supports, MgO exhibited a high and stable activity. It provided CO yield of 93% and H<sub>2</sub> yield of 90%, which remained unchanged during the period of study of 50 h. Al<sub>2</sub>O<sub>3</sub> provided a high CO yield initially, however, rapidly decayed. All the other supports exhibited low CO yields and CaO showed also low stabilities.

The carbon dioxide reforming of methane over the reduced supported Rh catalysts was investigated by Wang and Ruckenstein (2000). Two kinds of oxides, reducible (CeO<sub>2</sub>, Nb<sub>2</sub>O<sub>5</sub>, Ta<sub>2</sub>O<sub>5</sub>, TiO<sub>2</sub>, and ZrO<sub>2</sub>) and irreducible (Al<sub>2</sub>O<sub>3</sub>, La<sub>2</sub>O<sub>3</sub>, MgO, SiO<sub>2</sub>, and Y<sub>2</sub>O<sub>3</sub>) were used as supports. Among the irreducible metal oxides, Al<sub>2</sub>O<sub>3</sub>, La<sub>2</sub>O<sub>3</sub> and MgO provided stable catalytic activities during the period of study. However, deactivation occurred over the SiO<sub>2</sub> and Y<sub>2</sub>O<sub>3</sub> supported catalysts. Most of the reducible oxides provided much lower yields to CO and H<sub>2</sub> than the irreducible ones, and they were not suitable supports for Rh in the CO<sub>2</sub> reforming of methane. In summary, MgO and Al<sub>2</sub>O<sub>3</sub> were the most promising supports; they provided a stable high activity with a CO yield and a H<sub>2</sub> yield at the high space velocity of 60000 ml/h/g.

Ferreira-Aparicio *et al.* (2000) studied carbon dioxide reforming of methane over two ruthenium catalysts supported on silica and alumina. The accumulation of carbon adspecies formed from methane decomposition on the metallic particles finally promoted carbon dioxide dissociation and induced rapid deactivation of the catalyst. The alumina support provided an alternate route for CO<sub>2</sub>

activation by producing formate intermediates on its surface that subsequently decomposed and released CO. This bifunctional mechanism, in which the hydroxyl groups of the support played a key role, induced greater stability on the Ru/Al<sub>2</sub>O<sub>3</sub> catalyst by significantly decreasing the rate of carbon deposition on the metal.

Ni catalysts supported on  $\gamma$ -Al<sub>2</sub>O<sub>3</sub>, ZrO<sub>2</sub> and  $\gamma$ -Al<sub>2</sub>O<sub>3</sub>-ZrO<sub>2</sub> were studied in the synthesis gas reactions by Pompeo *et al.* (2004). The Ni/ $\gamma$ -Al<sub>2</sub>O<sub>3</sub>-ZrO<sub>2</sub> catalyst showed a very good performance in relation to the initial activity and selectivity, comparable to that of the Ni/ $\gamma$ -Al<sub>2</sub>O<sub>3</sub> catalyst. Concerning the deactivation, the modification of the  $\gamma$ -Al<sub>2</sub>O<sub>3</sub> supported with ZrO<sub>2</sub> led to a higher stability, due to the strong inhibition of the carbon formation during the reaction. These results suggested that ZrO<sub>2</sub> promoted the gasification of adsorbed intermediates, which were precursors of carbon formation and showed that high amounts of graphitic carbon were deposited on Ni/ $\gamma$ -Al<sub>2</sub>O<sub>3</sub> catalyst during CO<sub>2</sub> reforming reaction, while lesser amounts of deposited carbon were observed on Ni/ $\gamma$ -Al<sub>2</sub>O<sub>3</sub>-ZrO<sub>2</sub> (approximately one order lower).

Ni supported on Al<sub>2</sub>O<sub>3</sub> has been modified by the novel metal to increase the stability and activities for carbon dioxide reforming of methane. The detail of studies was as follows:

The effects of the preparation method for Mn-promoted Ni/Al<sub>2</sub>O<sub>3</sub> catalysts on the catalytic activity and stability for carbon dioxide reforming of methane were investigated by Seok *et al.* (2002). A coprecipitated catalyst, Ni-MnO<sub>x</sub>/MnAl<sub>2</sub>O<sub>4</sub>, showed higher coke resistance and more stable activity than that of an impregnated Ni/MnO/Al<sub>2</sub>O<sub>3</sub> catalyst. For the impregnated Ni/MnO/Al<sub>2</sub>O<sub>3</sub> catalyst, an addition of potassium stabilized its catalytic activity, to the level achieved by coprecipitated Ni-MnO<sub>x</sub>/MnAl<sub>2</sub>O<sub>4</sub> catalyst. These results indicated that the high stable Ni/Al<sub>2</sub>O<sub>3</sub> catalyst for the carbon dioxide reforming of methane can be prepared by addition of both potassium and manganese as promoters.

Valentini *et al.* (2003) studied the CO<sub>2</sub> reforming of CH<sub>4</sub> performed over V-promoted Ni/Al<sub>2</sub>O<sub>3</sub>. The results showed the role of vanadium doping of the Al<sub>2</sub>O<sub>3</sub> catalyst in the carbon dioxide reforming of methane. Vanadium induced microstructural changes in the metallic Ni on Al<sub>2</sub>O<sub>3</sub> catalysts. The preliminary analysis indicated that the vanadium doping avoided the formation of the aluminate spinel phase. There was significant increase in the methane conversion by V-promoted Ni/Al<sub>2</sub>O<sub>3</sub> catalysts. Moreover, vanadium doping reduced the amount of carbon deposition.

CuNi/Al<sub>2</sub>O<sub>3</sub> catalysts were prepared by Lee *et al.* (2004) to investigate the effects of Cu addition to Ni/Al<sub>2</sub>O<sub>3</sub> catalyst in CO<sub>2</sub> reforming of methane. The 1 wt.% Cu adding to Ni/Al<sub>2</sub>O<sub>3</sub> catalyst enhanced the stability and activity of Ni/Al<sub>2</sub>O<sub>3</sub> catalyst. However, the addition of more than 5 wt.% Cu caused rapid deactivation of catalyst.

### **The Conversion of Synthesis Gas to Hydrocarbons**

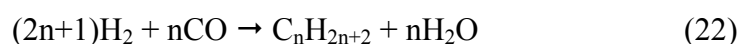
#### **1. Fischer-Tropsch (FT) Synthesis**

Fischer-Tropsch synthesis is a method for the synthesis of hydrocarbons and other aliphatic compounds. In this process, synthesis gas, a mixture of hydrogen and carbon monoxide, is reacted in the presence of an iron or cobalt catalyst. A lot of heat is evolved, and such products as methane, synthetic gasoline and waxes, and alcohols are made, with water or carbon dioxide is produced as byproducts. An important source of the hydrogen-carbon monoxide gas mixture is the gasification of coal and reforming process. This process was named after Franz Fischer and Hans Tropsch, the German coal researchers who discovered it in 1923.

Since the invention of the original process by the German researchers Franz Fischer and Hans Tropsch, working at the Kaiser Wilhelm Institute in the 1920s, many refinements and adjustments have been made, and the term "Fischer-Tropsch" now applies to a wide variety of similar processes (Fischer-Tropsch synthesis or Fischer-Tropsch chemistry).

The process was invented in petroleum-poor but coal-rich Germany to produce liquid fuels. It was used by Germany and Japan during World War II to produce alternative fuels. Germany's yearly synthetic fuel production reached more than 124,000 barrels per day from 25 plants (approximately 6.5 million tons in 1944).

The original Fischer-Tropsch process is described by the following chemical equation:



The mixture of carbon monoxide and hydrogen was called synthesis gas or syngas. The resulting hydrocarbon products are refined to produce the desired synthetic fuel. The carbon dioxide and carbon monoxide is generated by partial oxidation of coal and wood-based fuels. The utility of the process is primarily in its role in producing fluid hydrocarbons or hydrogen from a solid feedstock, such as coal or solid carbon-containing wastes of various types. Non-oxidative pyrolysis of the solid material produces syngas which can be used directly as a fuel without being taken through Fischer-Tropsch transformations. If liquid petroleum-like fuel, lubricant, or wax is required, the Fischer-Tropsch process can be applied. Finally, if hydrogen production is to be maximized, the water gas shift reaction can be performed, generating only carbon dioxide and hydrogen and leaving no hydrocarbons in the product stream. Fortunately shifts from liquid to gaseous fuels are relatively easy to make. Table 2 summarizes the history of FT synthesis.

## **2. Catalyst**

Many investigators have published results following the studies involving the Fischer-Tropsch (FT) reaction with different catalysts. FT processes with iron (Zhang *et al.*, 2006 and Luo and Davis, 2000) or cobalt (Iglesia, 1997 and Schulz, 1999) catalysts have to acknowledge the specific catalyst features. With iron catalyst,

substantial gas recycling is practically limited because of inhibition by the produced water. With cobalt catalyst, no water inhibition occurs and the conversion per pass is higher. Furthermore, with cobalt catalyst the selectivity is strongly depend on the partial pressures of CO and H<sub>2</sub>, in particular a sufficient high CO partial pressure should be maintained in order to avoid excessive methane formation. With iron catalyst, carbon accumulation on the catalyst is avoided. So, the life time of cobalt catalyst is much longer than that of iron catalyst. Fixed bed reactors are suited for low temperature FT synthesis, aiming at a high average molecular weight of the product (Schulz, 1999). Thus, cobalt catalyst is a promising catalyst for the synthesis of fuels and chemicals via the Fischer-Tropsch process.

Many studies have been carried out Fischer-Tropsch using different supports for cobalt loading, including alumina (Bechara, *et al.*, 2001 and Hosseini, *et al.*, 2004), titania (Zennaro, *et al.*, 2000), silica (Khodakov, *et al.*, 1997; Sun, *et al.* 2000 and Tsubaki, *et al.*, 2001.), etc.

The studies of the influence of average pore diameter of silica support on the physical and chemical properties of supported cobalt catalysts and their performances in the Fischer-Tropsch synthesis were investigated by Saib *et al.* (2002), the metal crystallite size and degree of reduction were found to increase with increasing pore diameter of the support for supports with an average pore diameter larger or equal to 40 Å. In impregnated catalysts, the metal crystallites seemed to appear in clusters on the support. With increasing average pore diameter, the size of these clusters increased.

In the Fischer-Tropsch synthesis, the supported catalyst of 100Å pore diameter was proved to be the most active and selective catalyst for hydrocarbon formation. SBA-15 is one kind of the mesoporous silica that has a large pore size and has had interest to be used as catalyst supports to synthesise longer hydrocarbons.

Table 3 History of FT synthesis.

Year	FT synthesis
1902	Sabatier and Senderen reported that methane was formed from synthesis gas on the Ni catalyst.
1923	Fischer and Tropsch reported that liquid hydrocarbon products were formed from synthesis gas on Ni, Fe, Co and Ru catalysts.
1936-1944	Commercial production plants were commissioned in Germany (Co based catalyst used in fixed-bed reactor).
1950	Hydrocal started operating plant in USA (Fe based catalyst used in fixed fluidized-bed reactor).
Mid 1950's	Plants in Germany and USA were shutdown because of discovery of abundant crude oil in the middle east of Asia.
1955	Sasol started the first plant in South Africa (Fe based catalyst used in fixed-bed and circulating fluidized-bed reactor).
1980-1983	Sasol continuously started the second plant and the third plant in South Africa (Fe based catalyst used in circulating and fixed fluidized-bed reactor, respectively).
1994	Shell started operating plant in Malaysia (Co based catalyst used in fixed-bed reactor). Hydrocarbon products were formed via synthesis gas, which obtained from natural gas.

Source: Satterfield (1991)

Khodakov *et al.* (2002) studied the pore size effects on Fischer-Tropsch reaction rates and selectivities over cobalt catalysts at atmospheric pressure using periodic (SBA-15 and MCM-41) and commercial mesoporous silicas as catalytic supports. Fischer-Tropsch reaction rates were found much higher on cobalt catalysts with the pore diameter exceed 30 Å than on the narrow pore catalysts, and a larger pore diameter of catalyst also led to significantly higher C<sub>5+</sub> selectivities. The catalytic effects were interpreted in terms of different cobalt particle sizes and reducibilities in the wide pore and narrow pore silicas that, the size of supported

cobalt species strongly increased, depended on the pore size, with increasing in catalyst pore diameter.

The influence of cobalt loading, cobalt precursor, and promoters on the mesoporous Co/SBA-15 catalysts for the Fischer-Tropsch synthesis has been investigated by Martínez *et al.* (2003). For Co/SBA-15 catalysts prepared from Co (II) nitrate, the metal dispersion decreased and the extent of cobalt reduction increased with cobalt loading. A maximum CO conversion was found for the sample with approximately 30 wt.% Co loading. The addition of approximately 1 wt.% Re enhanced the reducibility of cobalt oxides and increased the catalyst activity. Rhenium also favored the formation of long-chain *n*-paraffins (C<sub>10+</sub>) while decreasing methane selectivity. Promotion of cobalt with Mn significantly improved cobalt dispersion but decreased its reducibility, producing catalysts that were less active than the unpromoted one.

Ohtsuka *et al.* (2004) used mesoporous molecular sieves (MCM-41 and SBA-15) with different pore diameters as supports of Co catalysts. The performances in Fischer-Tropsch synthesis have been examined for the purpose of efficient production of C<sub>10</sub>–C<sub>20</sub> fraction as the main component of diesel fuel. The catalyst with the diameter of 8.3 nm of SBA-15 gave the highest CO conversion of 72%. The characterization of catalyst after FT synthesis strongly suggested the high stability of Co/SBA-15 in the dispersion and reducibility of the oxide species and in the mesoporous structure. The C<sub>10</sub>–C<sub>20</sub> selectivities were 30% at 203 °C over Co(20N)/SBA-15 catalyst.

Wei *et al.* (2004) used hexadecylpyridinium chloride as a template to synthesize the mesoporous zirconium silicate materials (Zr-MPS) at room temperature in a short time. The products, Zr-MPS, were structurally analogous to MCM-41. When Zr-MPS materials were used as the support of Co catalysts for Fischer-Tropsch synthesis, the higher selectivity for C<sub>5+</sub> hydrocarbons and the lower selectivity for CH<sub>4</sub> were obtained. It was noticed that the increment of Zr content in the silica framework was related to the Co metal crystallites of supported Zr-MPS catalyst.

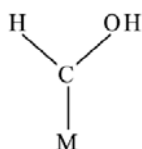


### 3. Reaction Mechanism

A mechanism for Fischer-Tropsch synthesis was quite complex and difficult to propose the existent procedures. Unlike many reactions, the Fischer-Tropsch synthesis converts two of the simplest compounds,  $H_2$  and  $CO$ , into a complex array of products, consisting predominantly of alkenes and alkanes but also varieties of minor compounds including a range of oxygenate compounds. In the following, major mechanisms have been proposed and in some cases were introduced in a slightly modified form.

The original carbide mechanism for the formation of hydrocarbon and oxygenate products with the Fischer-Tropsch synthesis (FTS) included the formation of the metal carbide followed by hydrogenation of the metal carbide to produce the various products (Davis, 2001).

In the 1950s, the oxygenate (enol) mechanism gained widespread acceptance (Davis, 2001). This mechanism involves the chemisorption of  $CO$  which reacts with adsorbed hydrogen to form a unit species such as:



Where M is metal active site. This structure grows by a combination of condensation and water elimination steps using adjacent groups on the site of active metal. This enol group can condense as depicted in Figure 3.

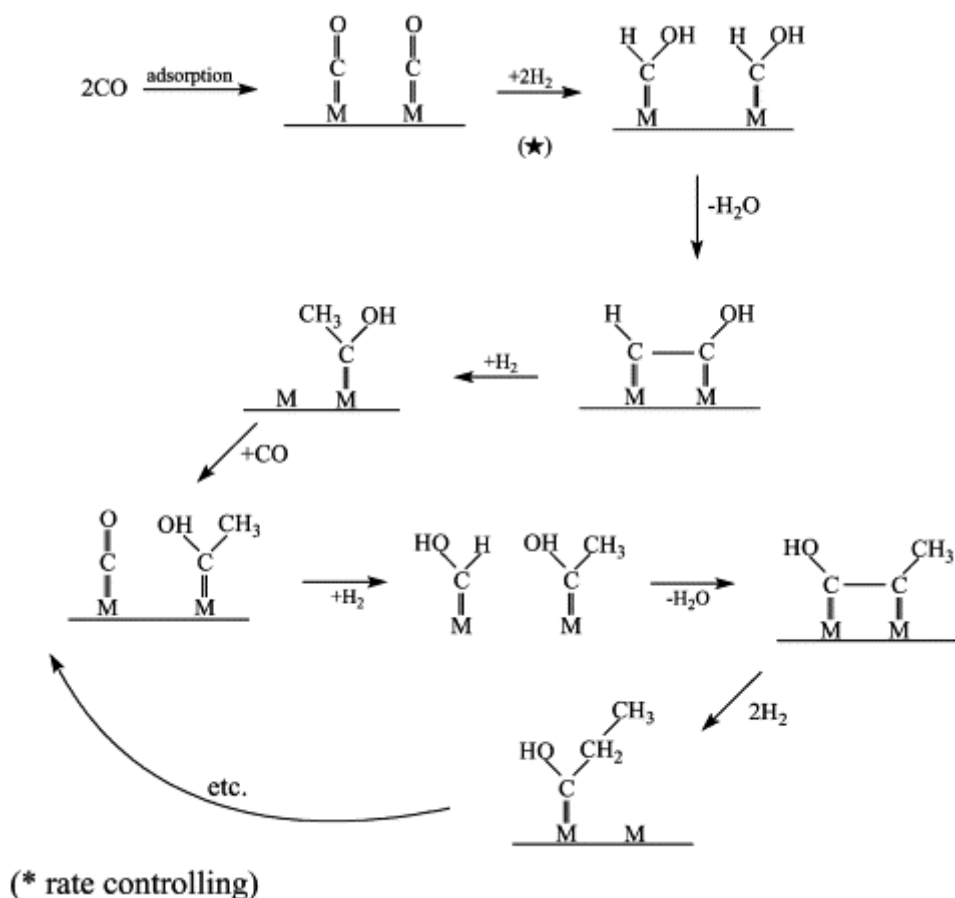


Figure 3 Scheme of the oxygenate (enol) mechanism.

The oxygenate mechanism that involved the reaction between CO and adsorbed hydrogen has been proposed. Besides, an insertion mechanism composed of the insertion of CO into a metal-methyl or metal-methylene carbon bond was also proposed. The inserted metal-methyl or metal-methylene is then hydrogenated to produce an alcohol or alkene; the alcohol or alcohol precursor can also eliminate oxygen to produce an alkene product. The scheme of this mechanism is shown in Figure 4.

With the general availability of surface science instruments, it was found that CO adsorbs on single crystal metal surfaces to produce a surface covered with carbon, and little oxygen. This led to the conclusion that the CO chemisorbs and dissociates to adsorbed C and O. This step is followed by the rapid hydrogenation of adsorbed O to

produce water. The hydrogenation of adsorbed carbon to form  $\text{CH}_2$  is much slower. This advanced mechanism was proposed by Maitlis (1989) and is shown in Figure 5.

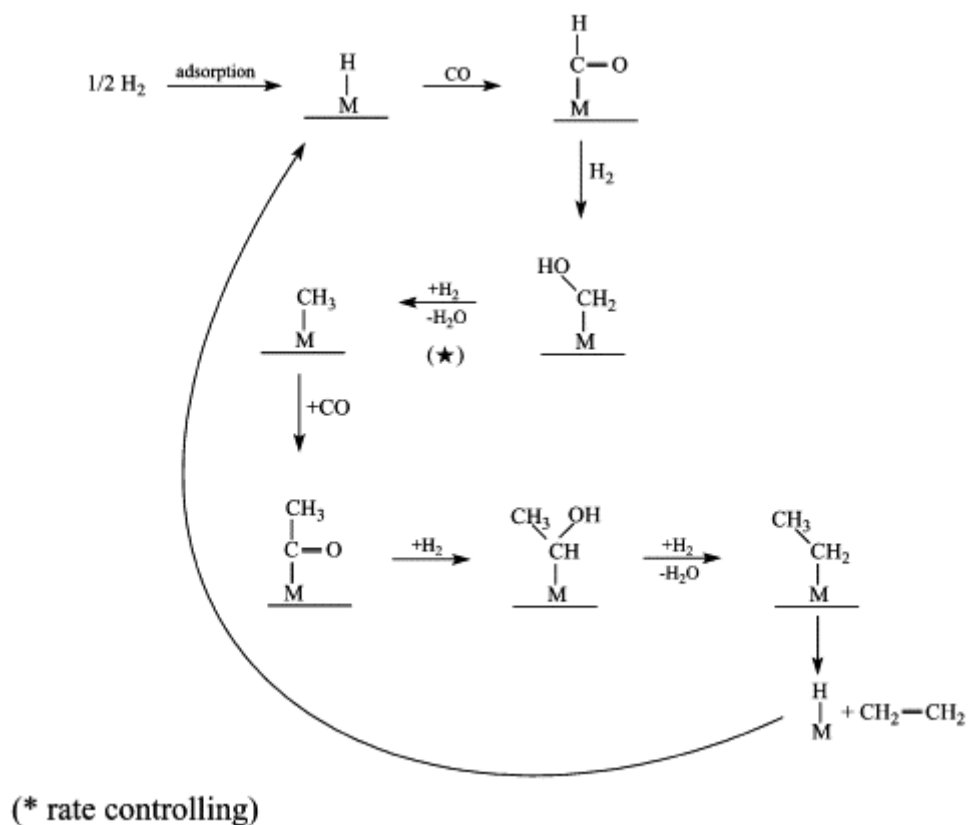


Figure 4 The insertion of CO into a metal-methyl or metal-methylene carbon bond.

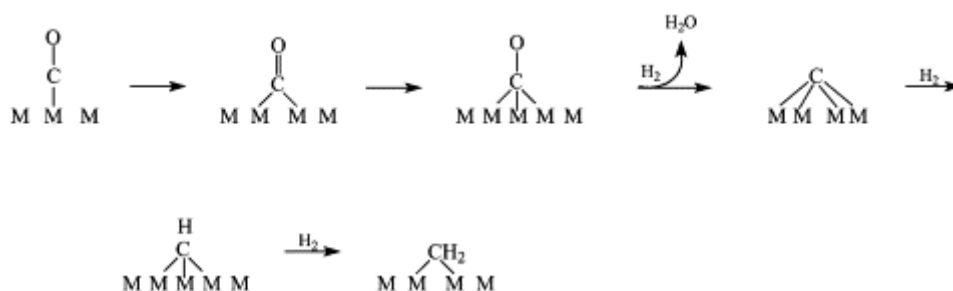


Figure 5 An advanced mechanism for the insertion of CO into a metal-methyl or metal-methylene carbon bond.

A more complicated version of advanced mechanism which proposed by Maitlis has been provided by Dry (1993) and is shown in Figure 6. This mechanism involved the adsorption and dissociation of CO to form adsorbed C and O on the metal active site, then followed by the hydrogenation and the removal of water to form the surface of CH<sub>2</sub>. The chain propagation of higher hydrocarbon was performed by insertion of CH<sub>2</sub> to the next same site that reacted with the adsorbed C and O which formed from the adsorption and dissociation of CO.

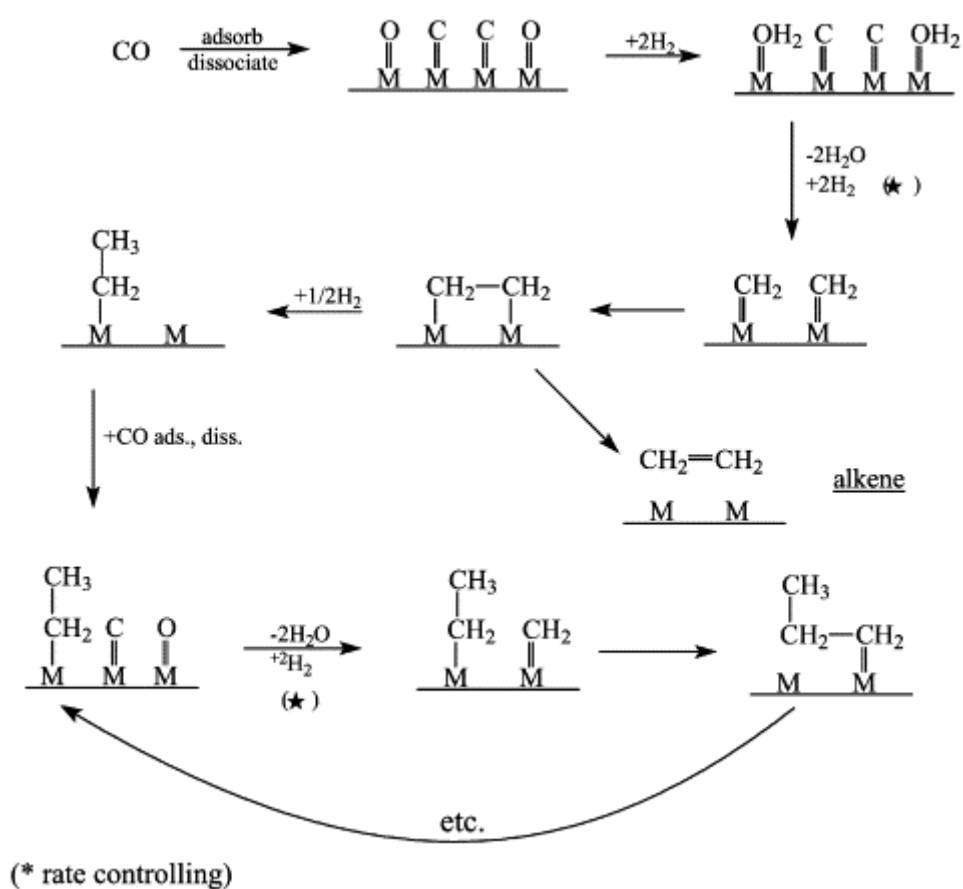


Figure 6 An insertion mechanism purposed by Dry (1993)

Blyholder *et al.* (1976) offered the following mechanism for the reaction of CO, H<sub>2</sub> and C<sub>2</sub>H<sub>4</sub> on a cobalt catalyst as shown in Figure 7. The mechanisms were quite similar to as suggested above, however, CO adsorbed onto the same site of CH<sub>x</sub> species, then inserted to the CH<sub>x</sub> species and reacted with the nearby site of adsorbed H to form the higher-chain CH<sub>x</sub> species. The next step was the adsorption and insertion of CO onto the same site of higher-chain CH<sub>x</sub> species.

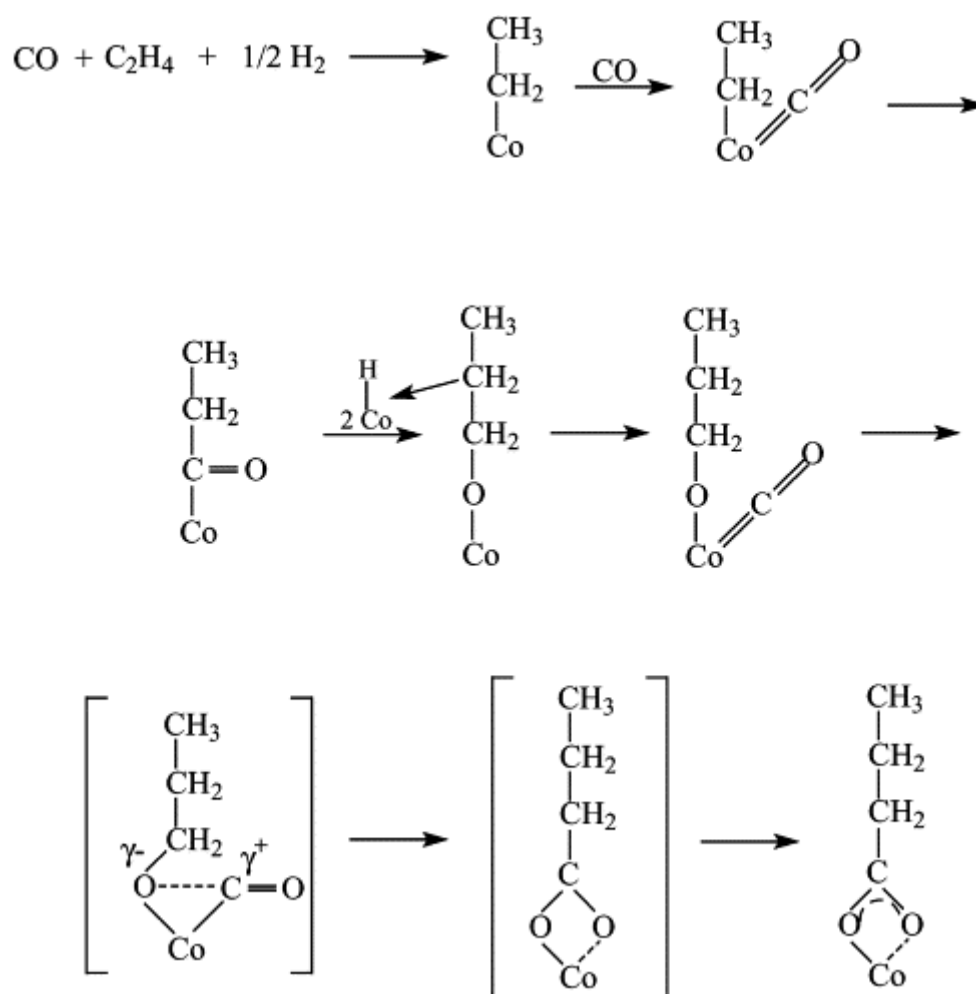


Figure 7 The mechanism for the reaction of CO, H<sub>2</sub> and C<sub>2</sub>H<sub>4</sub> on a cobalt catalyst.

A similar adsorption model has been proposed by Kolbel and Tillmetz (1974). A pathway similar to the above would account for the chain initiation by  $\text{CO}_2$  as shown in Figure 8.

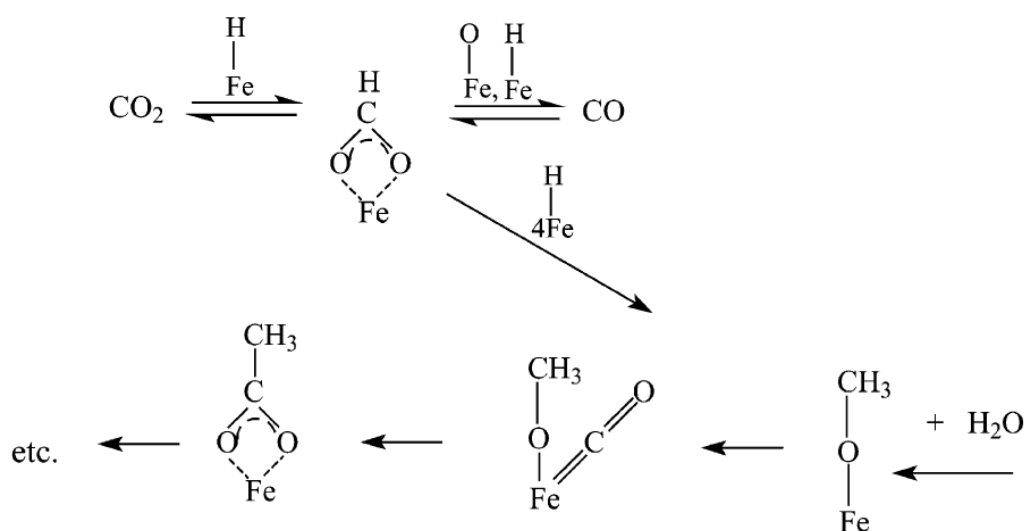


Figure 8 The adsorption model has been proposed by Kolbel and Tillmetz (1974).

From the scheme of mechanism as shown in Figure 8,  $\text{CO}_2$  reacted with adsorbed  $\text{H}$  on the metal active site to form the  $\text{COOH}$  species while the reversible reaction between of  $\text{COOH}$  species, and  $\text{CO}$  and adsorbed  $\text{O}$  and  $\text{H}$  were occurred.  $\text{COOH}$  species reacted with adsorbed  $\text{H}$  to form water and  $\text{CH}_3\text{O}$  species, similar to the mechanism above,  $\text{CO}$  adsorbed onto the same site of  $\text{CH}_3\text{O}$  species and inserted into  $\text{CH}_3\text{O}$  species. The chain growth of hydrocarbon was occurred by the adsorption of  $\text{CO}$  on metal site and followed by reacted with the adsorbed  $\text{H}$ .

FT synthesis is currently of considerable interest for commercial application in production of fuels such as LPG, gasoline, and diesel fuel because of the production of high quality and clean burning fuel.

From the survey on literatures, the synthesis of liquid fuels from carbon dioxide and methane via the two-stage process consisting reforming process and Fischer-Tropsch synthesis is the promising process. Due to our objectives to find out the best conditions for synthesis of liquid fuels using the two-stage reactor, the optimum conditions for both reforming process and Fischer-Tropsch synthesis were investigated. For the first process, carbon dioxide reforming of methane was performed over 5 wt.%Ni/Al<sub>2</sub>O<sub>3</sub> catalyst at the conditions as follows: CH<sub>4</sub>:CO<sub>2</sub> molar ratio of 1, total gas pressure of 10 atm, total flow rate of 50 ml/min and the temperature range of 500-750 °C. For the second process, Fischer-Tropsch synthesis was performed over Co/SBA-15 catalyst with the variation of reaction temperature (200-280 °C), amounts of cobalt loading (10-30 wt.%) and metal promoters (lithium, sodium and potassium) at the conditions as follows: CH<sub>4</sub>:CO<sub>2</sub> molar ratio of 1, total gas pressure of 10 atm and total flow rate of 50 ml/min. The details of the experiment were described in materials and methods.

## MATERIALS AND METHODS

### Chemicals and Equipments

#### 1. Chemicals

##### **1.1 Chemicals for Catalyst Preparation**

- 1.1.1 Nickel nitrate ( $\text{Ni}(\text{NO}_3)_3 \cdot 6\text{H}_2\text{O}$ , 97.0 % purity, Univar)
- 1.1.2 Cobalt nitrate ( $\text{Co}(\text{NO}_3)_2 \cdot 6\text{H}_2\text{O}$ , 99.0 % purity, Fluka)
- 1.1.3 Lithium nitrate ( $\text{LiNO}_3$ , 98.0 % purity, Panreac)
- 1.1.4 Sodium nitrate ( $\text{NaNO}_3$ , 99.0 % purity, Univar)
- 1.1.5 Potassium nitrate ( $\text{KNO}_3$ , 99.5 % purity, Univar)
- 1.1.6 Hydrochloric acid ( $\text{HCl}$ , 36.5 -38.0 wt.% purity, J.T. Baker)
- 1.1.7 Rice husk ash
- 1.1.8 Sodium hydroxide ( $\text{NaOH}$ , 99.0 % purity, Merck)
- 1.1.9 Pluronic P123 ( $\text{C}_5\text{H}_{14}\text{O}_4$ , Aldrich, product code No. 435-465)
- 1.1.10 Aluminum oxide ( $\text{Al}_2\text{O}_3$ , 100 % purity, Fluka)
- 1.1.11 Distilled water

##### **1.2 Chemicals for the Two-Stage Synthesis of Liquid Fuel from Carbon Dioxide and Methane**

- 1.2.1 Feed gases
  - Methane ( $\text{CH}_4$ , 99.99 % purity, TIG)
  - Carbon dioxide ( $\text{CO}_2$ , 99.5 % purity, SCE)
  - Oxygen ( $\text{O}_2$ , 99.5% purity, Linde)
  - Hydrogen ( $\text{H}_2$ , 99.99 % purity, TIG)
  - Nitrogen ( $\text{N}_2$ , 99.99 % purity, TIG)



### 1.2.2 Standard gases

- Carbon monoxide (CO, 99.99 % purity, TIG)
- Mixture of 5 % carbon monoxide (CO), 5 % carbon dioxide (CO<sub>2</sub>), 5 % methane (CH<sub>4</sub>), 5 % ethylene (C<sub>2</sub>H<sub>4</sub>), 5 % ethane (C<sub>2</sub>H<sub>6</sub>), 5 % propylene (C<sub>3</sub>H<sub>6</sub>) and 5 % propane (C<sub>3</sub>H<sub>8</sub>) in nitrogen (N<sub>2</sub>) balance (Messer)
- 5 % i-Butane (i-C<sub>4</sub>H<sub>10</sub>) in nitrogen (N<sub>2</sub>) balance (TIG)

### 1.2.3 Standard liquid hydrocarbons

- n-Pentane (n-C<sub>5</sub>H<sub>12</sub>, 99.64 % purity, Fischer chemicals)
- n-Hexane (n-C<sub>6</sub>H<sub>14</sub>, 99 % purity, Merck)
- n-Heptane (n-C<sub>7</sub>H<sub>16</sub>, 99.5 % purity, Fluka)
- n-Octane (n-C<sub>8</sub>H<sub>18</sub>, 99 % purity, Merck)
- n-Nonane (n-C<sub>9</sub>H<sub>20</sub>, 99 % purity, Merck)
- n-Decane (n-C<sub>10</sub>H<sub>22</sub>, 99 % purity, Merck)
- n-Undecane (n-C<sub>11</sub>H<sub>24</sub>, 97 % purity, Fluka)
- n-Dodecane (n-C<sub>12</sub>H<sub>26</sub>, 99 % purity, Merck)
- n-Tridecane (n-C<sub>13</sub>H<sub>28</sub>, 99 % purity, Fluka)
- n-Tetradecane (n-C<sub>14</sub>H<sub>30</sub>, 99 % purity, Fluka)
- n-Pentadecane (n-C<sub>15</sub>H<sub>32</sub>, 99 % purity, Fluka)
- Toluene (C<sub>7</sub>H<sub>8</sub>, 99.64% purity, Fischer chemicals)
- Octanol (C<sub>8</sub>H<sub>17</sub>OH, 99.5 % purity, Unilab)

### 1.2.4 Sand as the inert bed (40-200 mesh, Fluka)

### 1.2.5 Quartz wool as the catalyst bed support (Alltech)

## 2. Equipments

### 2.1 Equipments for Catalyst Preparation

- 2.1.1 Digital weighing machine (AT 400Metler, Toledo)
- 2.1.2 Magnetic hot plate and stirrer (SLR Model, Schott)
- 2.1.3 Oven (ED53 Model, Binder)
- 2.1.4 Furnace (ELF 10/6 Model, Carbolite)
- 2.1.5 Desicator

2.1.6 Digital hot plate and stirrer (Schott, SLR)

2.1.7 Autoclave

2.1.8 Sieve analysis (Retsch, VIBRO)

2.1.9 Electro mantle (Barnstead, EM1000/C)

## **2.2 Equipments for the Two-Stage Synthesis of Liquid Fuel from Carbon Dioxide and Methane**

### **2.2.1 Catalytic reaction testing unit**

- Pressure regulator
- Mass flow controller (GFC117 Model, Aalborg)
- Thermocouple (K type)
- Electric heater
- Temperature controller
- Furnace (MTF 12/38/250 Model, Carbolite)
- Flexible heating tape (100 Volt)
- Voltage transformer (0-240 Volt)
- Bubble flow meter

### **2.2.2 Gas analysis unit**

- Gas chromatograph equipped with thermal conductivity detector (TCD) (GC-8A Model, Shimadzu) and chromatopac data processor (C-R8A Model, Shimadzu)
- Gas chromatograph equipped with flame ionization detector (FID) (GC-8A Model, Shimadzu) and chromatopac data processor (C-R8A Model, Shimadzu)
- Gas syringe (Gastight#1002 Model, Hamilton)
- Liquid syringe (Microliter#80377 Model, Hamilton)

## **Experimental Preparation**

### **1. Catalytic Reaction Testing Unit**

The catalytic reaction testing unit for two-stage synthesis of liquid fuel from carbon dioxide and methane is shown in Figure 9. It consists of a feed flow measuring and controlling system (1), a furnace-equipped stainless steel tube reactor (2) and a sampling system (3). The catalytic reaction testing unit was designed to operate under heated and pressurized conditions. The details of this unit are as follows:

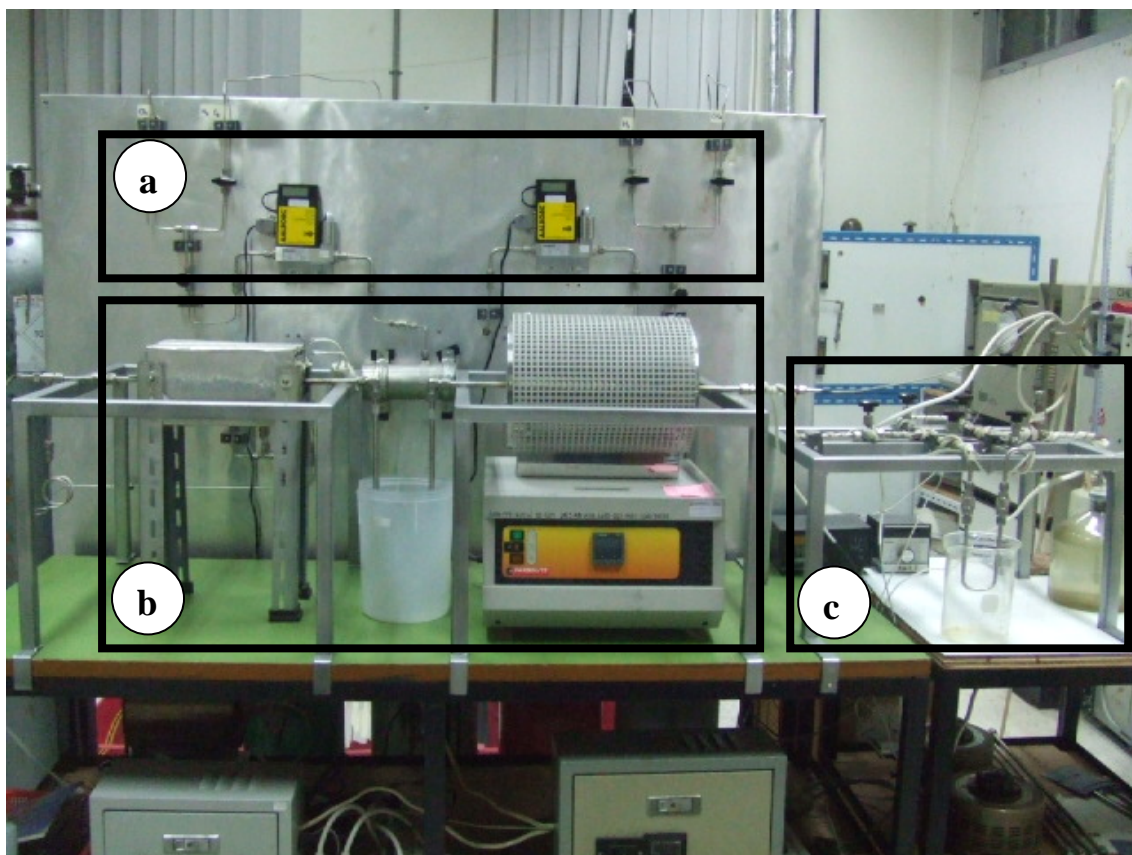


**Figure 9** Catalytic reaction testing unit: (a) a feed flow measuring and controlling system, (b) a furnace-equipped stainless steel tube reactor and (c) a sampling system.

### 1.1 The Feed Flow Measuring and Controlling System

This unit was connected to feed gases consisted of methane, carbon dioxide, oxygen, hydrogen and nitrogen. Methane and carbon dioxide were used as feedstock gases, oxygen and hydrogen were used for catalyst calcination and reduction, respectively. Nitrogen was used for monitoring system leakage. Flow rates of all feed gases were measured and controlled by Aalborg mass flow controller (Figure 10). The feedstock gases were mixed in cylinder before introduced into the reactor.

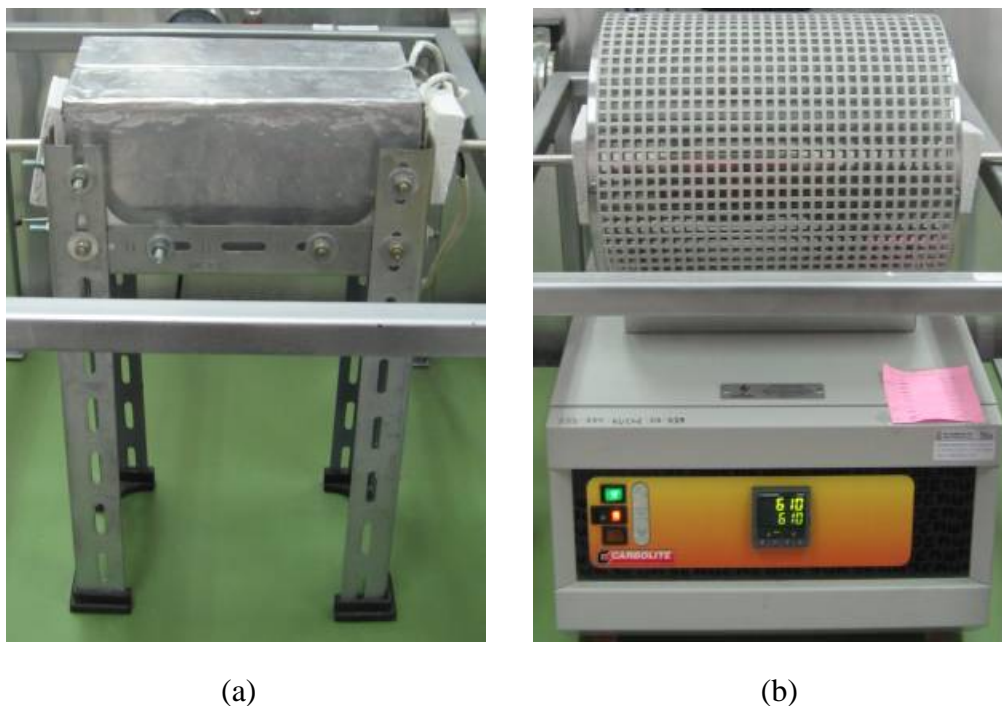


Figure 10 Aalborg mass flow controller.

### 1.2 The Pack Bed Reactor

The two-stage INCONEL tubes were used as the fixed-bed reactors. In the first-stage reforming reactor, the INCONEL tube was heated with an electric heater (Figure 11a) controlled by the temperature controller. A thermocouple connected to a temperature controller was inserted inside the INCONEL tubes in order to measure and control the temperature of the catalyst bed. Between the first-stage reforming reactor outlet and the second-stage Fischer-Tropsch (FT) reactor inlet, the reactor tube was cooled down by water at room temperature. In the second-stage FT reactor, the INCONEL tube was heated in the Carbolite furnace (Figure 11b). A thermocouple was also inserted inside the INCONEL tubes to measure and control the temperature

of the catalyst bed. In both reactors, different types of catalysts were placed in the isothermal zone of reactors between quartz wool layers as the schemes shown in Figures 12a and 12b.



**Figure 11** (a) The first-stage reforming reactor equipped with the electric heater (b) the second-stage FT reactor equipped with the Carbolite furnace.

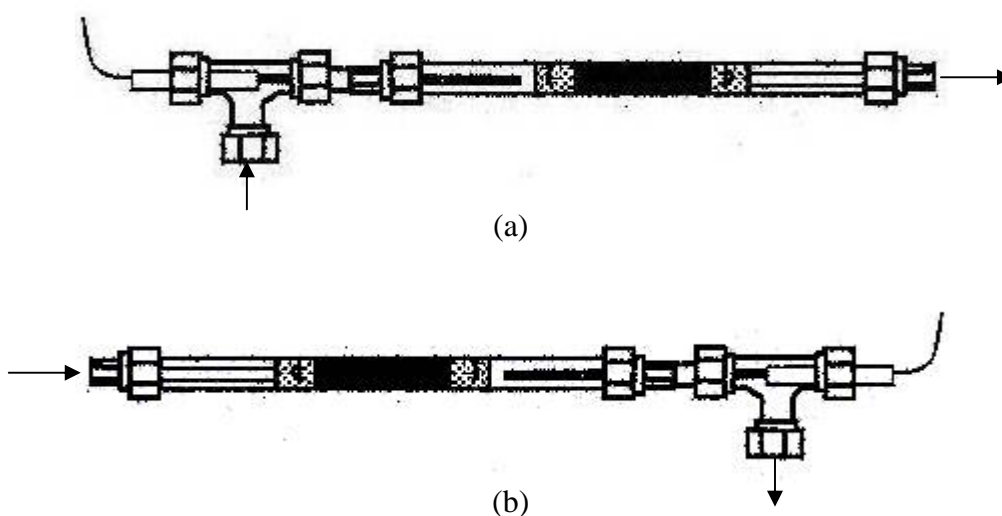


**Figure 12** Schemes of (a) the first-stage reforming reactor and (b) the second-stage FT reactor.

### 1.3 The Sampling System

The reaction gas mixtures were immediately sampled by a gas syringe through a heated sampling port or subsequently sampled by a liquid syringe after collecting at a U-tube cooling trap connecting to quick release valves as shown Figure 13. Samples were analyzed by gas chromatographs. Between the reactor outlet and the sampling port and U-tube, the gas mixtures were heated by heating tape to prevent condensation. Exit gas mixtures were trapped by water before venting to atmosphere and the exit flow rate was measured by a bubble flow meter.



Figure 13 Heated sampling valve and U-tube cooling trap connecting to quick release valves.

## 2. Gas Analysis Unit

Gas analysis unit consisted of Shimadzu gas chromatograph and chromatopac data processor. The amounts of CO, CO<sub>2</sub> and CH<sub>4</sub> were monitored by gas chromatograph with thermal conductivity detector (TCD) and a Porapak-Q column, as shown in Figure 14. Helium was used as both carrier gas and internal standard gas for TCD.



Figure 14 Shimadzu gas chromatograph equipped with thermal conductivity detector and chromatopac data processor.

The conditions for analysis of CO, CO<sub>2</sub>, CH<sub>4</sub> were:

- |                                 |     |                             |
|---------------------------------|-----|-----------------------------|
| - Primary gas pressure          | 200 | kPa (2 kg/cm <sup>2</sup> ) |
| - He carrier gas 1 pressure     | 100 | kPa (1 kg/cm <sup>2</sup> ) |
| - He carrier gas 2 pressure     | 100 | kPa (1 kg/cm <sup>2</sup> ) |
| - Injector/Detector temperature | 60  | °C                          |
| - Initial column temperature    | 60  | °C                          |
| - Final column temperature      | 60  | °C                          |
| - Bridge current supply         | 70  | mA                          |
| - Attenuation                   | 512 |                             |

The amounts of C<sub>2</sub>-C<sub>15</sub> hydrocarbons are analyzed by gas chromatography with flame ionization detector (FID) and both a Porapak-Q column for C<sub>2</sub>-C<sub>4</sub> hydrocarbons and an OV-101 column for C<sub>5</sub>-C<sub>15</sub> hydrocarbons, as shown in Figure 15. Helium was used as the carrier gas, while hydrogen and air were used as the combustion gas for FID.

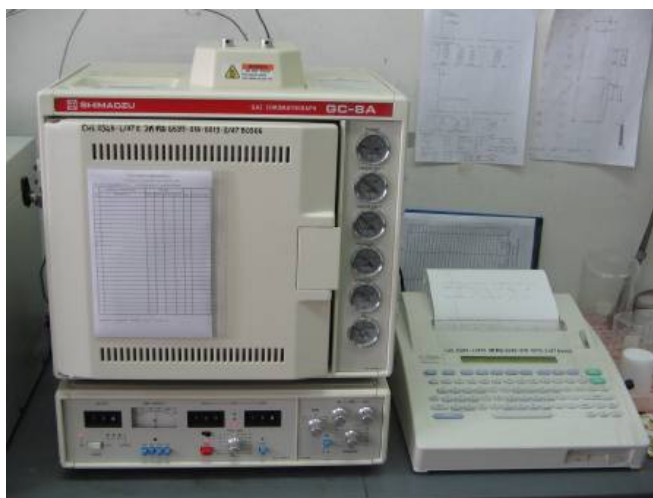


Figure 15 Shimadzu gas chromatograph equipped with flame ionization detector and chromatopac data processor.

The conditions for analysis of C<sub>2</sub>-C<sub>4</sub> hydrocarbons were:

- Primary gas pressure	200	kPa (2 kg/cm <sup>2</sup> )
- He carrier gas 1 pressure	100	kPa (1 kg/cm <sup>2</sup> )
- H <sub>2</sub> gas 1 pressure	60	kPa (0.6 kg/cm <sup>2</sup> )
- Air pressure	50	kPa (0.5 kg/cm <sup>2</sup> )
- Injector/Detector temperature	160	°C
- Initial column temperature	160	°C
- Final column temperature	160	°C
- Range	100	
- Attenuation	512	



The conditions for analysis of C<sub>5</sub>-C<sub>15</sub> hydrocarbons were:

- Primary gas pressure	200	kPa (2 kg/cm <sup>2</sup> )
- He carrier gas 2 pressure	50	kPa (1 kg/cm <sup>2</sup> )
- H <sub>2</sub> gas 2 pressure	60	kPa (0.6 kg/cm <sup>2</sup> )
- Air pressure	50	kPa (1 kg/cm <sup>2</sup> )
- Injector/Detector temperature	60	°C
- Initial column temperature	30	°C
- Final column temperature	230	°C
- Temperature program rate	10	°C/min
- Holding time	5	min
- Range	100	
- Attenuation	512	

The details of qualitative and quantitative analysis results from gas chromatograph are shown in Appendix A.

### **Experimental Procedures**

In this research, the experiment was divided into 2 sections: (1) preparation of SBA-15 mesoporous silica support and Ni/Al<sub>2</sub>O<sub>3</sub> and Co/SBA-15 catalysts (at different Co loadings and promoters) by wet impregnation method, and (2) synthesis of liquid fuels from carbon dioxide and methane using the two-stage reactor.

#### **1. Preparation of SBA-15 Mesoporous Silica Support and Co/SBA-15 Catalysts**

The support material and catalysts used in this experiment consist of SBA-15 mesoporous silica support and Ni/Al<sub>2</sub>O<sub>3</sub> and Co/SBA-15 catalysts (at different cobalt loadings and promoters). The detail of preparation methods were described as follows:

### 1.1 Synthesis of SBA-15 Mesoporous Silica Support

The equipment used in the synthesis of SBA-15 mesoporous silica support was set up as shown in Figure 16.



Figure 16 The setup of equipment for hydrolysis and condensation reactions.

1.1.1 A solution of Pluronic P123 was prepared by dissolving 0.00875 mol of Pluronic P123 in 200 mL of distilled water under stirring with room temperature.

1.1.2 The temperature of resulting solution was increased from room temperature to 50 °C and hold there with stirring for 5 minutes, after that the solution was cooled down to room temperature.

1.1.3 Sodium silicate solution based on a mol of silica was added to the mixture and mixed properly.

1.1.4 After that, 4 mol of HCl was quickly added under vigorous stirring at room temperature to 40 °C for 24 h.

1.1.5 The resulting gel was then transferred into a Teflon-lined autoclave and heated statically at 100 °C under autogeneous pressure for 24 h.

1.1.6 The solid products were separated from the mixture by filtration, then washed with large amounts of warm distilled water.

1.1.7 The washed product was dried at 140 °C for 3 h and calcined at 500 °C for 6 h. All of the synthesis step can be summarized as shown in Figure 17.

The detail of SBA-15 mesoporous silica synthesis has been reported by Nanta-ngern (2005).

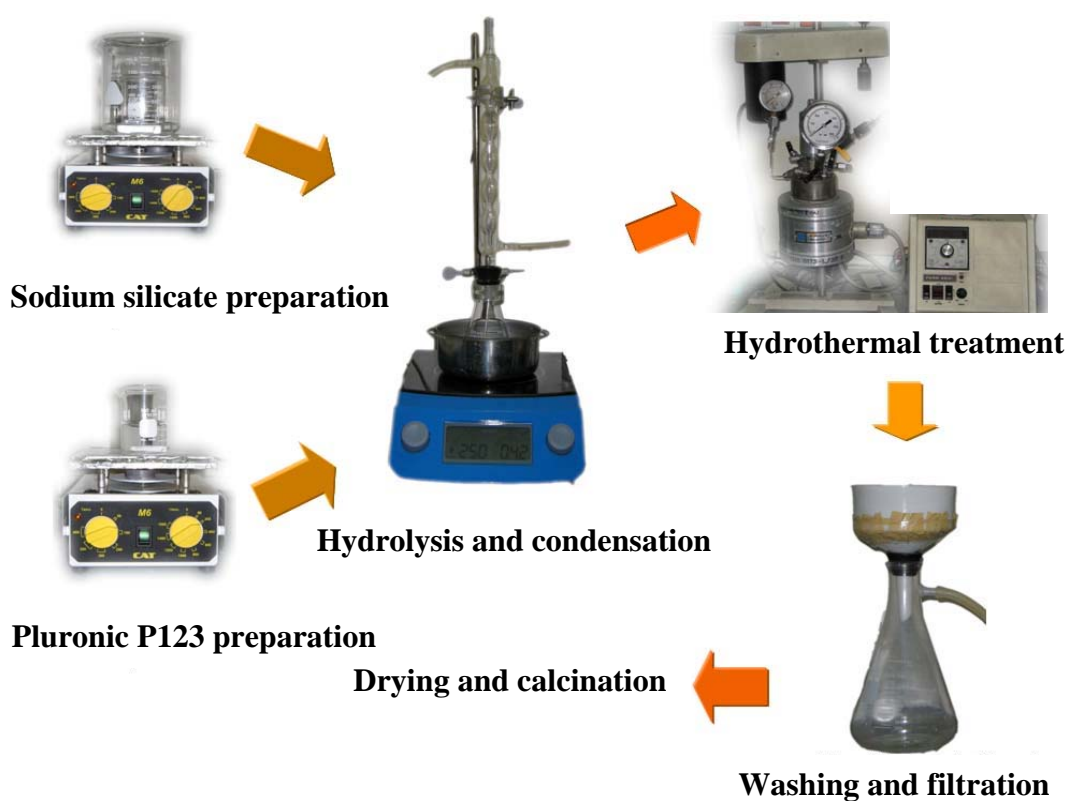


Figure 17 Scheme of mesoporous silica synthesis process.

## 1.2 Ni/Al<sub>2</sub>O<sub>3</sub> Catalyst Preparation

For Ni/Al<sub>2</sub>O<sub>3</sub> catalyst preparation, nickel nitrate salt (Ni(NO<sub>3</sub>)<sub>3</sub>·6H<sub>2</sub>O) was used as a metal precursor. The nickel metal of 5 wt.% was loaded on alumina via the wet impregnation method as the following procedures:

1.2.1 A required amount of an aqueous solution of nickel nitrate salt was mixed with alumina powder.

1.2.2 The mixture was agitated at room temperature for 1 h and dried at 120 °C for 24 h.

1.2.3 The dried product was calcined in air at 550 °C for 4 h. The catalyst granules were obtained.

1.2.4 The obtained catalyst granules were crushed and sieved to 200 mesh, this catalyst was denoted as 5Ni/Al<sub>2</sub>O<sub>3</sub> catalyst and used for reforming reaction of carbon dioxide and methane.

### **1.3 Co/SBA-15 Catalyst Preparation**

In this research, cobalt supported on SBA-15 was used as the catalyst for synthesis of liquid fuels from carbon dioxide and methane in the second-stage reactor. The amounts of cobalt loading on SBA-15 mesoporous silica support were 10, 20 and 30 wt.%. Co supported on SBA-15 support was promoted with Lithium (Li), Sodium (Na) and Potassium (K) metal element in the form of nitrate salt.

1.3.1 SBA-15 with difference cobalt loading. Cobalt nitrate salt was used as a metal precursor. The cobalt metal of 10, 20 and 30 wt.% were loaded on SBA-15 mesoporous silica via the wet impregnation method. The procedure was as follows:

1.3.1.1 A required amount of an aqueous solution of cobalt nitrate salt was mixed with SBA-15 mesoporous silica powder.

1.3.1.2 The mixture was agitated at room temperature for 1 h and dried at 120 °C for 24 h.

1.3.1.3 The dried product was calcined in air at 550 °C for 4 h. The catalyst granules were obtained.

1.3.1.4 The obtained catalyst granules were crushed and sieved to 200 mesh and this catalyst was denoted as 10Co/SBA-15, 20Co/SBA-15 and 30Co/SBA-15 catalysts, respectively.

1.3.2 20Co/SBA-15 with different metal promoters. 20 wt.% Co and metal promoters including Li, Na and K were loaded on SBA-15 mesoporous silica via impregnation method. The procedure was as follows:

1.3.2.1 A required amount of an aqueous solution of cobalt nitrate salt and each metal promoter ( 0.1 wt.% Li, 0.3 wt.% Na and 0.5 wt.% K or 0.0045 mol% each ) were separately mixed with SBA-15 mesoporous silica powder.

1.3.2.2 The mixture was agitated at room temperature for 1 h and dried at 120 °C for 24 h.

1.3.2.3 The dried product was calcined in air at 550 °C for 4 h. The catalyst granules were obtained.

1.3.2.4 The obtained catalyst granules were crushed and sieved to a powder of 200 mesh and this catalyst was denoted as 0.1Li-20Co/SBA-15, 0.3Na-20Co/SBA-15 and 0.5K-20Co/SBA-15 catalyst, respectively.

The catalyst support and metal supported catalysts obtained from these preparation methods were characterized by X-ray fluorescence spectroscopy (XRF), N<sub>2</sub> adsorption analysis and transmission electron microscopy (TEM) for their elemental components, surface area, morphology and elemental distribution.

## **2. Two-Stage Synthesis of Liquid Fuels from Carbon Dioxide and Methane**

Before testing the catalytic performance, catalyst pretreatment procedures were undertaken in the reactor to obtain an active form of catalyst. The 5Ni/Al<sub>2</sub>O<sub>3</sub> catalyst was placed in the first-stage reforming reactor (3/8 in. outer diameter) with the bed length of 4 cm. The Co/SBA-15 catalyst was placed in the second-stage FT reactor (3/8 in. outer diameter) with the bed length of 4 cm. The catalysts were firstly calcined in oxygen atmosphere at 500 °C for 1 h and flow rate of 60 ml/min (NTP), flushed with nitrogen and followed by reduction in hydrogen atmosphere at 400 °C for 2 h and flow rate of 60 ml/min (NTP), and finally flushed and cooled with nitrogen. After activation, the catalysts were ready for the catalytic performance test.

In this research, the liquid fuels target product was synthesized from carbon dioxide and methane under pressurized condition of 10 atm. Methane reforming with carbon dioxide reaction was occurred in the first stage reactor, while Fischer-Tropsch (FT) synthesis was occurred in the second stage FT reactor. In the first-stage reforming reactor, carbon dioxide and methane gases were converted to synthesis gas on the 5Ni/Al<sub>2</sub>O<sub>3</sub> catalyst at the temperature of 500-750 °C. The reaction gas mixtures from the first-stage reforming reactor were directly introduced to the second-stage reactor. In the second-stage FT reactor, synthesis gas was converted to liquid fuels on the Co/SBA-15 catalyst, respectively at the temperature of 200-280 °C.

The details of experimental conditions performed in this research were categorized by the sequence of experiment as shown in Table 4.

**Table 4** The details of experimental conditions

Series of experiment <sup>1</sup>	1 <sup>st</sup> stage reactor		2 <sup>nd</sup> stage reactor	
	Catalysts	Temperature <sup>2</sup> (°C)	Catalysts	Temperature (°C)
Thermal reaction	Sand	500-750	-	-
	Sand	a	Sand	200-280
Catalytic reaction: catalyst supports	Al <sub>2</sub> O <sub>3</sub>	500-750	-	-
	Al <sub>2</sub> O <sub>3</sub>	a	SBA-15	200-280
Catalytic reaction: metal-supported catalysts	Ni/Al <sub>2</sub> O <sub>3</sub>	500-750	-	-
	Ni/Al <sub>2</sub> O <sub>3</sub>	a	Co/SBA-15	200-280

<sup>1</sup> The operating conditions were as follows: CH<sub>4</sub>:CO<sub>2</sub> molar ratio, 1:1; total gas pressure, 10 atm; total flow rate, 50 ml/min.

<sup>2</sup> a = optimum temperature of which maximum CO yield was produced at CH<sub>4</sub>:CO<sub>2</sub> molar ratio of 1; total gas pressure of 10 atm; total flow rate of 50 ml/min.

All reaction and product gas mixtures were analyzed by gas chromatograph. The data of conversion and selectivity calculated from gas chromatograph results and the details of calculations were shown in Appendix B.

## RESULTS AND DISCUSSION

In this research, liquid fuels in the range of gasoline to diesel are synthesized from carbon dioxide and methane via reforming reaction and Fischer-Tropsch (FT) synthesis in a two-stage reactor. The influences of catalytic temperatures (200, 220, 240, 260 and 280 °C), amounts of cobalt catalyst loading (10, 20 and 30 wt.% Co) and metal promoter types (lithium: Li, sodium: Na and potassium: K) are investigated at conditions as follow: CH<sub>4</sub>/CO<sub>2</sub> molar ratio of 1, total gas pressure of 10 atm and total flow rate of 50 ml/min (NTP).

In this part, results and discussion were separated into 3 sections consisting of catalyst characterization, thermal reaction investigation and catalytic reaction investigation. In the first section, chemical and physical properties of catalyst supports (Al<sub>2</sub>O<sub>3</sub> and SBA-15 mesoporous silica) and metal-supported catalysts (Ni/Al<sub>2</sub>O<sub>3</sub> and Co/SBA-15) prepared by wet impregnation method were characterized. In the second section, the thermal reactions of catalyst supports and metal-supported catalysts with temperature variations were considered for comparison of conversion and selectivity between thermal reaction and catalytic reaction. For the last section, the catalytic performances of metal-supported catalysts and metal-supported catalysts with metal promoters with temperature variations were investigated.

### **Catalyst Characterization**

The Al<sub>2</sub>O<sub>3</sub> and SBA-15 mesoporous silica supports, and Ni/Al<sub>2</sub>O<sub>3</sub> and Co/SBA-15 catalysts prepared by wet impregnation methods were characterized using X-ray fluorescence spectroscopy (XRF), N<sub>2</sub> adsorption analysis and transmission electron microscopy (TEM) for their chemical and physical properties.

#### **1. X-Ray Fluorescence Spectroscopy**

The XRF analysis results confirm the compositions of active metals on the catalyst supports as shown in Table 5.



Table 5 The chemical compositions of catalysts.

Catalysts	Component	Composition (wt.%)
5Ni/Al <sub>2</sub> O <sub>3</sub>	NiO	5.8
	Al <sub>2</sub> O <sub>3</sub>	94.2
10Co/SBA-15	CoO	15.2
	SiO <sub>2</sub>	83.4
	Others	1.4
20Co/SBA-15	CoO	27.4
	SiO <sub>2</sub>	70.3
	Others	2.3
30Co/SBA-15	CoO	31.1
	SiO <sub>2</sub>	68.9
0.1Li-20Co/SBA-15	Li <sub>2</sub> O	0.2
	CoO	21.6
	SiO <sub>2</sub>	78.2
0.3Na-20Co/SBA-15	Na <sub>2</sub> O	0.4
	CoO	20.7
	SiO <sub>2</sub>	78.9
0.5K-20Co/SBA-15	K <sub>2</sub> O	0.6
	CoO	20.3
	SiO <sub>2</sub>	79.1

From Table 5, the compositions of nickel impregnated onto Al<sub>2</sub>O<sub>3</sub> support is 4.5 wt.% for 5Ni/Al<sub>2</sub>O<sub>3</sub> catalyst and cobalt impregnated onto SBA-15 mesoporous silica support are 11.9, 21.5 and 24.5 wt.% for 10Co/SBA-15, 20Co/SBA-15 and 30Co/SBA-15 catalysts, respectively. The metal compositions of lithium, sodium and potassium as the promoters on 20Co/SBA-15 catalyst are 0.1, 0.3 and 0.5 wt.% for 0.1Li-20Co/SBA-15, 0.3Na-20Co/SBA-15 and 0.5K-20Co/SBA-15 catalysts, respectively.

Thus, the amounts of metal catalyst loaded on supports in each case are quite close to that of the desired amounts of active metal loading.

## **2. N<sub>2</sub> Adsorption Analysis**

Nitrogen adsorption isotherms of Al<sub>2</sub>O<sub>3</sub> and SBA-15 mesoporous silica supports, and 5Ni/Al<sub>2</sub>O<sub>3</sub>, 10Co/SBA-15, 20Co/SBA-15, 30Co/SBA-15, 0.1Li-20Co/SBA-15, 0.3Na-20Co/SBA-15 and 0.5K-20Co/SBA-15 catalysts were measured with nitrogen adsorption/desorption technique using the Autosorb-1 analyzer.

The nitrogen adsorption isotherms of catalyst supports and metal-supported catalysts are shown in Figures 18-20. The isotherms exhibit a typical hysteresis loop for capillary condensation in the pores of catalyst supports, metal-supported catalysts and metal-supported catalysts with metal promoters. The nitrogen adsorption isotherms for SBA-15 mesoporous silica support present a sharp inflection at a relative pressure in the range of 0.45-0.75 of which narrow than that of Al<sub>2</sub>O<sub>3</sub> support (present a sharp inflection at a relative pressure in the range of 0.4–1.0). This indicates the uniformity of mesopores structure of SBA-15 support.

Figure 18 shows the nitrogen adsorption isotherms of the first-stage reforming catalyst. Volume of nitrogen adsorbed on 5Ni/Al<sub>2</sub>O<sub>3</sub> catalyst is lower than that of Al<sub>2</sub>O<sub>3</sub> support at all relative pressures ( $P/P_0$ ). The lesser nitrogen adsorbed volume of 5Ni/Al<sub>2</sub>O<sub>3</sub> catalyst reveals the existence of nickel loaded on Al<sub>2</sub>O<sub>3</sub> support. For second-stage FT catalyst, the nitrogen adsorption isotherms are shown in Figure 19 and Figure 20. From Figure 19, the shape of the nitrogen adsorption isotherms of cobalt-supported catalysts was similar to that of the original SBA-15 mesoporous silica (as the isotherms of catalysts containing 10, 20 and 30 wt% Co), suggested that the mesoporous structure of SBA-15 mesoporous silica was mostly retained after cobalt impregnation. From Figure 19, the inflection isotherms of cobalt-supported catalysts occur at the same relative pressure (0.45-0.75) as compared with that of the

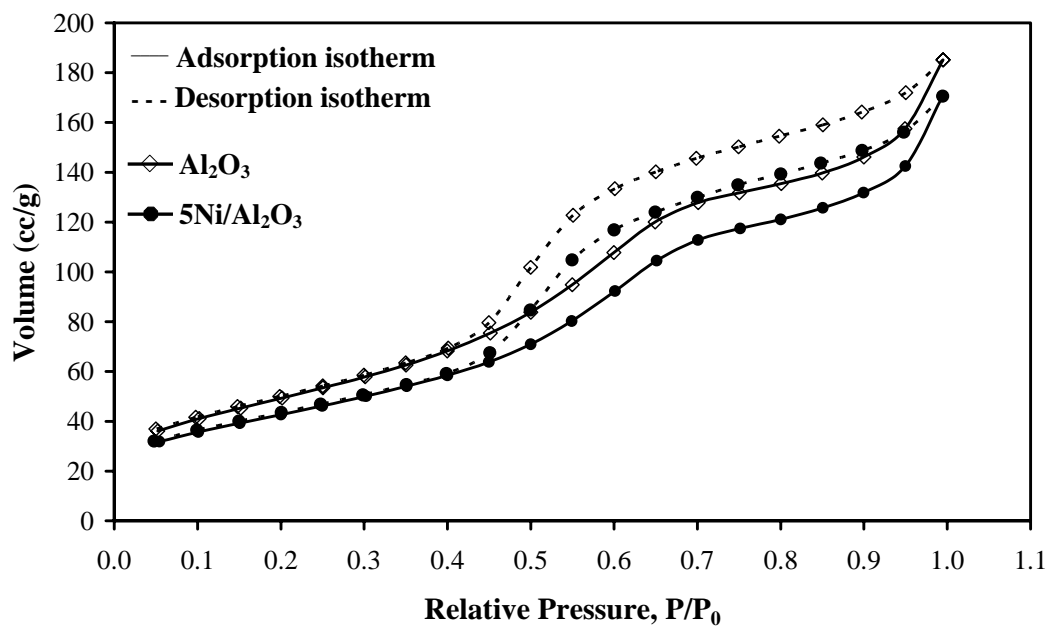


Figure 18 Nitrogen sorption isotherms of  $\text{Al}_2\text{O}_3$  support and  $5\text{Ni}/\text{Al}_2\text{O}_3$  catalyst.

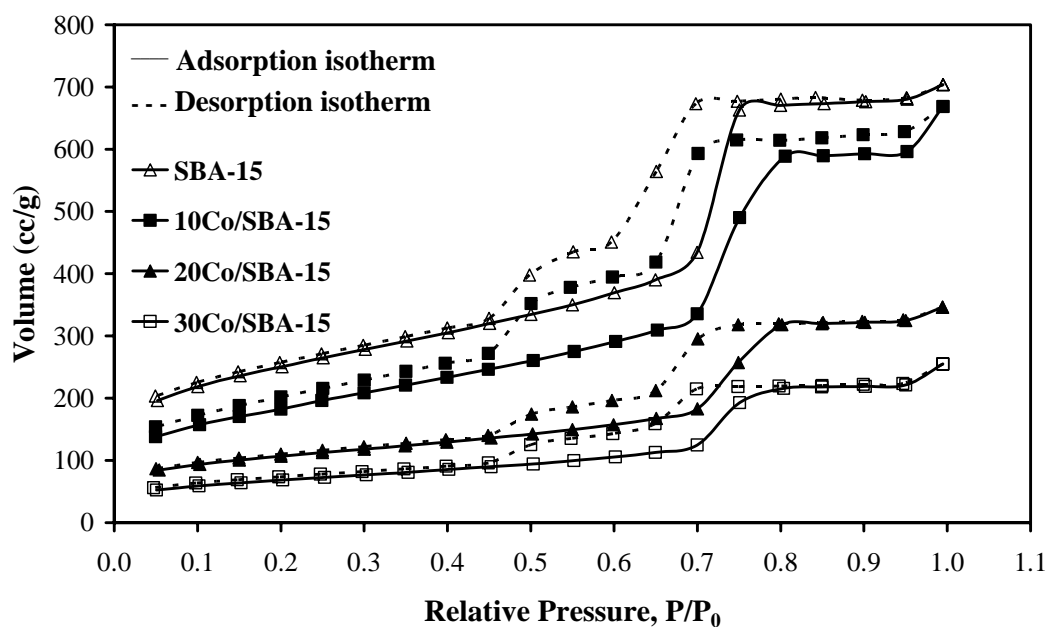
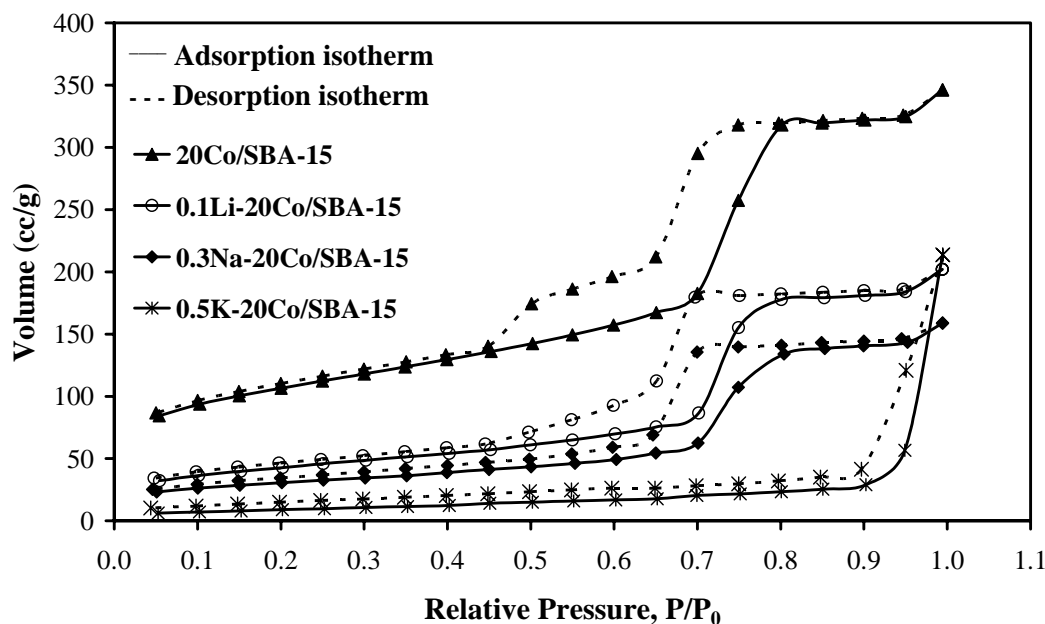


Figure 19 Nitrogen sorption isotherms of SBA-15 support,  $10\text{Co}/\text{SBA-15}$ ,  $20\text{Co}/\text{SBA-15}$  and  $30\text{Co}/\text{SBA-15}$  catalysts.



**Figure 20** Nitrogen sorption isotherms of 20Co/SBA-15, 0.1Li-20Co/SBA-15, 0.3Na-20Co/SBA-15 and 0.5K-20Co/SBA-15 catalysts.

SBA-15 mesoporous silica support. The BJH pore diameters in Table 6, also indicate and confirm a quite constant of the mean pore diameter after cobalt impregnation. These results are similar to the first-stage reforming catalyst and show the decrement of volume for nitrogen adsorbed on SBA-15 mesoporous silica support with the increment of cobalt loading amounts.

For cobalt-supported catalysts with metal promoters, the results are similar to nitrogen adsorption isotherms of cobalt-supported catalysts (as the isotherms of catalysts containing 10, 20 and 30 wt% Co) as shown in Figure 20. The sharp inflection isotherms of 0.1Li-20Co/SBA-15, 0.3Na-20Co/SBA-15 and 0.5K-20Co/SBA-15 catalysts at a relative pressure in the range of 0.45-0.8 also indicate the regularity of SBA-15 mesoporous silica support and a quite constant mean pore diameter (confirm by BJH pore diameter as shown in Table 6) although the large amounts of cobalt and metal promoters are loaded onto the support.

From Figure 20, it is observed that the inflection of isotherms has been shifted from the relative pressure ( $P/P_0$ ) of 0.45 in the case of 20Co/SBA-15 catalyst to 0.50, 0.65 and 0.90 in the cases of 0.1Li-20Co/SBA-15, 0.3Na-20Co/SBA-15 and 0.5K-20Co/SBA-15 catalysts, respectively. This may be explained that the desorption of nitrogen gas from the surface of catalyst during nitrogen adsorption/desorption analysis was occurred by reduction of pressure. The reduction of pressure at lower content was easily occurred with a lesser pore volume of catalyst, therefore the inflection isotherms of the lesser pore volume for 0.1Li-20Co/SBA-15, 0.3Na-20Co/SBA-15 and 0.5K-20Co/SBA-15 catalysts were shifted from 0.45 of 20Co/SBA-15 catalyst to the higher relative pressure at 0.5, 0.65 and 0.9, respectively.

The results of BET surface areas, pore diameters and total pore volume of  $\text{Al}_2\text{O}_3$ , SBA-15, 5Ni/ $\text{Al}_2\text{O}_3$ , 10Co/SBA-15, 20Co/SBA-15, 30Co/SBA-15, 0.1Li-20Co/SBA-15, 0.3Na-20Co/SBA-15 and 0.5K-20Co/SBA-15 catalysts measured by Autosorb-1 analyzer are shown in Table 6.

**Table 6** BET surface area, pore diameter and total pore volume of supports and catalysts cobalt.

Catalysts	BET surface area ( $\text{m}^2/\text{g}$ )	BJH pore diameter (nm)	Total pore volume (cc/g)
$\text{Al}_2\text{O}_3$	182	4.3	0.29
5Ni/ $\text{Al}_2\text{O}_3$	157	4.9	0.27
SBA-15	848	7.8	1.02
10Co/SBA-15	645	7.8	1.01
20Co/SBA-15	359	7.8	0.50
30Co/SBA-15	235	7.8	0.38
0.1Li-20Co/SBA-15	151	7.8	0.31
0.3Na-20Co/SBA-15	106	7.8	0.25
0.5K-20Co/SBA-15	94	7.8	0.21

Figures 18-20 and Table 6 show the results of metal introduction onto catalyst supports that lead to the decrement of both BET surface area and total pore volume. Both BET surface area and total pore volume are significantly decreased with the catalysts of higher cobalt and metal promoters loading. The surface areas drop from 182 to 157 m<sup>2</sup>/g for Al<sub>2</sub>O<sub>3</sub> support and 5Ni/Al<sub>2</sub>O<sub>3</sub> catalyst and drop from 848 to 645, 359 and 235 m<sup>2</sup>/g for SBA-15 mesoporous silica support and 10Co/SBA-15, 20Co/SBA-15 and 30Co/SBA-15 catalysts, respectively. For cobalt-supported catalysts with metal promoters, surface areas drop from 359 to 151, 106 and 94 m<sup>2</sup>/g for 20Co/SBA-15 catalyst and 0.1Li-20Co/SBA-15, 0.3Na-20Co/SBA-15 and 0.5K-20Co/SBA-15 catalysts, respectively. The results of surface areas and pore volumes change of SBA-15 mesoporous silica support and cobalt-supported catalysts are similar to that of Khodakov *et al.* (2003) who studied the effect of support mesoporous structure and cobalt content on cobalt dispersion and reducibility using two series of Fischer–Tropsch (FT) silica supported cobalt catalysts. They found that BET surface areas and total pore volume of SBA-15 mesoporous silica support drop from 887 to 249 m<sup>2</sup>/g and 1.91 to 0.38 cm<sup>3</sup>/g when amounts of cobalt loading were increased from 0 to 35 %.

The decrement of the surface areas and pore volume but quite constant in pore diameter are likely due to a partial plugging of support pores by metal species which corresponding to the result of nitrogen adsorption isotherms as shown in Figure 19. The plugging causes the pores inaccessible for nitrogen adsorption (Khodakov *et al.*, 2003 and Ohtsuka *et al.*, 2004).

### **3. Transmission Electron Microscopy (TEM)**

The morphology of catalyst supports, metal-supported catalysts and cobalt-supported catalysts with metal promoters was characterized by TEM. The TEM images of Al<sub>2</sub>O<sub>3</sub>, SBA-15, 5Ni/Al<sub>2</sub>O<sub>3</sub>, 10Co/SBA-15, 20Co/SBA-15, 30Co/SBA-15, 0.1Li-20Co/SBA-15, 0.3Na-20Co/SBA-15 and 0.5K-20Co/SBA-15 catalysts are shown in Figures 21-23.

The TEM image of  $\text{Al}_2\text{O}_3$  support is shown in Figure 21(a). The structure of  $\text{Al}_2\text{O}_3$  support is not quite uniform in pore size and structure. The dark color on  $\text{Al}_2\text{O}_3$  support which corresponding to nickel metal species is shown in Figure 21(b). Normally, the characteristic of metal on TEM image is shown as a dark area. From Figure 21(b), it can be obviously seen that the structure of nickel metal is appeared as a spherical area of which darker than that of the  $\text{Al}_2\text{O}_3$  support. Figure 22(a) shows the highly ordered hexagonal structure of SBA-15 mesoporous silica support of which uniformly arranged along parallel direction to the  $c$  axis. The dark color on SBA-15 mesoporous silica support is corresponding to cobalt metal species as shown in Figures 22(b)-22(d).

TEM images of cobalt-supported catalysts with metal promoters are shown in Figure 23. The TEM images along the direction perpendicular and parallel to the  $c$  axis of 0.1Li-20Co/SBA-15, 0.3Na-20Co/SBA-15 and 0.5K-20Co/SBA-15 catalysts are shown in Figures 23(a)-23(f), respectively. Similar to Figure 22, the dark color on SBA-15 mesoporous silica support is corresponding to cobalt metal and metal promoter species. Unfortunately, the obtained TEM images of cobalt-supported catalysts with metal promoters exhibit all metal species (cobalt, lithium, sodium and potassium) only in the form of rather dark color.

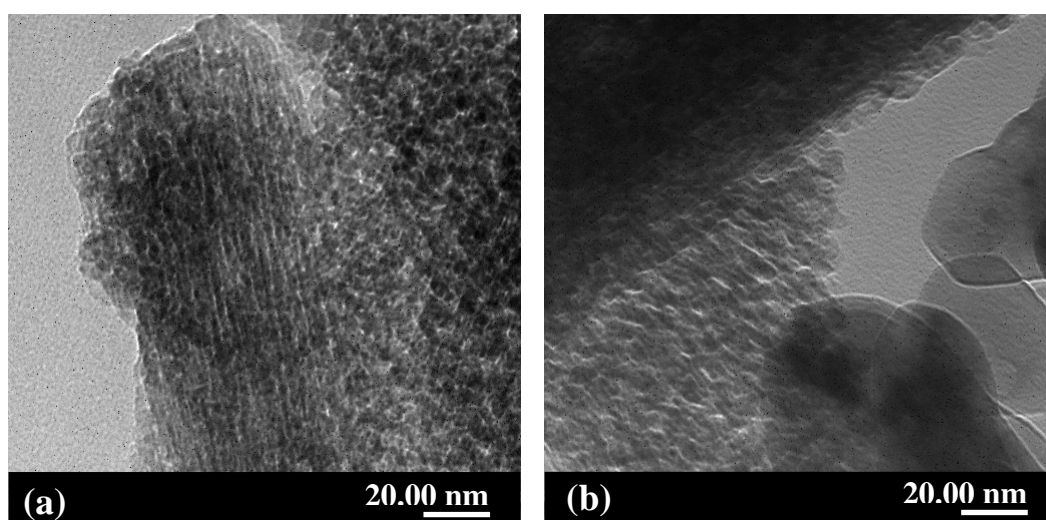


**Figure 21** TEM images of (a)  $\text{Al}_2\text{O}_3$  support (b) 5Ni/ $\text{Al}_2\text{O}_3$  catalyst.

As shown in Figures 21-23, the TEM images of 5Ni/Al<sub>2</sub>O<sub>3</sub>, 10Co/SBA-15, 20Co/SBA-15, 30Co/SBA-15, 0.1Li-20Co/SBA-15, 0.3Na-20Co/SBA-15 and 0.5K-20Co/SBA-15 catalysts reveal highly dispersion of active metal phases on the cross sectional arrays of Al<sub>2</sub>O<sub>3</sub> and SBA-15 mesoporous silica supports, no agglomeration is observed. As the results, the SBA-15 mesoporous silica structure of cobalt-supported catalyst and cobalt-supported catalysts with metal promoters are clearly remained after the cobalt impregnation and calcination.

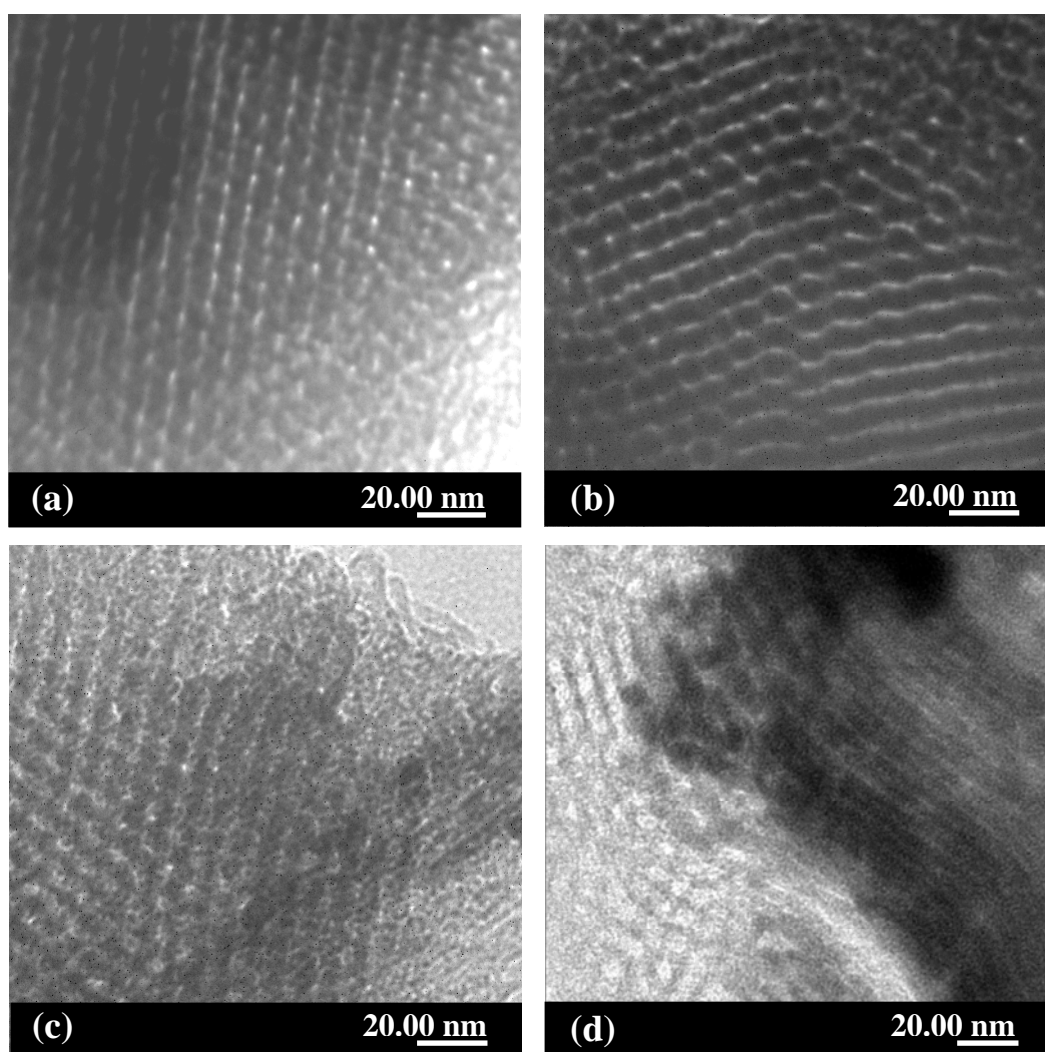


**Figure 22** TEM images of (a) SBA-15 support (b) 10Co/SBA-15 catalyst  
(c) 20Co/SBA-15 catalyst (d) 30Co/SBA-15 catalyst.



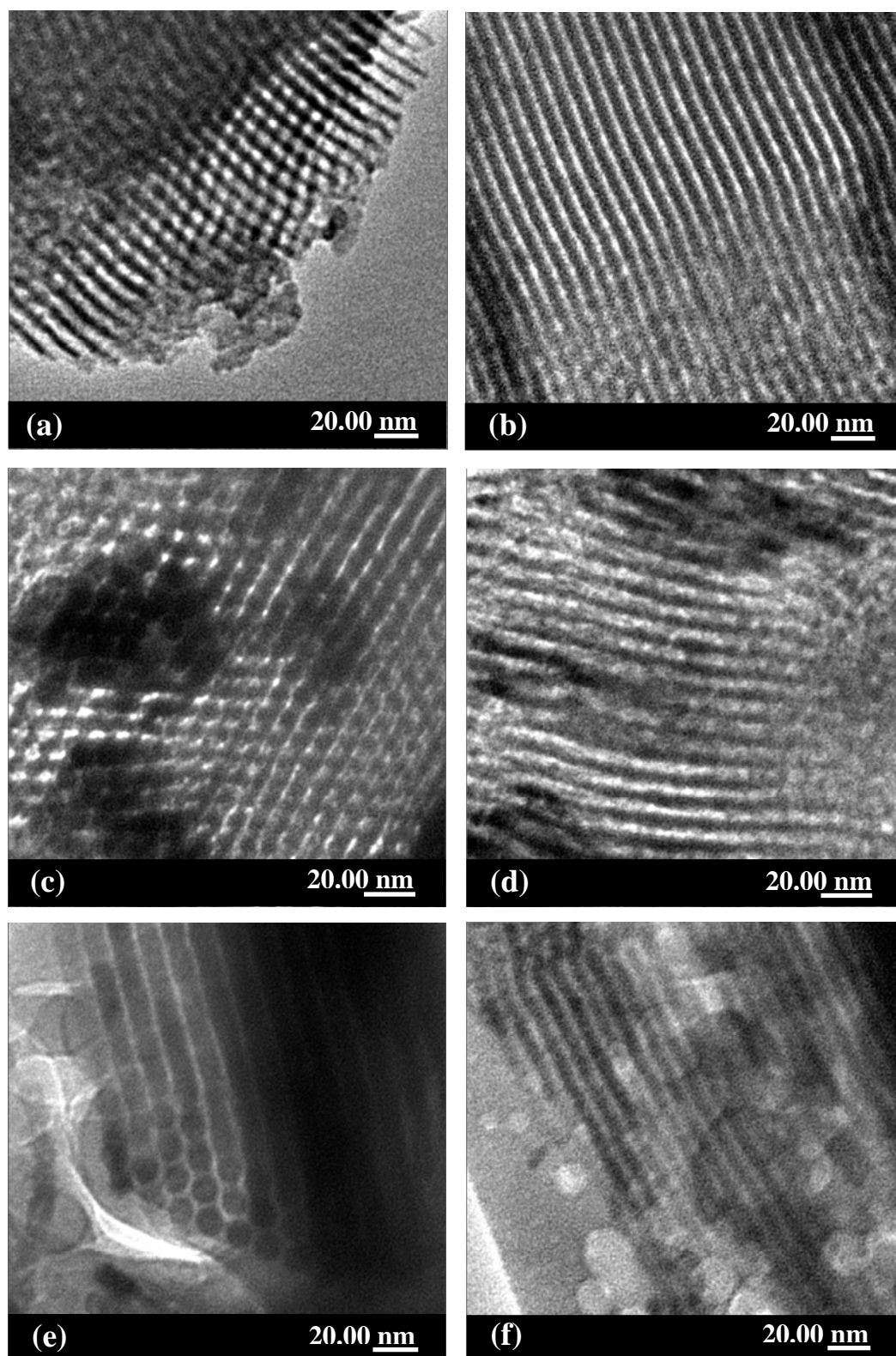


**Figure 23** TEM images along the direction perpendicular and parallel to the c axis of (a) and (b) 0.1Li-20Co/SBA-15 catalyst, (c) and (d) 0.3Na-20Co/SBA-15 catalyst and (e) and (f) 0.5K-20Co/SBA-15 catalyst.

### Thermal Reaction Investigation

Before investigating the performance of catalysts for two-stage synthesis of liquid fuels from carbon dioxide and methane, thermal reactions with temperature variations over sand as an inert packing material were investigated. The conversion and selectivity of products were identified.

In the first-stage reforming reactor, the conversion of carbon dioxide and methane to synthesis gas was investigated at the temperature range of 500-750 °C. The other operating conditions were fixed as follows: CH<sub>4</sub>/CO<sub>2</sub> molar ratio of 1, total gas pressure of 10 atm and total flow rate of 50 ml/min (NTP). The results of carbon dioxide and methane conversions for thermal reaction with temperature variations in the first-stage reforming reactor are shown in Figure 24.

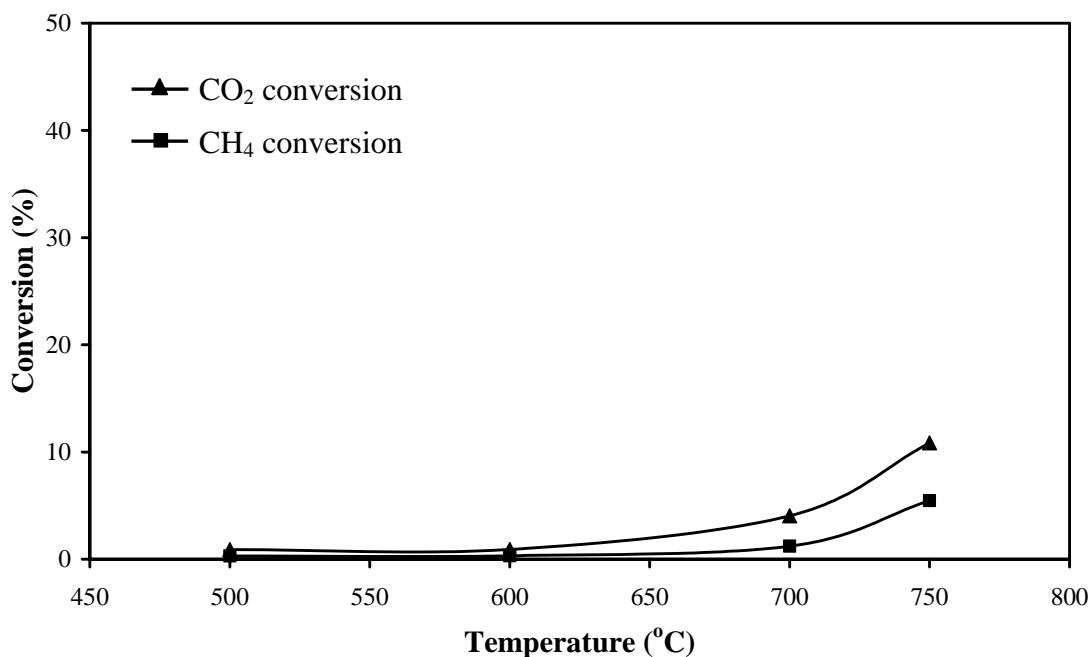
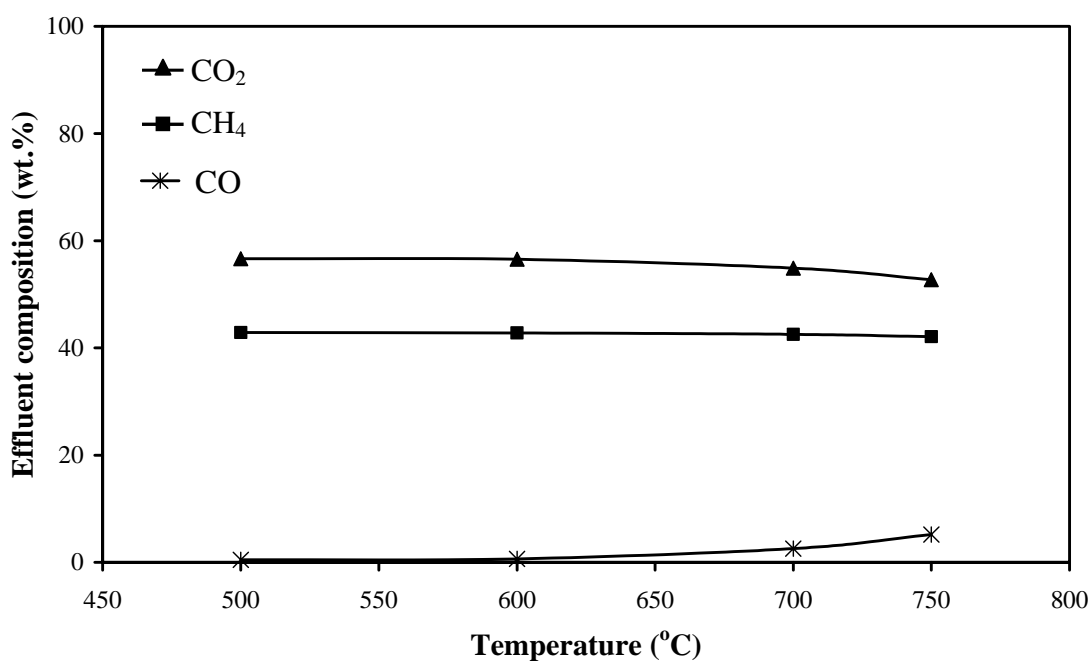


Figure 24 Effect of temperature on the CO<sub>2</sub> and CH<sub>4</sub> conversions in the first-stage reforming reactor packed with sand.

It can be seen from Figure 24 that  $\text{CO}_2$  and  $\text{CH}_4$  conversions on sand in a first-stage reforming reactor were slightly increased with increasing the temperature.  $\text{CO}_2$  conversions and  $\text{CH}_4$  conversions increase to 12.1 times and 18.3 times when the temperature is increased from 500 to 750 °C. It was implied that without catalyst or with thermal reaction only, the conversion of carbon dioxide reforming of methane is quite low and almost the same at the temperature range of 500-750 °C.

Effluent compositions with temperature variations in the first-stage reforming reactor are shown in Figure 25.



**Figure 25** Effect of temperature on the effluent compositions in the first-stage reforming reactor packed with sand.

Regarding the effluent composition of the outlet gaseous from a first-stage reforming reactor as shown in Figure 25, it was found that carbon monoxide occur as a main product.  $\text{CO}$  concentration in the effluent was increased while increasing temperature, while  $\text{CH}_4$  and  $\text{CO}_2$  concentration in the effluent were decreased while

increasing temperature. CO concentrations are 0.5, 0.6, 2.6 and 5.2 wt.% at 500, 600, 700 and 750 °C, respectively.

In the second-stage FT reactor, the conversion of synthesis gas to hydrocarbon products on sand as an inert packing material was also investigated at the temperature of 200-280 °C. The other operating conditions were fixed as follows: CH<sub>4</sub>/CO<sub>2</sub> molar ratio of 1, total gas pressure of 10 atm and total flow rate of 50 ml/min (NTP). The result of conversion and selectivity with temperature variations in the second-stage FT reactor are shown in Figure 26.

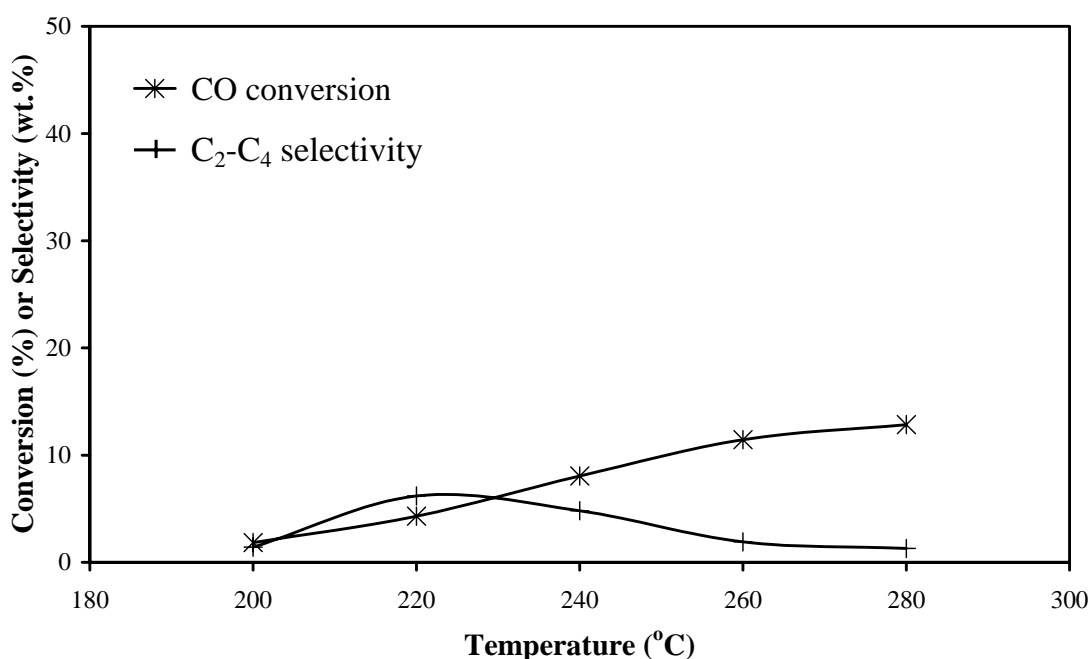


**Figure 26** Effect of temperature on the CO conversion and hydrocarbon selectivity in the second-stage FT reactor packed with sand.

From Figure 26, it can be seen that CO conversion on sand as an inert bed in a second-stage FT reactor gradually increases with increasing temperature. CO conversions are 1.8 % at 200 °C and 12.9 % at 280 °C. C<sub>2</sub>-C<sub>4</sub> gaseous hydrocarbons are produced from synthesis gas. The C<sub>2</sub>-C<sub>4</sub> selectivities obtained in the temperature

range of 200-280 °C are gradually decreased from 6.6 wt.% to 3.8 wt.% at the temperature of 220 and 280 °C, respectively.

Effluent composition and hydrocarbon selectivity obtained from the second-stage FT reactor operated at various temperatures are shown in Figures 27 and 28, respectively.

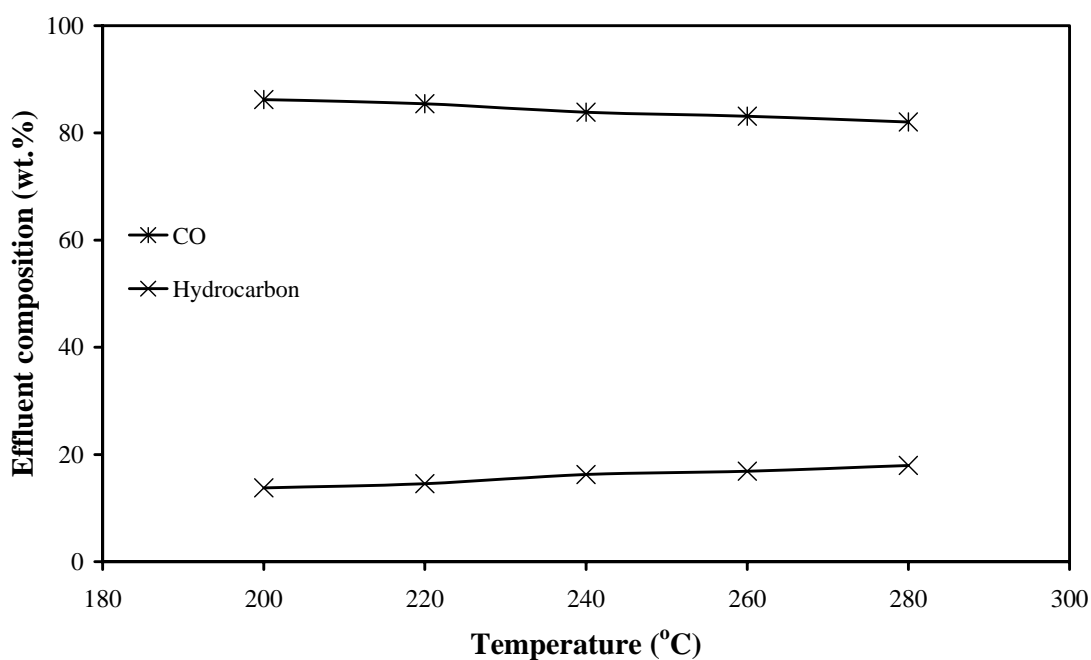


**Figure 27** Effect of temperature on the effluent composition in the second-stage FT reactor packed with sand.

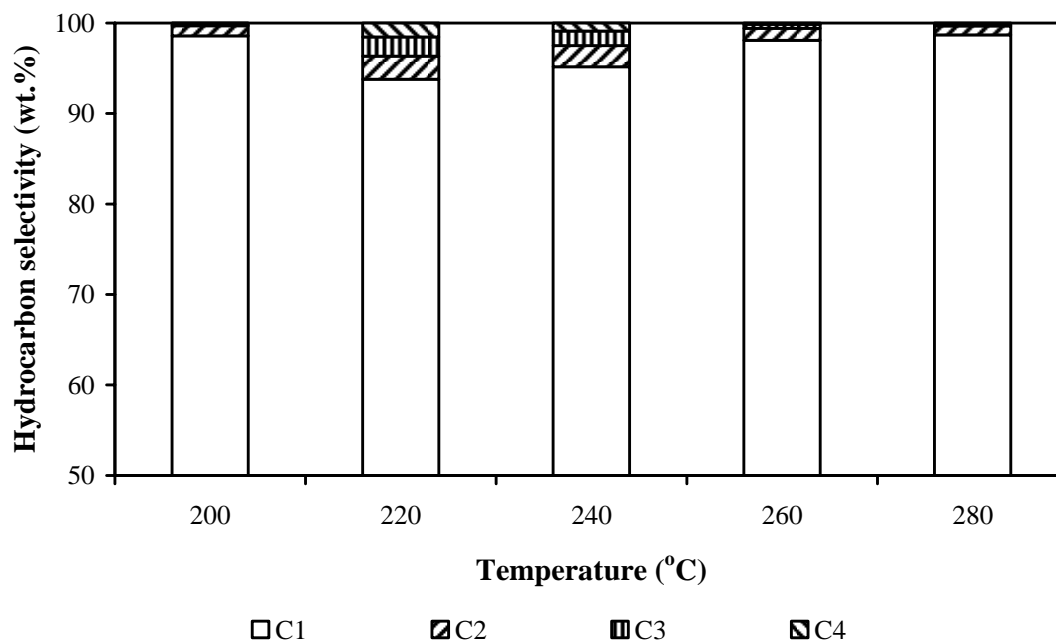


**Figure 28** Effect of temperature on hydrocarbon selectivity in the second-stage FT reactor packed with sand.

Regarding the effluent composition from Figure 27, it was found that the concentration of total gaseous hydrocarbons, mainly methane in the effluent almost decreases with increasing temperature while CO concentration decreases with increasing temperature.

From Figure 28, it was observed that C<sub>1</sub>-C<sub>4</sub> gaseous hydrocarbons, mainly methane, are produced from synthesis gas. Few higher hydrocarbon products can be produced from synthesis gas via thermal reaction.

From the experimental results the hydrocarbon products are proposed to be occurred from the decomposition of H<sub>2</sub> to H adatoms and consecutive insertion of H adatoms to weakly bond between C and O via FT synthesis as shown in Equation 23.



Where  $m$  is the number of hydrogen atoms per carbon and  $n$  is the average length of hydrocarbon chain.

### **Catalytic Reaction Investigation**

The catalytic performance of metal-supported catalysts for two-stage synthesis of liquid fuels from carbon dioxide and methane was investigated in series as follows: 1) the conversion of carbon dioxide and methane to synthesis gas on  $\text{Al}_2\text{O}_3$  and  $5\text{Ni}/\text{Al}_2\text{O}_3$  catalysts in the first-stage reforming reactor 2) catalytic performances of cobalt-supported catalysts and cobalt-supported catalysts with metal promoters in sequence for the conversion of synthesis gas to hydrocarbon products in the second-stage FT reactor.

#### **1. Conversion of Carbon Dioxide and Methane to Synthesis Gas**

$\text{Ni}/\text{Al}_2\text{O}_3$  catalyst was reported as a promising catalyst in terms of conversion and selectivity for carbon dioxide and methane conversions to synthesis gas. Ferreira-aparicio *et al.* (1998) found that 5 %  $\text{Ni}/\text{Al}_2\text{O}_3$  catalyst showed higher activity and stability than 5 %  $\text{Co}/\text{Al}_2\text{O}_3$ , 1 %  $\text{Ni}/\text{SiO}_2$  and 1 %  $\text{Co}/\text{SiO}_2$  catalysts in the temperature range of 400-750 °C for methane reforming with carbon dioxide reaction. Moreover, Lu and Wang (1999) found that 5 wt.% nickel loading on alumina exhibited higher conversion with lower deactivation than other loadings varying from 2 to 20 wt.% nickel for methane reforming with carbon dioxide reaction. Thus, in this part, 5 %  $\text{Ni}/\text{Al}_2\text{O}_3$  catalyst was selected to use for the conversion of carbon dioxide and methane to synthesis gas.

##### **1.1 Catalytic Performance of $\text{Al}_2\text{O}_3$ and $\text{Ni}/\text{Al}_2\text{O}_3$ Catalysts**

In the first-stage reforming reactor, the conversion of carbon dioxide and methane to synthesis gas was performed to determine the conversion of  $\text{Al}_2\text{O}_3$  and  $5\text{Ni}/\text{Al}_2\text{O}_3$  catalysts at the temperature of 500-750 °C. The other operating conditions were fixed as follows:  $\text{CH}_4/\text{CO}_2$  molar ratio of 1, total gas pressure of 10 atm and total

flow rate of 50 ml/min (NTP). The results of CO<sub>2</sub> and CH<sub>4</sub> conversions on Al<sub>2</sub>O<sub>3</sub> support and 5Ni/Al<sub>2</sub>O<sub>3</sub> catalyst at various temperatures in the first-stage reforming reactor are shown in Figure 29.

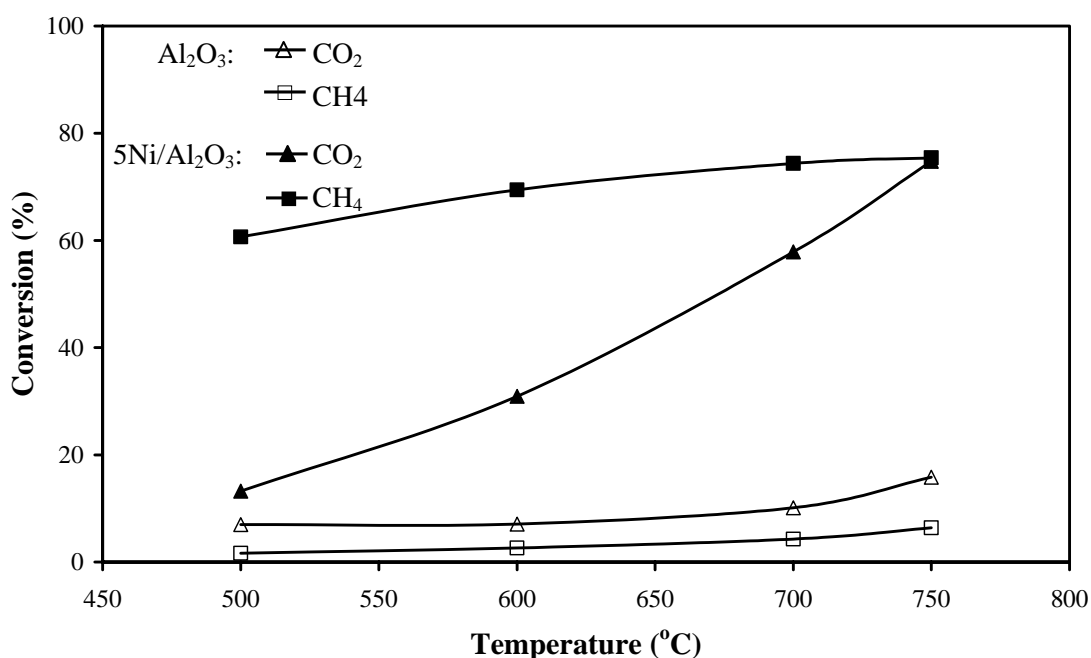


**Figure 29** Effect of temperature on CO<sub>2</sub> and CH<sub>4</sub> conversions of Al<sub>2</sub>O<sub>3</sub> and 5Ni/Al<sub>2</sub>O<sub>3</sub> catalyst in the first-stage reforming reactor.

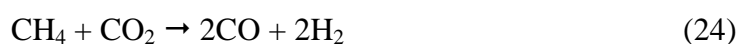
From Figure 29, it can be seen that CO<sub>2</sub> and CH<sub>4</sub> conversions of Al<sub>2</sub>O<sub>3</sub> and 5Ni/Al<sub>2</sub>O<sub>3</sub> catalyst increase with increasing temperature. Comparing between Al<sub>2</sub>O<sub>3</sub> support and 5Ni/Al<sub>2</sub>O<sub>3</sub> catalyst, it was found that 5Ni/Al<sub>2</sub>O<sub>3</sub> catalyst shows higher activity than Al<sub>2</sub>O<sub>3</sub> support at the temperature of 500-750 °C. Moreover, CO<sub>2</sub> conversion of 5Ni/Al<sub>2</sub>O<sub>3</sub> catalyst is 4.7 times higher than that of Al<sub>2</sub>O<sub>3</sub> support and 6.7 times higher than that of sand (without catalyst or thermal reaction) at the temperature of 750 °C. On 5Ni/Al<sub>2</sub>O<sub>3</sub> catalyst, the highest CO<sub>2</sub> conversion of 75 % and CH<sub>4</sub> conversion of 76 % are achieved at the temperature of 750 °C. For this reaction, lower pressure is favored for higher conversion (Fujimoto *et al.*, 1992). However, elevated pressure of 10 atm is performed since this reaction should be combined with the following reaction of FT synthesis. These conversion results are



quite similar to the results of Lu and Wang (1999) who reported that CH<sub>4</sub> and CO<sub>2</sub> conversions of Ni/Al<sub>2</sub>O<sub>3</sub> catalyst were 84 % and 86 %, respectively at temperature of 700 °C and total gas pressure of 1 atm. For the conversion of carbon dioxide and methane to synthesis gas on 5Ni/Al<sub>2</sub>O<sub>3</sub> catalyst at the CH<sub>4</sub>/CO<sub>2</sub> mole ratio of 1, temperature of 750 °C, total gas pressure of 10 atm and total flow rate of 50 ml/min (NTP), the synthesis gas produced by this reaction has a high CO content, which is effective for the FT synthesis of higher hydrocarbons. According to methane reforming with carbon dioxide reaction, this reaction favors higher temperature for synthesis gas production, thus operating at temperature range of 500-750 °C, synthesis gas yield can be increased.

### 1.2 Possible Mechanism for Synthesis Gas Formation on Ni/Al<sub>2</sub>O<sub>3</sub> Catalyst

In this part of catalytic performance of Al<sub>2</sub>O<sub>3</sub> and 5Ni/Al<sub>2</sub>O<sub>3</sub> catalysts, the conversion of carbon dioxide and methane to synthesis gas was performed. It was found that carbon monoxide occurs as a major product from carbon dioxide reforming of methane. Thus, it can be proposed that synthesis gas is produced via carbon dioxide reforming of methane reaction as shown in Equation 24.



Kroll *et al.* (1997) reported that the reaction between carbon dioxide and methane on active site surface (a) of reduced Ni/SiO<sub>2</sub> catalyst was feasibly started with methane activation. Alstrup and Tavares (1992) suggested that the activation of methane proceeded via Equations 25 to 28, producing short-lived CH<sub>x</sub> residues and at the tail-end of the chain, carbon has been formed.





Where (a) is active site.

$\text{CH}_x$  is the intermediate species of  $\text{CH}_4$ .

$\text{CH}_{x(a)}$  is the intermediate species of  $\text{CH}_4$  that adsorbed on active site.

$\text{H}_{(a)}$  is the hydrogen species that adsorbed on active site.

The dissociation of  $\text{CH}_4$  alone is generally very limit on the reduced active metal surfaces, however this process can be enhanced by adsorbed O produced on the metal surface via carbon dioxide activation as was reported by Kroll *et al.* (1997). Wang and Au (1997), and Edwards and Maitra (1995) gave a similar suggestion for the possible carbon dioxide activation which was proposed as follows:

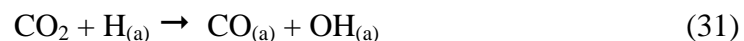


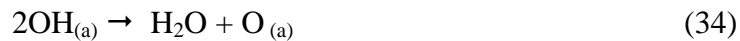
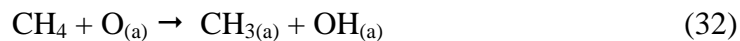
Where  $\text{CO}_{(a)}$  is the carbon dioxide species that adsorbed on active site.

$\text{O}_{(a)}$  is the oxygen species that adsorbed on active site.

$\text{C}_{(a)}$  is the carbon species that adsorbed on active site.

In addition, Edwards and Maitra (1995) also suggested that when both  $\text{CH}_4$  and  $\text{CO}_2$  were present, their self-decomposition were enhanced via Equations 31 to 34. Thus, the dissociation of  $\text{CH}_4$  was facilitated by adsorbed oxygen. The dissociation of  $\text{CO}_2$  was also promoted by adsorbed hydrogen and possibly by other  $\text{CH}_x$  residues. It should be suggested that the desired reforming reaction products and the following reactions also need to be considered:

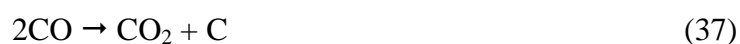




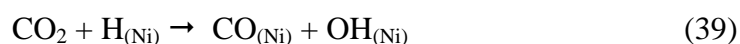
Equation 34 revealed the formation of undesired H<sub>2</sub>O which then competed with CO<sub>2</sub> for subsequent reactions with carbon formed by the dissociation of CH<sub>4</sub>. Furthermore, steam was always observed via the reverse water gas-shift (RWGS) and occurred as a side reaction for methane reforming with carbon dioxide as shown in Equation 35.



Moreover, from this experiment it was found that 5Ni/Al<sub>2</sub>O<sub>3</sub> catalyst is deactivated by carbon formation which is occurred as proposed in Equations 36 and 37.



Therefore, in this experiment we can conclude that the overall reactions for carbon dioxide reforming of methane occur in parallel and series with other competing reactions (Equations 25-37). The simplified reaction mechanism of carbon dioxide reforming of methane on Ni/Al<sub>2</sub>O<sub>3</sub> catalyst can be proposed as follows:





Where (Ni) is nickel active site

From Equations 37-39, CH<sub>4</sub> activation is occurred on the Ni active site surface to yield CH<sub>x</sub> species and hydrogen. CO<sub>2</sub> activation and H-promoted CO<sub>2</sub> dissociation are occurred on the Ni active site surface. After that CH<sub>x</sub> species then react with O species originated from CO<sub>2</sub> activation to yield intermediate CH<sub>x</sub>O species and decompose on the Ni active site surface to yield H<sub>2</sub> and CO.

## **2. Conversion of Synthesis Gas to Liquid Hydrocarbon Products**

The reaction and product gas mixtures from carbon dioxide reforming of methane reaction on 5Ni/Al<sub>2</sub>O<sub>3</sub> catalyst at the CH<sub>4</sub>/CO<sub>2</sub> molar ratio of 1, temperature of 750 °C, total gas pressure of 10 atm and total flow rate of 50 ml/min (NTP) in the first-stage reforming reactor were directly introduced into the second-stage FT reactor. It was found that cobalt-supported catalysts show high activity and selectivity for FT synthesis. Mesoporous silica materials are well-known common support for cobalt catalyst in the research regarding the larger hydrocarbon synthesis. SBA-15 mesoporous silica is selected to use as the support for cobalt catalyst because of their large, uniform pore size and structure, and high surface area. Therefore, it is expected that this support can improve both activity and selectivity of liquid fuels production on the cobalt-supported catalysts. Thus, in this part, conversions of synthesis gas to hydrocarbon products in the range of liquid fuels on catalyst support (SBA-15 mesoporous silica support), cobalt-supported catalysts (10Co/SBA-15, 20Co/SBA-15, 30Co/SBA-15) and cobalt-supported catalysts with metal promoters (0.1Li-20Co/ SBA-15, 0.3Na-20Co/SBA-15 and 0.5K-20Co/SBA-15 catalysts) were investigated.

## 2.1 Catalytic Performance of Catalyst Support and Cobalt-Supported Catalysts

In the second-stage FT reactor, synthesis gas conversion to hydrocarbon products in the range of liquid fuels was performed and the catalytic performance of SBA-15 mesoporous silica support, 10Co/SBA-15, 20Co/SBA-15 and 30Co/SBA-15 catalysts with the temperature range of 200-280 °C was considered to determine the effect of cobalt loading amounts on CO conversion and hydrocarbon selectivity. The operating conditions were fixed as follows: H<sub>2</sub>/CO molar ratio of 1, total gas pressure of 10 atm and total flow rate of 50 ml/min (NTP). The results of CO conversion and hydrocarbon selectivity with temperature variations on SBA-15 mesoporous silica support and 10Co/SBA-15, 20Co/SBA-15 and 30Co/SBA-15 catalysts in the second-stage FT reactor are shown in Figures 30-34, respectively.

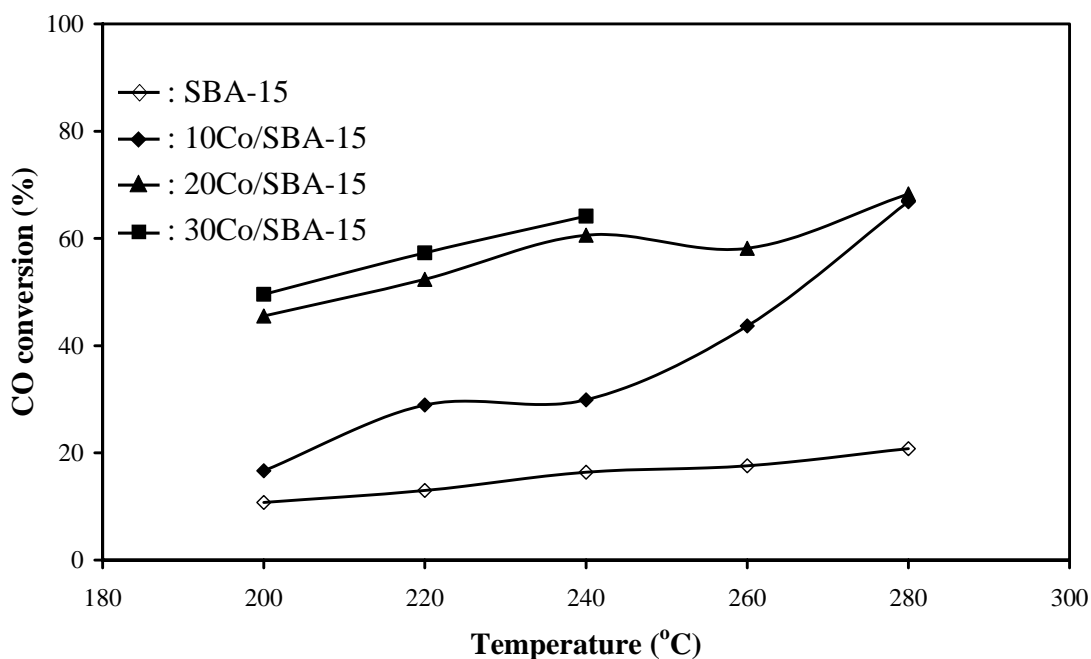


**Figure 30** Effect of temperature on CO conversion over SBA-15 support, 10Co/ SBA-15, 20Co/SBA-15 and 30Co/SBA-15 catalysts in the second-stage FT reactor.

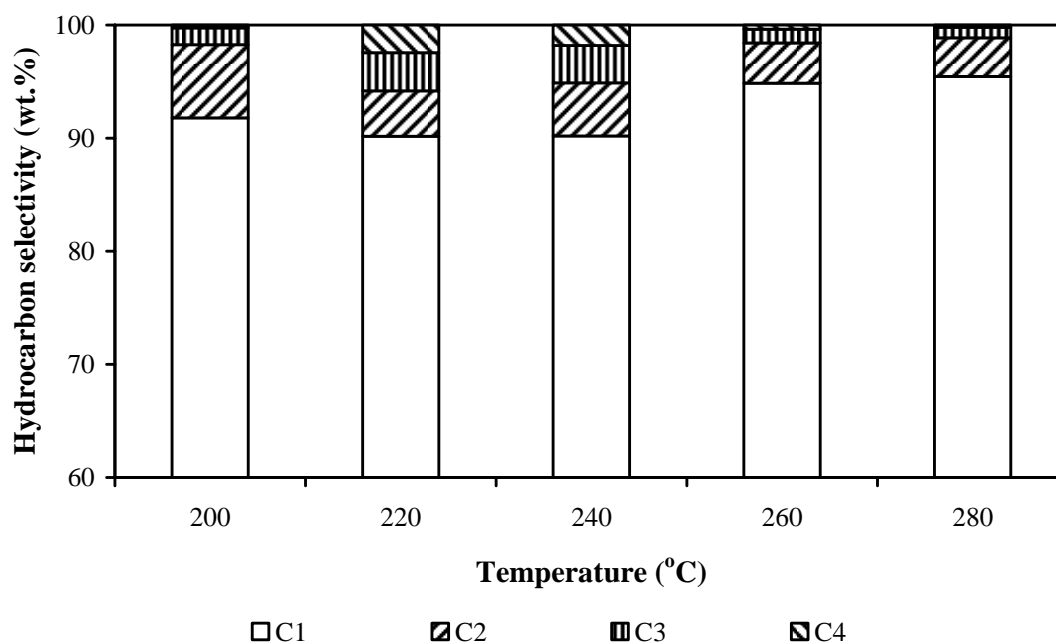


Figure 31 Effect of temperature on hydrocarbon selectivity over SBA-15 support in the second-stage FT reactor.

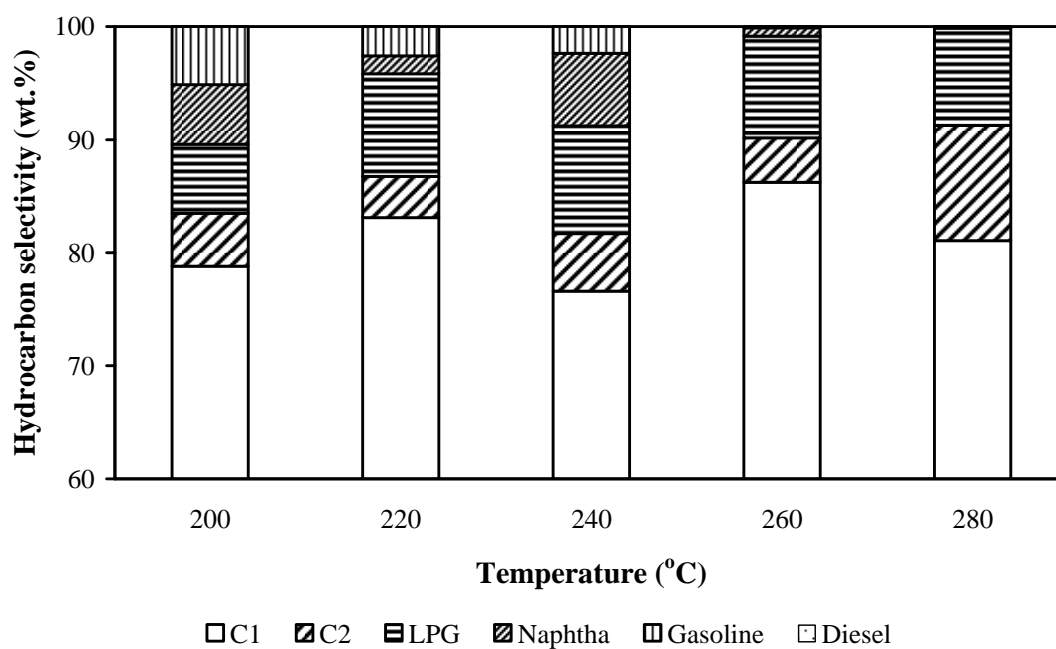
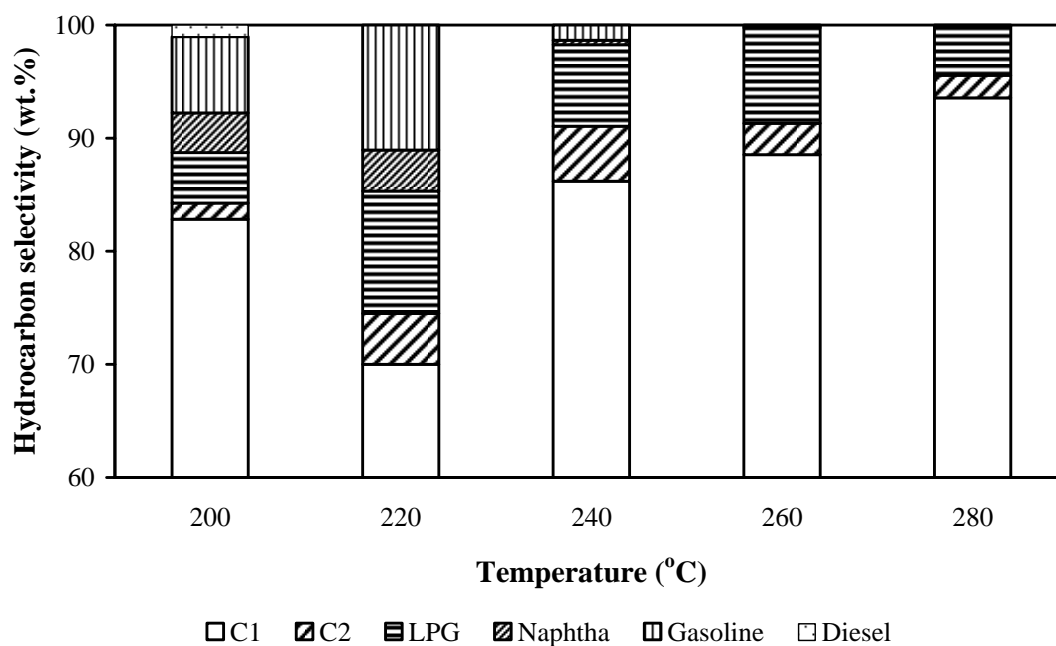
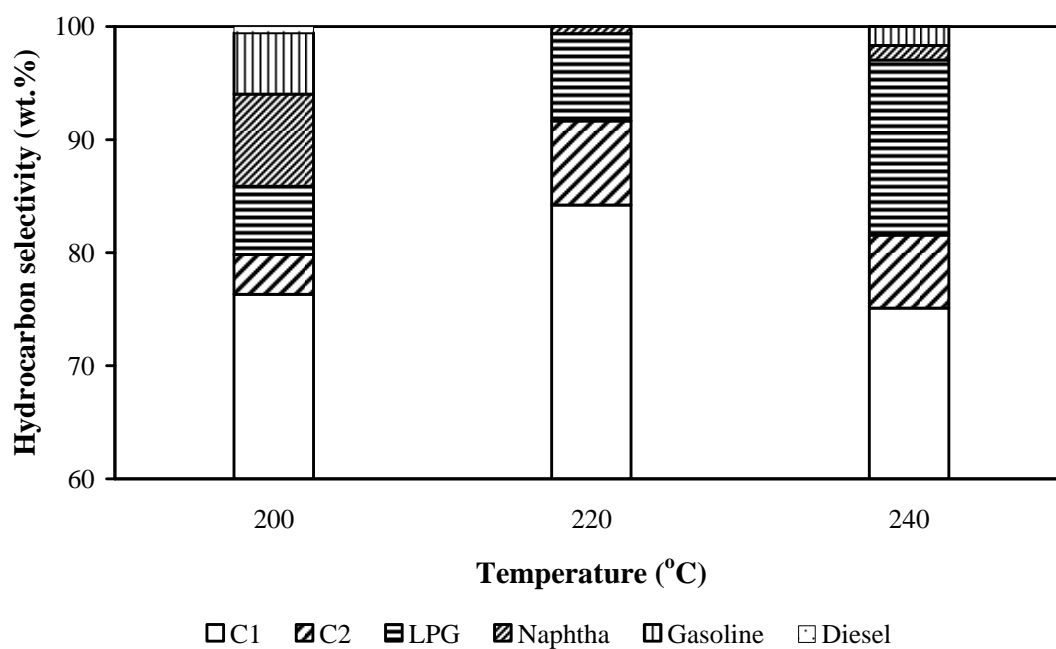


Figure 32 Effect of temperature on hydrocarbon selectivity over 10Co/SBA-15 catalyst in the second-stage FT reactor.



**Figure 33** Effect of temperature on hydrocarbon selectivity over 20Co/SBA-15 catalyst in the second-stage FT reactor.



**Figure 34** Effect of temperature on hydrocarbon selectivity over 30Co/SBA-15 catalyst in the second-stage FT reactor.

From Figure 30, CO conversions over SBA-15 mesoporous silica support, 10Co/SBA-15, 20Co/SBA-15 and 30Co/SBA-15 catalysts increase with the increasing temperature. CO conversions on SBA-15 mesoporous silica support are 10.8, 13.0, 16.4, 17.6 and 20.8 % at the temperature range of 200-280 °C. With 10Co/SBA-15 catalyst the CO conversion increases from 16.8 % to 66.8% when increasing temperature in the range of 200-280 °C, respectively. For 20Co/SBA-15 catalyst, CO conversions are quite higher than those of with 10Co/SBA-15 catalyst at the same reaction temperature. When the amounts of cobalt loading are increased to 30 wt.% for 30Co/SBA-15 catalyst, CO conversions are 49.6, 57.3 and 64.2 % at the temperature of 200, 220 and 240 °C, respectively. It can be clearly seen that CO conversions are increased with increasing both the reaction temperature and amounts of cobalt loading. The similar trend of cobalt loading effect was mentioned by Martínez et al. (2003) who studied the effect of cobalt loading (10-40 wt.%) on the physico-chemical and catalytic properties of mesoporous Co/SBA-15 catalysts for the FT reaction at 220 °C. They found that CO conversions were increased from 13.2-33.1 % with increasing amounts of cobalt loading from 10-30 wt.%, respectively.

As shown in Figure 31, only C<sub>1</sub>-C<sub>4</sub> gaseous hydrocarbons, mainly methane, are produced from synthesis gas on SBA-15 mesoporous silica support. Interestingly, not only C<sub>1</sub>-C<sub>4</sub> gaseous hydrocarbons but also C<sub>5+</sub> liquid hydrocarbons are synthesized on cobalt-supported catalysts. The selectivities (as weight percent) to the different FT synthesis products obtained from 10Co/SBA-15, 20Co/SBA-15 and 30Co/SBA-15 catalysts are presented in Figures 32-34, respectively. As observed with 10Co/SBA-15 catalyst in Figure 32, hydrocarbon products ranging from C<sub>1</sub>-C<sub>10</sub> are produced and the largest hydrocarbon (in this case, C<sub>10</sub>) is obtained at 200 °C and 240 °C. C<sub>1</sub> and C<sub>2</sub> selectivities are slightly increased with increasing temperature, while the selectivities of naphtha and gasoline range hydrocarbons are slightly decreased. Moreover, LPG is almost not changed with the temperature range of 220-280 °C.

As shown in Figure 33, the hydrocarbon products of 20Co/SBA-15 catalyst are rather similar to that of 10Co/SBA-15 catalyst, but the largest



hydrocarbon product (in this case,  $C_{15}$ ) is found at only 200 °C. Furthermore,  $C_1$  selectivity slightly increases with the increasing temperature. In contrast,  $C_2$ , LPG, naphtha and gasoline selectivities slightly decrease with increasing temperature.

For 30Co/SBA-15 catalyst, the hydrocarbon products are rather similar to that of 10Co/SBA-15 catalyst, especially 20Co/SBA-15 catalyst, the largest hydrocarbon product (in this case,  $C_{15}$ ) is found at only 200 °C as shown in Figure 34.  $C_1$  and  $C_2$  selectivities are not significantly changed with increasing temperature while LPG selectivity slightly increases with the increase of temperature. On the other hand, the selectivities of naphtha and gasoline are gradually decreased with increasing temperature. Like 20Co/SBA-15 catalyst, diesel is found only at 200 °C.

Although the highest CO conversion of 10Co/SBA-15 and 20Co/SBA-15 catalysts and 30Co/SBA-15 catalyst are obtained at the temperature of 280 °C and 240 °C, however as our preferable products, the highest  $C_{5+}$  selectivity is obtained at the temperature range of 200-220 °C. From Figures 32-34, it can be clearly observed that liquid fuels selectivities are slightly decreased with increasing catalytic temperatures, especially hydrocarbon products in the range of diesel of which prefer to occur only at 200 °C.

Since FT synthesis is the reaction of carbon monoxide and hydrogen to produce hydrocarbons and oxygenate products, Schulz (1999) revealed the short history and present trends of Fischer-Tropsch synthesis and suggested that FT chain growth in a general way, may be visualized as a repeated reaction sequence in which hydrogen atoms are added to carbon and oxygen, the C-O bond is split and a new C-C bond is formed. Because of the strongly exothermic reaction of FT synthesis (Schulz, 1999) and also that of  $\Delta G^\circ < 0$  kJ/mol at temperature below 350 °C (Wender, 1996), the FT chain growth prefers to occur at lower temperature as of the exothermic nature of the FT reaction. Chain initiation of hydrocarbon is decreased with the increase of catalytic temperatures. Therefore, it requires a lower temperature for thermodynamics of heavy hydrocarbon production. Our result is good agreement with that of Fujimoto *et al.* (1992) who studied the synthesis of liquid hydrocarbons under pressurized

conditions. They found that cobalt catalyst was quite sensitive to reaction temperature with respect to both activity and selectivity, while the products selectivity shifted to light hydrocarbons at higher temperature. They also reported that the CO conversion was increased with increasing reaction temperature; this result is consistent with that of Calleja *et al.* (1995) who studied the effect of process variables on the activity of a Co/HZSM-5 zeolite bifunctional catalyst for the conversion of synthesis gas to hydrocarbons. They found that the light hydrocarbons (mainly methane) favored higher temperatures in the range of 240-320 °C and heavier hydrocarbons, mainly C<sub>6+</sub>, were more sensitive to temperature, undergoing cracking and dealkylation reactions that become increasingly important with increasing temperature. Therefore, it can be concluded that the catalytic temperature is the essential factor to manipulate the selectivity of liquid fuels.

The effect of cobalt loading amounts on liquid fuels selectivities were considered at two temperature ranges. At the temperature range of 200-220 °C, when amounts of cobalt loading increased from 10 to 20 wt.%, the liquid fuels selectivities increase from 10.4 to 11.3 % and 4.2 to 14.7 % at 200 and 220 °C, respectively and the liquid fuels selectivities increased from 11.3 % to 14.1 % when amounts of cobalt loading increased from 20 to 30 wt.% at 200 °C. As mentioned regarding the effect of temperature, it can be realized that this lower temperature range is suitable for promoting the FT reaction and the chain initiation. These results are similar to that of Calleja *et al.* (1995) who suggested that there was a balance between two trends: the hydrogenation reactions yielding C<sub>6+</sub> hydrocarbons and the optimum temperature approximately 200-220 °C. Iglesia *et al.* (1992) studied the effect of metal dispersion and support on FT synthesis rate and selectivity at conditions that favored for C<sub>5+</sub> hydrocarbons formation (200 °C, 20 atm, H<sub>2</sub>/CO = 2). They found that transport restrictions by a high site density with cobalt loading amounts within catalyst pellets increased the residence time and the readsorption probability of reactive olefins and led to higher C<sub>5+</sub> yields and more paraffinic products.

At the temperature range of 240-280 °C, when amounts of cobalt loading increase from 10 to 20 wt.%, the liquid fuels selectivities decrease from 8.8 to 1.7 %,

0.9 to 0.2 % and 0.2 to 0.1 % at 240, 260 and 280 °C, respectively. When amounts of cobalt loading increase from 20 to 30 wt.%, the liquid fuels selectivities slightly increase from 1.7 to 3.0 % at 240 °C. The alternate decrease of liquid fuels selectivities may be caused by the higher temperature that is not suitable for Fischer-Tropsch reaction. Although the amounts of cobalt loading was increased to 30 wt.%, the chain initiation is decreased with increasing amounts of cobalt loading at this temperature range. Liquid fuels selectivities of FT synthesis over cobalt supported catalysts reflect a complex interplay of catalytic temperatures and amounts of cobalt loading to readsorption and chain initiation of carbon atoms.

## **2.2 Catalytic Performance of Cobalt-Supported Catalysts with Metal Promoters**

From the previous part regarding the catalytic performance of supports and cobalt-supported catalysts, the largest hydrocarbon product in the range of diesel is found only at temperature of 200 °C and the maximum yield is observed with 30Co/SBA-15 catalysts. Therefore, the effect of metal promoter types was selected to investigate under these conditions. Thus, the catalytic performances of 0.1Li-20Co/SBA-15, 0.3Na-20Co/SBA-15 and 0.5K-20Co/SBA-15 at the temperature of 200 °C were performed to determine the effect of each metal promoter (Li,Na,K) on CO conversion and hydrocarbon selectivity. The other operating conditions were fixed as follows: H<sub>2</sub>/CO molar ratio of 1, total gas pressure of 10 atm and total flow rate of 50 ml/min (NTP). The results of CO conversion and hydrocarbon selectivity with the variations of metal promoters in the second-stage FT reactor are shown in Figures 35 and 36.

Notice that the amount of metal promoter was loaded on the 20Co/SBA-15 catalyst at the same molar basis, as the result when compared by weight basis the weight ratio of Li : Na : K was 1 : 3 : 5 and the obtain catalyst were then denoted as weight basis as follows: 0.1Li-20Co/SBA-15, 0.3Na-20Co/SBA-15 and 0.5K-20Co/SBA-15, respectively.

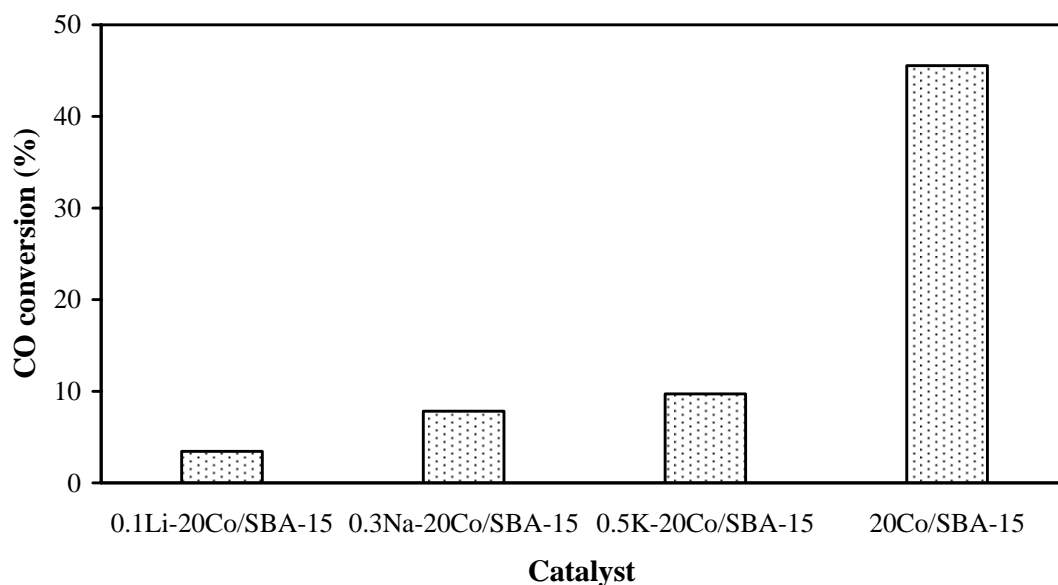


**Figure 35** Effect of metal promoter on CO conversion of 0.1Li-20Co/ SBA-15, 0.3Na-20Co/SBA-15 and 0.5K-20Co/SBA-15 catalysts in the second-stage FT reactor.

As shown in Figure 35, CO conversions of 0.1Li-20Co/SBA-15, 0.3Na-20Co/SBA-15 and 0.5K-20Co/SBA-15 catalysts are 3.5, 7.8 and 9.7 %, respectively. CO conversion was gradually increased with the increase of mass of the promoter from 0.1 wt.% Li, 0.3 wt.% Na and 0.5 wt.% K, respectively. However, it should be noted that the equal amount to 0.0045 mol% of each metal promoters were loaded on each cobalt-supported.

The effects of metal promoter types on the hydrocarbon selectivity of 0.1Li-20Co/SBA-15, 0.3Na-20Co/SBA-15 and 0.5K-20Co/SBA-15 catalysts are shown in Figure 36.

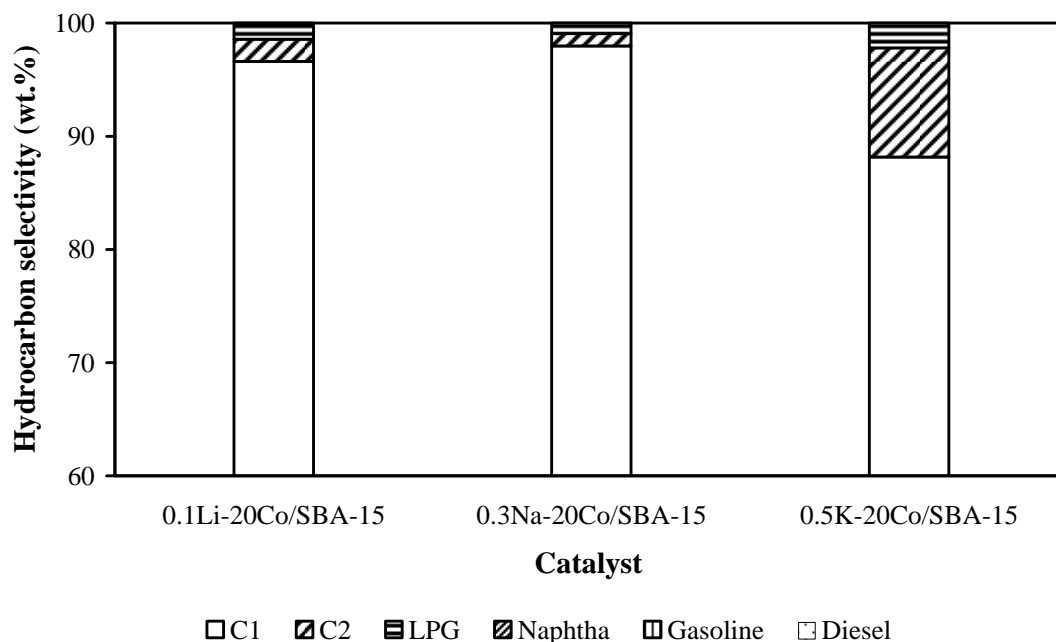


**Figure 36** Effect of metal promoter on hydrocarbon selectivity of 0.1Li-20Co/SBA-15, 0.3Na-20Co/SBA-15 and 0.5K-20Co/SBA-15 catalysts in the second-stage FT reactor.

From Figure 36, the effect of each metal promoter on hydrocarbon selectivity gave unsatisfied result when compare with 20Co/SBA-15 catalyst without metal promoter. Hydrocarbon products obtained with promoters are ranging from methane to LPG, and the largest hydrocarbon is  $C_4$  of which can be found in all conditions with our study. Methane is a main product for all cobalt-supported catalysts with metal promoters. Methane selectivities are 96.6, 98.0 and 88.2 wt.% for 0.1Li-20Co/SBA-15, 0.3Na-20Co/SBA-15 and 0.5K-20Co/SBA-15 catalysts, respectively. The highest  $C_2$  and LPG selectivities are 9.6 and 2.2 wt.% for 0.5K-20Co/SBA-15 catalysts. From this result, there are not significant effects of metal promoters on CO conversion and hydrocarbon selectivity, on the other hand, 20Co/SBA-15 catalyst promoted by potassium is of interesting that it can provide the higher  $C_2$  and LPG selectivities than that of 20Co/SBA-15 catalyst promoted by lithium or sodium.

From these results, the discussions about the promoter effects are presented as follows:

### **2.2.1 Effect of Lithium Promoter**

From Figure 36, methane, C<sub>2</sub> and LPG selectivities of 0.1Li-20Co/SBA-15 catalyst are 96.6, 2.0 and 1.3 %, respectively. Hydrocarbon products are produced ranging from methane to LPG, on the other hand, liquid fuels in the range of gasoline and diesel do not occurred on this catalyst. These results are similar to that of Ngantsoue-Hoc *et al.* (2002) who studied the impact of group I alkali metals on the activity of iron catalysts at medium pressure and at the same conversion levels, and they found that the relative impact of the alkali metal depends upon the conversion level. At low conversions of CO (< 40 %), quite similar to our result (< 10 %), lithium is nearly as effective as potassium on the catalytic activity but is the poorest promoter at high conversion levels. In the other point of view, they suggested that lithium should be considered as the inhibitor since it caused the decreased of the catalytic activity for CO conversion to the level below that of the unpromoted catalyst.

### **2.2.2 Effect of Sodium Promoter**

Methane, C<sub>2</sub> and LPG selectivities of 0.3Na-20Co/SBA-15 catalyst are 98.0, 1.1 and 0.9 %, respectively, as can be seen in Figure 36. Similar to the effect of lithium, hydrocarbon products are produced ranging from methane to LPG, however with this catalyst, liquid fuels in the range of gasoline and diesel can not occur. Xu *et al.* (1998) studied the hydrogenation of carbon dioxide over Na-Fe-Cu/zeolite composite catalysts and the effects of sodium on the catalytic activity at the condition of 200 °C and 20 atm. Xu *et al.* (1998) found that the addition of sodium at low concentration onto the catalyst caused the decrease of light hydrocarbons yield, of which significant decrease at higher levels of sodium addition.

### 2.2.3 Effect of Potassium Promoter

Almost similar to both the effect of lithium and sodium, hydrocarbon products are also produced ranging from methane to LPG. C<sub>2</sub> and LPG selectivities obtained in this case are higher than that of 0.1Li-20Co/SBA-15 and 0.3Na-20Co/SBA-15 catalysts. Methane, C<sub>2</sub> and LPG selectivities of 0.5K-20Co/SBA-15 catalyst are 88.2, 9.6 and 2.2 %, respectively. Li *et al.* (2001) studied the effects of potassium on the structural properties and the catalytic behavior of iron-based FTS catalysts, they concisely suggested that the addition of potassium inhibits the content of paraffin in FTS products. Ma *et al.* (2004) also studied the effects of cobalt loading and K, Ce, and Zr promoters on activities and selectivities of activated-carbon-supported cobalt (Co/AC) FTS catalysts under conditions of 240 °C, 24 atm and H<sub>2</sub>/CO ratio of 2 in a fixed-bed reactor. They found that the addition of potassium to the Co/AC catalyst significantly decreased the FTS activity and C<sub>2</sub>-C<sub>4</sub> selectivity because potassium acted as the inhibitor for FTS activity.

From Figure 36, the main products of 0.1Li-20Co/SBA-15, 0.3Na-20Co/SBA-15 and 0.5K-20Co/SBA-15 catalysts are methane, C<sub>2</sub> and LPG. From this result, potassium seems to be the best promoter when compared with lithium and sodium because it can promote the highest C<sub>2</sub> and LPG selectivities over 20Co/SBA-15 catalyst. Some reason was gave by Mirzaei et al. (2006), who studied the effect of difference supports (TiO<sub>2</sub>, SiO<sub>2</sub>, Al<sub>2</sub>O<sub>3</sub> and La<sub>2</sub>O<sub>3</sub>) and promoters (Li, Na, K Rb and Mg) on CO hydrogenation, suggested that the catalyst containing potassium promoter was more active and rather selective towards ethylene (C<sub>2</sub>) and propylene (C<sub>3</sub>) than the other promoted catalysts in the same alkaline group.

As shown in the results and mention above, the addition of alkaline promoters such as lithium, sodium and potassium onto the 20Co/SBA-15 catalyst negatively affects the hydrocarbon selectivity for the conversion of synthesis gas to liquid fuels. From the investigation of Praliaud *et al.* (1985) that studied the influence of the addition of alkaline promoters onto the catalyst on the kinetic parameters of various reactions and reported that alkali doping has been generally

interpreted in terms of electronic effect in which the electron-donating alkali additive may transfer electrons to the metallic phase and thus strengthen the bonds between metals and electron-acceptor molecules such as CO, N<sub>2</sub> while it may weaken the bonds between the metals and electron-donor elements such as hydrogen. Therefore, it is possible that the poor effect result of the addition of alkaline promoter attribute to the weakening of cobalt-hydrogen bond.

The alteration of CO conversion as a function of time on stream on 20Co/SBA catalyst at H<sub>2</sub>/CO molar ratio of 1, temperature of 200 °C, total gas pressure of 10 atm and total flow rate of 50 ml/min (NTP) is shown in Figure 37.

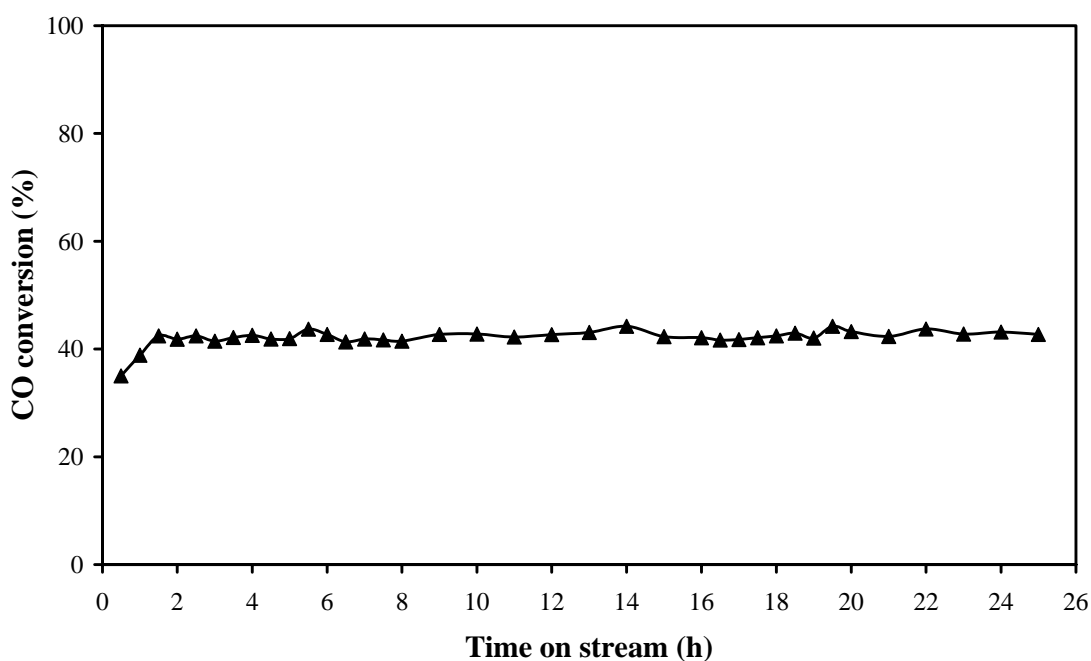


**Figure 37** The alteration of CO conversion as a function of time on stream of 20Co/SBA-15 catalyst in the second-stage FT reactor.

As shown in Figure 37, the CO conversion of 20Co/SBA-15 catalyst slightly increases in the first 2 h of reaction period. The CO conversion is quite constant during 25 h of reaction, it can be implied that 20Co/SBA-15 catalyst exhibits



a long-lived stability for liquid fuels synthesis during 25 h of catalytic performance test.

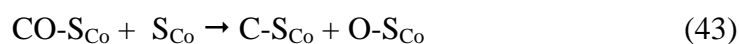
As of our finding, it can be concluded that SBA-15 mesoporous silica can be used as the support of cobalt metal catalyst for Fischer-Tropsch synthesis. These supports promote the dispersion of active metal phases as in good agreement with the result from TEM images. These improve the activity and selectivity of cobalt metal catalyst. Moreover, Co/SBA-15 mesoporous silica catalysts are promising catalysts for FT synthesis in the synthesis of liquid fuels from carbon dioxide and methane in the two-stage reactor.

### **2.3 Possible Mechanism of Fischer-Tropsch Reaction on Co/SBA-15 Catalysts**

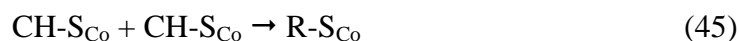
When reaction gas mixtures from the first-stage reforming reactor were introduced to the second-stage FT reactor, the reactions of these reactant gas mixtures were taken place over Co/SBA-15 catalyst. Due to the main products from the first-stage reforming reactor are carbon monoxide and hydrogen, the possible reaction which occurs in the second-stage FT reactor has been proposed. When the reaction gas was directly introduced into the second-stage FT reactor, the expected mechanism is started with the adsorption of CO and H<sub>2</sub> on the metal active site of cobalt as shown in Equations 41 and 42:



After that, the dissociation of CO on the site of cobalt metal is occurred as shown in Equation 43.



Then, the reaction between adsorbed carbon species and adsorbed hydrogen species is occurred and chain propagation is continued as the following equations:



Finally, the chain termination is occurred as Equation 46:



Where  $\text{S}_{\text{Co}}$  is cobalt active site.

$\text{C-S}_{\text{Co}}$  is adsorbed carbon on cobalt active site.

$\text{O-S}_{\text{Co}}$  is adsorbed oxygen on cobalt active site.

$\text{H-S}_{\text{Co}}$  is adsorbed hydrogen on cobalt active site.

$\text{R-S}_{\text{Co}}$  is adsorbed hydrocarbon products on cobalt active site.

Our expected mechanism of Fischer-Tropsch reaction over cobalt-supported catalyst with the mechanism of the other researchers has been revealed. Overett *et al.* (2000) suggested that the Fischer-Tropsch reaction yielded predominantly straight chain hydrocarbons ( $\alpha$ -olefins and alkanes) and it is agree in general that the reaction may be concerned as a methylene polymerization reaction where the monomer unit ( $=\text{CH}_2$ ), is not initially present. The products are formed via hydrogenation of CO to generate the methylene monomer, initiation of chain growth, followed by chain propagation and chain termination steps. Wojciechowski *et al.* (1988) inferred that the adsorption of CO and  $\text{H}_2$  species on the catalyst surface resulting in the decomposition of  $\text{H}_2$  and CO to hydrogen adatoms, adsorbed C and O, respectively. Ponec *et al.* (1979) suggested the possible mechanism the dissociative adsorption of hydrogen proceeded on two free active sites as shown in Equation 47:



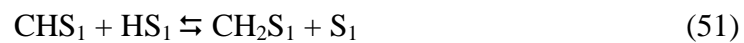
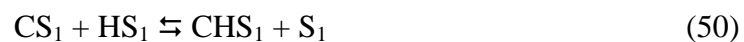
$S_1$  was denoted as a metal active site where hydrocarbons could be formed. Consequently, carbon monoxide adsorbed associatively on the other metal active site:



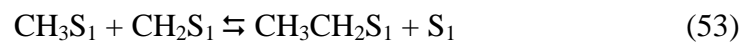
Adsorbed CO or  $COS_1$  could be dissociated in a second step:



As Wojciechowski *et al.* (1988) suggested that the monomer unit for oligomerisation was  $CH_2$ , and its formation on surface carbon reacted with adsorbed dissociated hydrogen as shown in Equations 50 and 51:

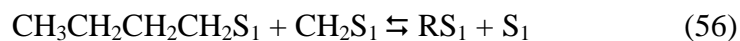


Brady *et al.* (1980) suggested a reaction between surface methylene and surface hydrogen to form a surface methyl, and that chain growth was propagated by the insertions of methylene into the metal-alkyl bond as shown in Equations 52 and 53, respectively:

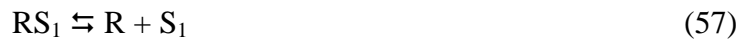


Termination of the chain growth gives  $\alpha$ -olefins or alkanes as shown in Equations 54-56:





After that, the weakly co-ordinated alkene desorbs from the surface yielding the product:



From Equation 57, R is the linear alkene or alkane. The reaction mechanism of FT synthesis is quite complex. The main reaction mechanism of FT synthesis consists of chain initiation, chain growth, and chain termination as sequences. It can be proposed that the possible reaction are consisted of chain initiation by  $\text{H}_2$  decomposition to form H adatoms, CO decomposition to form adsorbed C and O, and the surface reactions between theses species to form  $\text{CH}_x$  and OH, chain growth by the insertion of individual  $\text{CH}_2$  for oligomerization, and chain termination by desorption and H adatoms insertion.

## CONCLUSION

The effects of the catalytic temperature, the amount of cobalt loading and metal promoter types for liquid fuels synthesis from carbon dioxide and methane in the two-stage reactor have been investigated. Carbon dioxide reforming with methane was performed in the first-stage reforming reactor and the appropriate temperature to produce synthesis gas on 5Ni/Al<sub>2</sub>O<sub>3</sub> catalyst is 750 °C. At this temperature CO<sub>2</sub> conversion of 75 % and CH<sub>4</sub> conversion of 76 % are obtained.

The product gas mixtures from the first-stage reforming reactor were directly introduced to the second-stage FT reactor. It was found that CO conversion is strongly affected by both the catalytic temperature and the amount of cobalt loading. The maximum CO conversion of 68.3 % is obtained from 20Co/SBA-15 catalyst at 280 °C. The liquid fuels selectivity is strongly affected by the catalytic temperature. For Co/SBA-15 catalysts, gaseous hydrocarbon selectivities are slightly increased while liquid fuels selectivity in range of naphtha to diesel slightly decrease with the increasing temperature. The maximum liquid fuels selectivity of 14.1 % is obtained at 200 °C.

The selectivity to liquid fuels is also strongly affected by the amount of cobalt loading in the temperature range of 200-220 °C. Liquid fuels selectivity is slightly increased with the increase of cobalt loading amount. The highest liquid fuels selectivity of 14.1 % is obtained from 30Co/SBA-15 catalyst.

In the scope of our research, we found that metal promoters on 20Co/SBA-15 catalyst including lithium, sodium and potassium are not quite satisfied for the promotion of liquid fuels selectivity. The maximum CO conversion of 9.7 % is obtained from 0.5K-20Co/SBA-15 catalyst and the largest hydrocarbon products is C<sub>4</sub>. Lithium, sodium or potassium added on 20Co/SBA-15 catalyst should be viewed as reaction inhibitors since they decrease the activity for CO conversion and the production of liquid fuels in the FT synthesis stage.

Regarding the experimental products, the possible mechanisms for the conversion of carbon dioxide and methane to synthesis gas on Ni/Al<sub>2</sub>O<sub>3</sub> catalyst and the conversion of synthesis gas to hydrocarbon products on Co/SBA-15 catalysts have been proposed.

## LITERATURE CITED

- Alstrup, I. and M.T. Tavares 1992. The kinetics of carbon formation from  $\text{CH}_4 + \text{H}_2$  on a silica-supported nickel catalyst. **Journal of Catalysis** 135: 147-155.
- Asami, K., X. Li, K. Fujimoto, Y. Koyama, A. Sakurama, N. Kometani and Y. Yonezawa 2003.  $\text{CO}_2$  reforming of  $\text{CH}_4$  over ceria-supported metal catalysts. **Catalysis Today** 84: 27-31.
- Bechara, R., D. Balloy and D. Vanhove 2001. Catalytic properties of  $\text{Co}/\text{Al}_2\text{O}_3$  system for hydrocarbon synthesis. **Applied Catalysis A: General** 207: 343-353.
- Blyholder, G., D. Shihabi, W.V. Wyatt and R. Bartlett 1976. Adsorption and interaction of  $\text{C}_2\text{H}_4$ ,  $\text{H}_2$ ,  $\text{CO}$ , and organic acids on Fe, Co, and Ni. **Journal of Catalysis** 43: 122-130.
- Bradford, M.C.J. and M.A. Vannice 1999. The role of metal-support interactions in  $\text{CO}_2$  reforming of  $\text{CH}_4$ . **Catalysis Today** 50: 87-96.
- Buyevskaya, O.V., M. Rothaemel, H.W. Zanthoff and M. Baerns 1994. Transient studies on reaction steps in the oxidative coupling of methane over catalytic surfaces of  $\text{MgO}$  and  $\text{Sm}_2\text{O}_3$ . **Journal of Catalysis** 146: 346-357.
- Calleja, G., A. Lucas and R. Grieken 1995.  $\text{Co}/\text{HZSM-5}$  catalyst for syngas conversion: influence of process variables. **Fuel** 74: 445-451.
- Davis, B.H. 2001. Fischer-Tropsch synthesis: current mechanism and futuristic needs. **Fuel Processing Technolog** 71(1-3):157-166.

- Dissanayake, D., K.C.C. Kharas, J.H. Lunsford and M.P. Rosynek 1993. Catalytic partial oxidation of methane over Ba-Pb, Ba-Bi, and Ba-Sn perovskites. **Journal of Catalysis** 139: 652-663.
- Drago, R.S., K. Jurczyk, N. Kob, A. Bhattacharyya and J. Masin 1998. Partial oxidation of methane to syngas using NiO-supported catalysts. **Catalysis Letters** 51: 177-181.
- Edwards, J.H. and A.M. Maitra 1995. The chemistry of methane reforming with carbon dioxide and its current and potential applications. **Fuel Processing Technology** 42: 269-289.
- Elmasides, C. and X.E. Verykios 2001. Mechanistic study of partial oxidation of methane to synthesis gas over modified Ru/TiO<sub>2</sub> catalyst. **Journal of Catalysis** 203: 477-486.
- Erdohelyi, A., J. Cserenyi and F. Solymosi 1993. Activation of CH<sub>4</sub> and its reaction with CO<sub>2</sub> over supported Rh catalysts. **Journal of Catalysis** 141: 287-299.
- Fathi, M., F. Monnet, Y. Schuurman, A. Holmen and C. Mirodatos 2000. Reactive oxygen species on platinum gauzes during partial oxidation of methane into synthesis gas. **Journal of Catalysis** 190: 439-445.
- Ferreira-Aparicio, P., A. Guerrero-Ruiz and I. Rodríguez-Ramos 1998. Comparative study at low and medium reaction temperatures of syngas production by methane reforming with carbon dioxide over silica and alumina supported catalysts. **Applied Catalysis A: General** 170: 177-187.
- \_\_\_\_\_, I. Rodríguez-Ramos, J.A. Anderson and A. Guerrero-Ruiz 2000. Mechanistic aspects of the dry reforming of methane over ruthenium catalysts. **Applied Catalysis A: General** 202: 183-196.



- Fujimoto, K., K. Omata, T. Nozaki, O. Yamazaki and Y. Han 1992. Selective synthesis of liquid hydrocarbons from carbon dioxide and methane. **Energy Conversion and Management** 33: 529-536.
- Grenoble, D.C. 1978. The chemistry and catalysis of the water/toluene reaction. The role of support and kinetic analysis. **Journal of Catalysis** 51: 212-220.
- Hosseini, S.A., A. Taeb, F. Feyzi and F. Yaripour 2004. Fischer-Tropsch synthesis over Ru promoted Co/ $\gamma$ -Al<sub>2</sub>O<sub>3</sub> catalysts in a CSTR. **Catalysis Communications** 5: 137-143.
- Iglesia, E. 1997. Design, synthesis, and use of cobalt-based Fischer-Tropsch synthesis catalysts. **Applied Catalysis A: General** 161: 59-78.
- \_\_\_\_\_, S.L. Soled and R.A. Fiato 1992. Fischer-Tropsch synthesis on cobalt and ruthenium. Metal dispersion and support effects on reaction rate and selectivity. **Journal of Catalysis** 137: 212-224.
- Khodakov, A.Y., A. Griboval-Constant, R. Bechara and V.L. Zholobenko 2002. Pore size effects in Fischer-Tropsch synthesis over cobalt-supported mesoporous silicas. **Journal of Catalysis** 206: 230-241.
- \_\_\_\_\_, J. Lynch, D. Bazin, B. Rebours, N. Zanier, B. Moisson and P. Chaumette 1997. Reducibility of cobalt species in silica-supported Fischer-Tropsch catalysts. **Journal of Catalysis** 168: 16-25.
- \_\_\_\_\_, R. Bechara and A. Griboval-Constant 2003. Fischer-Tropsch synthesis over silica supported cobalt catalysts: mesoporous structure versus cobalt surface density. **Applied Catalysis A: General** 254: 273-288.

- Knottenbelt, C. 2002. Mossgas “gas-to-liquid” diesel fuels-an environmentally friendly option. **Catalysis Today** 71: 437-445.
- Kodama, T., T. Shimizu, K. Shimizu and Y. Kitayam 2001. Thermochemical methane reforming using  $\text{WO}_3$  as an oxidant below 1173 K by a solar furnace simulator. **Solar Energy** 71: 315-324.
- Kolbel, H. and K.D. Tillmetz 1974. Model studies of the interaction of CO and  $\text{H}_2$  on transition metals: II. On the role of chemisorption complexes in primary reactions. **Journal of Catalysis** 34: 307-316.
- Kroll, V.C.H., Y. Schuurman, P. Ferreira-Aparicio and C. Mirodatos 1997. Use of transient kinetics techniques for studying the methane reforming by carbon dioxide. **Catalysis Today** 38(1): 129-135.
- Lee, J., E. Lee, O. Joo and K. Jung 2004. Stabilization of  $\text{Ni}/\text{Al}_2\text{O}_3$  catalyst by Cu addition for  $\text{CO}_2$  reforming of methane. **Applied Catalysis A: General** 269: 1-6.
- Li, C., C. Yu and S. Shen 2000. Role of the surface state of  $\text{Ni}/\text{Al}_2\text{O}_3$  in partial oxidation of  $\text{CH}_4$ . **Catalysis Letters** 67: 139-145.
- Li, S., A. Li, S. Krishnamoorthy and E. Iglesia 2001. Effects of Zn, Cu, and K promoters on the structure and on the reduction, carburization, and catalytic behavior of iron-based Fischer-Tropsch synthesis catalysts. **Catalysis Letters** 77:21-29.
- Luo, M. and B.H. Davis 2003. Fischer-Tropsch synthesis: activation of low-alpha potassium promoted iron catalysts. **Fuel Processing Technology** 83(1-3): 49-65.

- Ma, W., Y. Ding and L. Lin 2004. Fischer-Tropsch synthesis over activated-carbon-supported cobalt catalysts: effect of Co loading and promoters on catalyst performance. **Industrial and Engineering Chemistry Research** 43: 2391-2398.
- Mallens, E.P.J., J.H.B. Hoebink and G.B. Marin 1997. The reaction mechanism of the partial oxidation of methane to synthesis gas: A transient kinetic study over rhodium and a comparison with platinum. **Journal of Catalysis** 167: 43-56.
- Mariana, M.V., M. Souza, D.A.G. Aranda and M. Schmal 2001. Reforming of methane with carbon dioxide over Pt/ZrO<sub>2</sub>/Al<sub>2</sub>O<sub>3</sub> catalysts. **Journal of Catalysis** 204: 498-511.
- Martínez, A., C. López, F. Márquez and I. Díaz 2003. Fischer-Tropsch synthesis of hydrocarbons over mesoporous Co/SBA-15 catalysts: the influence of metal loading, cobalt precursor, and promoters. **Journal of Catalysis** 220: 486-499.
- Mirzaei, A.A., R. Habibpour, M. Faizi and E. Kashi 2006. Characterization of iron-cobalt oxide catalysts: Effect of different supports and promoters upon the structure and morphology of precursors and catalysts. **Applied Catalysis A: General** 301: 272-283.
- Ngantsoue-Hoc, W., Y. Zhang, R.J. Brien, M. Luo and B.H. Davis 2002. Fischer-Tropsch synthesis: activity and selectivity for group I alkali promoted iron-based catalysts. **Applied Catalysis A: General** 236: 77-89.
- Ohtsuka, Y., Y. Takahashi, M. Noguchi, T. Arai, S. Takasaki, N. Tsubouchi and Y. Wang 2004. Novel utilization of mesoporous molecular sieves as supports of cobalt catalysts in Fischer-Tropsch synthesis. **Catalysis Today** 89: 419-429.

- Oklany, J.S., K. Hou and R. Hughes 1998. A simulative comparison of dense and microporous membrane reactors for the steam reforming of methane. **Applied Catalysis A: General** 170: 13-22.
- Overett, M.J., R.O. Hill and J.R. Moss 2000. Organometallic chemistry and surface science: mechanistic models for the Fischer-Tropsch synthesis. **Coordination Chemistry Reviews** 206: 581-605.
- Qin, D., J. Lapszewicz and X. Jiang 1996. Comparison of partial oxidation and steam- $\text{CO}_2$  mixed reforming of  $\text{CH}_4$  to syngas on MgO-supported metals. **Journal of Catalysis** 159: 140-149.
- Praliaud, H., P. Turlier, P. Moral, G. A. Martin and J. A. Dalmon 1985. Influence of the nature of the support on the reducibility and catalytic properties of nickel: evidence for a new type of metal support interaction. **Applied Catalysis** 19(2): 287-300.
- Richardson, J.T. and S.A. Paripatyadar 1990. Carbon dioxide reforming of methane with supported rhodium. **Applied Catalysis** 61: 293-309.
- Rostrup-Nielsen, 1994. Catalysis and large-scale conversion of natural gas. **Catalysis Today** 21: 257-267.
- \_\_\_\_\_. 1984. Catalytic steam reforming. **Catalysis Reviews - Science and Engineering** 5: 1-117.
- \_\_\_\_\_. 1973. Activity of nickel catalysts for steam reforming of hydrocarbons. **Journal of Catalysis** 31: 173-199.

- Ruckenstein, E., and Y.H. Hu 1995. Carbon dioxide reforming of methane over nickel/alkaline earth metal oxide catalysts. **Applied Catalysis A: General** 133(1): 149-161.
- Ruckenstein, E. and H.Y. Wang 2000. Carbon dioxide reforming of methane to synthesis gas over supported cobalt catalysts. **Applied Catalysis A: General** 204: 257-263.
- \_\_\_\_\_ and Y.H. Hu 1998. Combination of CO<sub>2</sub> reforming and partial oxidation of methane over NiO/MgO solid solution catalysts. **Industrial and Engineering Chemistry Research** 37: 1744-1747.
- Saib, A.M., M. Claeys and E.V. Steen 2002. Silica supported cobalt Fischer-Tropsch catalysts: effect of pore diameter of support. **Catalysis Today** 71: 395-402.
- Satterfield, C.N. 1991. **Heterogeneous catalysis in industrial practice**. 2nd ed. McGraw-Hill, Inc., Singapore.
- Schulz, H. 1999. Short history and present trends of Fischer-Tropsch synthesis. **Applied Catalysis A: General** 186: 3-12.
- Schuurman, Y., V.C.H. Kroll, P. Ferreira-Aparicio and C. Mirodatos 1997. Use of transient kinetics techniques for studying the methane reforming by carbon dioxide. **Catalysis Today** 38: 129-135
- Seok, S., S.H. Choi, E.D. Park, S.H. Han and J.S. Lee 2002. Mn-promoted Ni/Al<sub>2</sub>O<sub>3</sub> catalysts for stable carbon dioxide reforming of methane. **Journal of Catalysis** 209: 6-15.

- Mariana M., V.M. Souza, A. Donato, G. Aranda and M. Schmal 2001. Reforming of methane with carbon dioxide over Pt/ZrO<sub>2</sub>/Al<sub>2</sub>O<sub>3</sub> catalysts. **Journal of Catalysis** 204(2): 498-511
- Sun, S., N. Tsubaki and K. Fujimoto 2000. The reaction performances and characterization of Fischer-Tropsch synthesis Co/SiO<sub>2</sub> catalysts prepared from mixed cobalt salts. **Applied Catalysis A: General** 202: 121-131.
- Torniainen, P.M., X. Chu and L.D. Schmidt 1994. Comparison of monolith-supported metals for the direct oxidation of methane to syngas. **Journal of Catalysis** 146: 1-10.
- Tsipouriari, V.A. and X.E. Verykios 2001. Kinetic study of the catalytic reforming of methane with carbon dioxide to synthesis gas over Ni/La<sub>2</sub>O<sub>3</sub> catalyst. **Catalysis Today** 64: 83-90.
- \_\_\_\_\_, Z. Zhang and X.E. Verykios 1998. Catalytic partial oxidation of methane to synthesis gas over Ni-based Catalysts: I. Catalyst performance characteristics. **Journal of Catalysis** 179: 283-291.
- Tsubaki, N., S. Sun and K. Fujimoto 2001. Different functions of the noble metals added to cobalt catalysts for Fischer-Tropsch synthesis. **Journal of Catalysis** 199: 236-246.
- Turlier, P., H. Praliaud, P. Moral, G.A. Martin and J.A. Dalmon 1985. Influence of the nature of the support on the reducibility and catalytic properties of nickel: evidence for a new type of metal support interaction. **Applied Catalysis** 19: 287-300.

- Valentini, A., N.L.V. Carreno, L.F.D. Probst, P.N. Lisboa-Filho, W.H. Schreiner, E.R. Leite and E. Longo 2003. Role of vanadium in Ni/Al<sub>2</sub>O<sub>3</sub> catalysts for carbon dioxide reforming of methane. **Applied Catalysis A: General** 255: 211-220.
- Van der Laan, G.P. and A.C.M. Beenackers 1999. Hydrocarbon selectivity model for the gas-solid Fischer-Tropsch synthesis on precipitated iron catalysts. **Industrial and Engineering Chemistry Research** 38: 1277-1290.
- Vernon, P.D.F., M.L.H. Green, A.K. Cheetham and A.T. Ashcroft 1992. Partial oxidation of methane to synthesis gas, and carbon dioxide as an oxidizing agent for methane conversion. **Catalysis Today** 13: 417-426.
- Wang, H.Y. and C.T. Au 1997. Carbon dioxide reforming of methane to syngas over SiO<sub>2</sub>-supported rhodium catalysts. **Applied Catalysis A: General** 155: 239-252.
- \_\_\_\_\_ and E. Ruckenstein 2000. Carbon dioxide reforming of methane to synthesis gas over supported rhodium catalysts: the effect of support. **Applied Catalysis A: General** 204: 143-152.
- Wang, S. and G.Q. Lu 1998. Reforming of methane with carbon dioxide over Ni/Al<sub>2</sub>O<sub>3</sub> catalysts: Effect of nickel precursor. **Applied Catalysis A: General** 169(2): 271-280.
- Wei, M., K. Okabe, H. Arakawa and Y. Teraoka 2004. Synthesis and characterization of zirconium containing mesoporous silicates and the utilization as support of cobalt catalysts for Fischer-Tropsch synthesis. **Catalysis Communications** 5: 597-603.

- Wender, I. 1996. Reaction of synthesis gas. **Fuel Processing Technology** 48: 189-297.
- Witt, P.M. and L.D. Schmidt 1996. Effect of flow rate on the partial oxidation of methane and ethane. **Journal of Catalysis** 163: 465-475.
- Wojciechowski, B.W. and J. Abbot 1988. The effect of temperature on the product distribution and kinetics of reactions of n-hexadecane on HY zeolite. **Journal of Catalysis** 109(2): 274-283.
- Xu, J. and G.F. Froment 1989. Methane steam reforming, methanation and water-gas shift: I Intrinsic kinetics. **AIChE Journal** 35: 88.
- Xu, Q., D. He, M. Fujiwara, M. Tanaka, Y. Souma and H. Yamanaka 1998. Hydrogenation of carbon dioxide over Fe–Cu–Na/zeolite composite catalysts: Na migration via solid-solid reaction and its effects on the catalytic activity. **Journal of Molecular Catalysis A: Chemical** 136: 161-168.
- Yan, Q.G., Z.S. Chao, T.H. Wu, W.Z. Weng, M.S. Chen and H.L. Wan 2000. Carbon deposition on Ni/Al<sub>2</sub>O<sub>3</sub> catalyst during partial oxidation of methane to syngas. **Studies in Surface Science and Catalysis** 130: 3549-3554.
- Zennaro, R., M. Tagliabue and C.H. Bartholomew 2000. Kinetics of Fischer-Tropsch synthesis on titania-supported cobalt. **Catalysis Today** 58: 309-319.
- Zhu, J., J.G. Ommen and L. Lefferts 2004. Reaction scheme of partial oxidation of methane to synthesis gas over yttrium-stabilized zirconia. **Journal of Catalysis** 225: 388-397.



Zhang, C.H., Y. Yang, B.T. Teng, T.Z. Li, H.Y. Zheng, H.W. Xiang and Y.W. Li  
2006. Study of an iron-manganese Fischer–Tropsch synthesis catalyst  
promoted with copper. **Journal of Catalysis**, 237(2): 405-415.

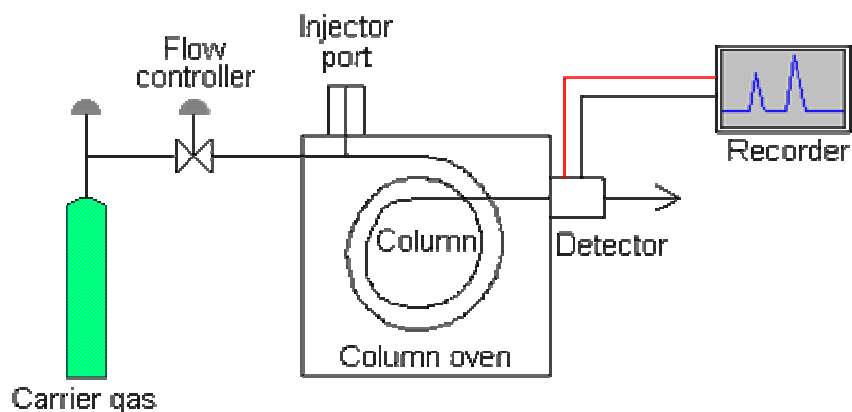
## **APPENDIX**

## **Appendix A**

### **Qualitative and Quantitative Results from Gas Chromatography**

### **Qualitative and Quantitative Results from Gas Chromatography**

The procedure of gas chromatography was carried out in a specially designed instrument. A gas chromatograph is consisted of a flowing mobile phase, an injector port, a separation column containing the stationary phase, a detector, and a data recording system as shown in Appendix Figure A1. An amount of gaseous or liquid mixture samples was injected into the instrument at injector port and was volatilized in a hot injection chamber. Then, it was swept by a flow of inert carrier gas (as a mobile phase) through a heated column which contains the stationary phase. As the gaseous or liquid mixture sample travel through the column, its components go back and forward at different rates, and thus separated into pure components. Before each compound exit the instrument, it passed through a detector. When the detector “sees” a compound, it sent an electronic signal to the recorder, which respond by printing a peak on a piece of paper.

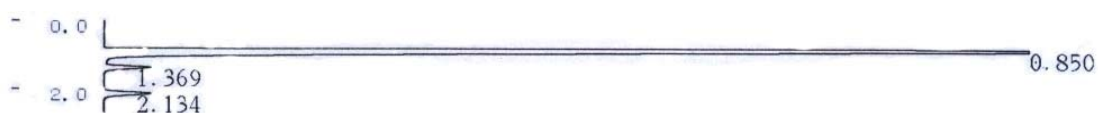


Appendix Figure A1 Scheme diagram of gas chromatograph.

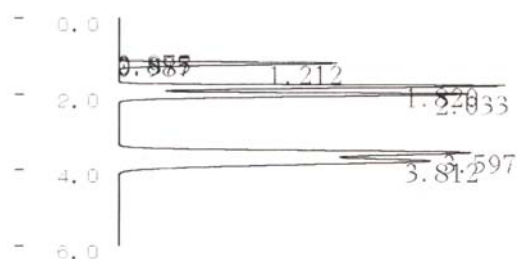
In this study, gas chromatography provided qualitative and quantitative data of a mixture of gaseous or liquid samples. Before analysis, gas chromatography conditions of Shimadzu GC-8A gas chromatograph with chromatopac data processor were prepared as mentioned in the experimental preparation. A known volume of gaseous mixture sample was injected into injector port by a syringe. Then, this

gaseous mixture sample was analyzed. The qualitative and quantitative data of a mixture of gaseous or liquid samples was reported by Shimadzu chromatopac data processor.

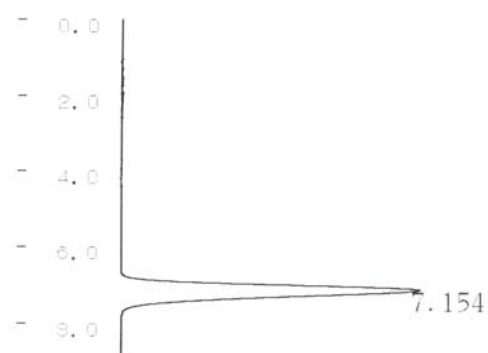
By gas chromatography, the qualitative analysis of a mixture of gaseous or liquid samples can be identified by comparing the retention time data between the samples and standard gases or liquids. The chromatogram of standard gases and liquids used in this study were shown in Appendix Figures A2-A4.



Appendix Figure A2 Chromatogram of standard gases for CO, CH<sub>4</sub> and CO<sub>2</sub>.

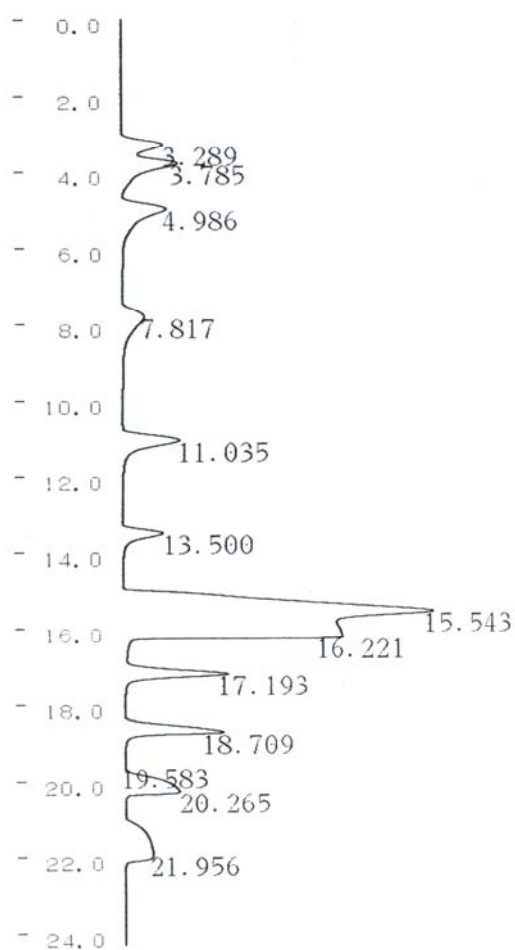


(a)



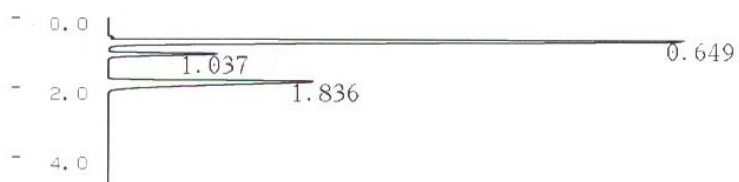
(b)

Appendix Figure A3 Chromatograms of standard gases for (a) C<sub>1</sub>-C<sub>3</sub> hydrocarbons and (b) C<sub>4</sub> hydrocarbon.

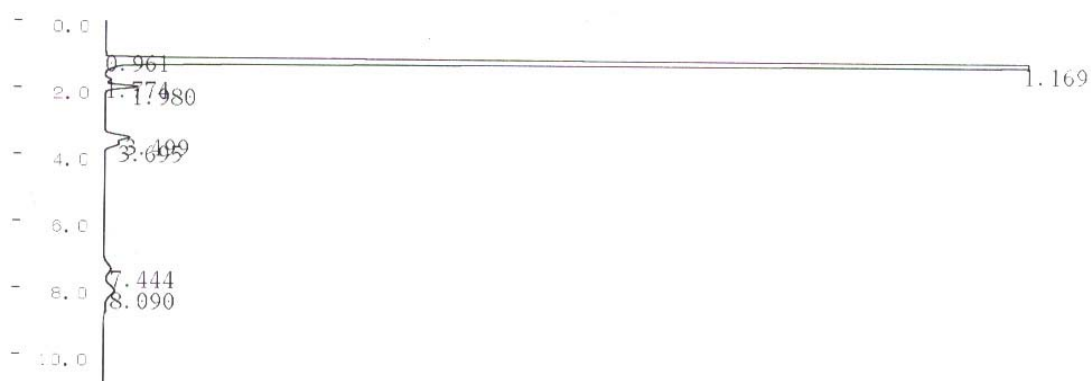


Appendix Figure A4 Chromatogram of standard liquid for C<sub>5</sub>-C<sub>15</sub> hydrocarbons.

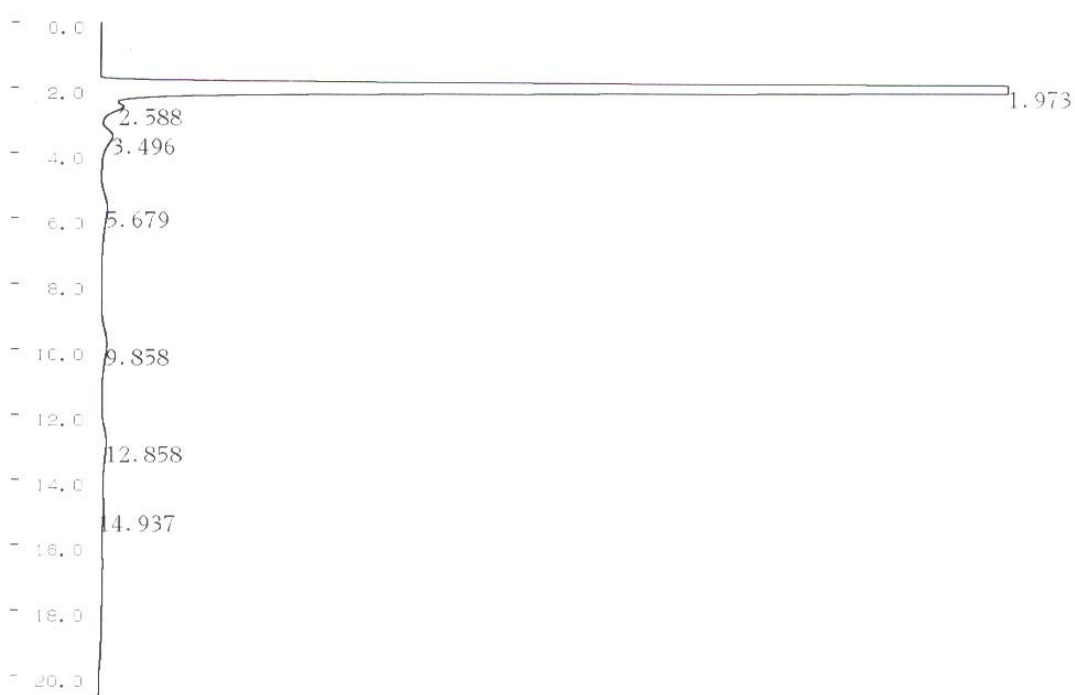
Some chromatograms obtained from the two-stage synthesis of liquid fuels from carbon dioxide and methane are shown in Appendix Figures A5-A7 as follows:



Appendix Figure A5 Chromatogram of synthesis gas over 5Ni/Al<sub>2</sub>O<sub>3</sub> catalyst at 750 °C from the first-stage reforming reactor.

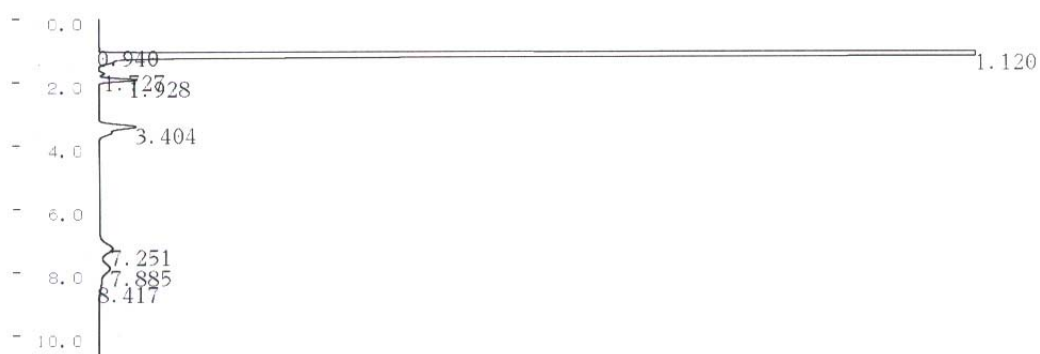


(a)



(b)

**Appendix Figure A6** Chromatograms of hydrocarbon products for (a) C<sub>1</sub>-C<sub>4</sub> and (b) C<sub>5</sub>+ over 10Co/SBA-15 catalyst at 200 °C from the second-stage FT reactor.



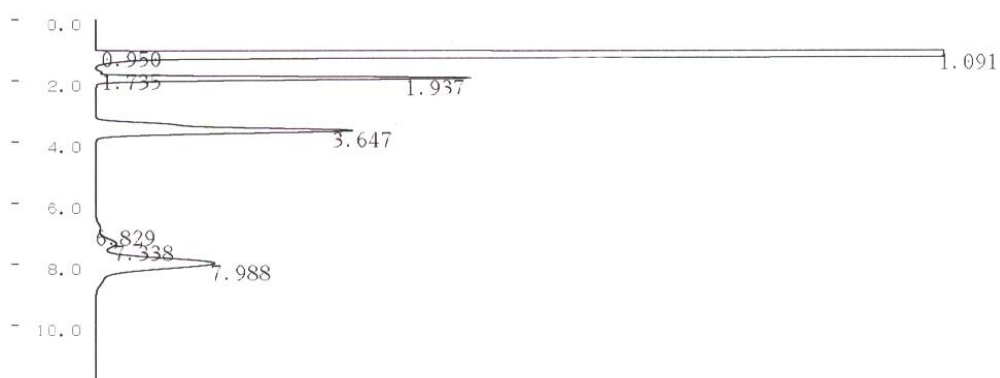
(a)



(b)

Appendix Figure A7 Chromatograms of hydrocarbon products for (a) C<sub>1</sub>-C<sub>4</sub> and (b) C<sub>5</sub>+ over 20Co/SBA-15 catalyst at 200 °C from the second-stage FT reactor.





(a)



(b)

**Appendix Figure A8** Chromatograms of hydrocarbon products for (a) C<sub>1</sub>-C<sub>4</sub> and (b) C<sub>5</sub>+ over 30Co/SBA-15 catalyst at 200 °C from the second-stage FT reactor.

The quantitative analysis of a mixture of gaseous or liquid samples can be obtained from the correlation between the amount of gas or liquid sample (mol) injecting into gas chromatograph and the area of sample obtained from gas chromatogram.

The calculation for the amount of each component in a standard gases mixture that can be calculated as follows:

$$\text{Amount of component i (mol)} = \frac{V_i \times T}{100 \times 22400} \quad (\text{A1})$$

Where  $V_i$  = % volume of component i ( $\text{cm}^3/\text{cm}^3$ )

$T$  = volume of standard gases mixture (mL)

The calculation for the amount of each component in a standard liquids mixture that can be calculated as follows:

$$\text{Amount of component i (mol)} = \frac{V_i \times T \times D \times P \times 10^{-7}}{\text{MW}} \quad (\text{A2}) \quad 11$$

Where  $V$  = % volume of component i ( $\text{cm}^3/\text{cm}^3$ )

$T$  = volume of liquid mixture ( $\mu\text{L}$ )

$D$  = density ( $\text{g}/\text{cm}^3$ )

$\text{MW}$  = molecular weight ( $\text{g}/\text{mol}$ )

$P$  = purity (%)

The correlation between these variables was characterized by a linear regression equation so-called “calibration curve”. All calibration curves for each standard gas and standard liquid used in this study are shown in Appendix Table A1.

Appendix Table A1 Equation of calibration curves for each standard gas and liquid.

Substance	Equation	R <sup>2</sup>
CO	$\text{mol} = 9.78 \times 10^{-11} \times \text{area}$	0.999
CO <sub>2</sub>	$\text{mol} = 1.28 \times 10^{-10} \times \text{area}$	0.989
CH <sub>4</sub>	$\text{mol} = 1.77 \times 10^{-10} \times \text{area}$	0.995
C <sub>2</sub> H <sub>4</sub>	$\text{mol} = 6.75 \times 10^{-13} \times \text{area}$	0.958
C <sub>2</sub> H <sub>6</sub>	$\text{mol} = 6.78 \times 10^{-13} \times \text{area}$	0.955
C <sub>3</sub> H <sub>6</sub>	$\text{mol} = 4.43 \times 10^{-13} \times \text{area}$	0.954
C <sub>3</sub> H <sub>8</sub>	$\text{mol} = 4.34 \times 10^{-13} \times \text{area}$	0.936
C <sub>4</sub> H <sub>10</sub>	$\text{mol} = 3.08 \times 10^{-13} \times \text{area}$	0.991
C <sub>5</sub> H <sub>12</sub>	$\text{mol} = 3.05 \times 10^{-13} \times \text{area}$	0.997
C <sub>6</sub> H <sub>14</sub>	$\text{mol} = 1.39 \times 10^{-13} \times \text{area}$	0.997
C <sub>7</sub> H <sub>16</sub>	$\text{mol} = 1.39 \times 10^{-13} \times \text{area}$	0.997
C <sub>8</sub> H <sub>18</sub>	$\text{mol} = 1.97 \times 10^{-13} \times \text{area}$	0.997
C <sub>9</sub> H <sub>20</sub>	$\text{mol} = 1.13 \times 10^{-13} \times \text{area}$	0.997
C <sub>10</sub> H <sub>22</sub>	$\text{mol} = 1.97 \times 10^{-13} \times \text{area}$	0.988
C <sub>11</sub> H <sub>24</sub>	$\text{mol} = 7.36 \times 10^{-14} \times \text{area}$	0.995
C <sub>12</sub> H <sub>26</sub>	$\text{mol} = 6.85 \times 10^{-14} \times \text{area}$	0.996
C <sub>13</sub> H <sub>28</sub>	$\text{mol} = 6.67 \times 10^{-14} \times \text{area}$	0.997
C <sub>14</sub> H <sub>30</sub>	$\text{mol} = 6.15 \times 10^{-14} \times \text{area}$	0.992
C <sub>15</sub> H <sub>32</sub>	$\text{mol} = 6.25 \times 10^{-14} \times \text{area}$	0.993

## **Appendix B**

### **Conversion and Selectivity Results**

### **Conversion and Selectivity Results**

The calculation for the conversion of carbon dioxide and methane to synthesis gas is shown as follows:

#### **Percent of CO<sub>2</sub> and CH<sub>4</sub> conversions**

$$\text{CO}_2 \text{ conversion} = (\text{CO}_{2\text{in}} - \text{CO}_{2\text{out}}) / \text{CO}_{2\text{in}} \times 100 \%$$

$$\text{CH}_4 \text{ conversion} = (\text{CH}_{4\text{in}} - \text{CH}_{4\text{out}}) / \text{CH}_{4\text{in}} \times 100 \%$$

#### **Percent of effluent composition for CO<sub>2</sub>, CH<sub>4</sub> and CO**

$$\text{Effluent composition of component } i = \frac{\text{mass of component } i}{\sum \text{mass of component } i} \times 100 \%$$

#### **Percent of CO conversion**

$$\text{CO conversion} = (\text{CO}_{\text{in}} - \text{CO}_{\text{out}}) / \text{CO}_{\text{in}} \times 100 \%$$

#### **Percent of effluent composition for CO and total hydrocarbon products**

$$\text{Effluent composition of component } i = \frac{\text{mass of component } i}{\sum \text{mass of component } i} \times 100 \%$$

#### **Percent of hydrocarbon selectivity for hydrocarbon products**

$$\text{Hydrocarbon selectivity of } i = \frac{\text{mass of hydrocarbon } i}{\sum \text{mass of hydrocarbon } i} \times 100 \%$$

Finally, all conversion results are reported as function of % mole (or mass) of feed that converted into product by mole (or mass) of feed introduced. All effluent composition results are reported as function of % mass by mass of total effluent compositions and all hydrocarbon selectivity results are also reported as function of %

mass by mass of total hydrocarbon products for the particular catalytic reaction system.

The example of calculation for conversion and selectivity can be shown in Appendix Table B1.

Appendix Table B1 Calculation of conversion and selectivity.

Description	Calculation
<u>1. The first-stage reforming reactor: thermal reaction packed with sand at 750 °C</u>	
Inlet: Area of CH <sub>4</sub> , CO <sub>2</sub>	175361, 322043
Calibration curve of CH <sub>4</sub> (mole)	$1.77 \times 10^{-10} \times \text{area}$
Calibration curve of CO <sub>2</sub> (mole)	$1.28 \times 10^{-10} \times \text{area}$
CH <sub>4</sub> amount	0.00003098 mol
CO <sub>2</sub> amount	0.00004116 mol
Outlet: Area of CH <sub>4</sub> , CO <sub>2</sub> , CO	165773, 287115, 36917
Calibration curve of CO (mole)	$9.78 \times 10^{-11} \times \text{area}$
CH <sub>4</sub> amount	0.00002929 mol (0.00046859 g)
CO <sub>2</sub> amount	0.00003669 mol (0.00016145 g)
CO amount	0.00000361 mol ( 0.00010106 g)
CH <sub>4</sub> conversion	6 %
CO <sub>2</sub> conversion	11 %
CH <sub>4</sub> effluent composition	42 %
CO <sub>2</sub> effluent composition	52 %
CO effluent composition	6 %

Description	Calculation
<b>2. The second-stage FT reactor: thermal reaction packed with sand at 200 °C</b>	
Inlet: CH <sub>4</sub> amount	0.00002929 mol
CO <sub>2</sub> amount	0.00003669 mol
CO amount	0.00000361 mol
Outlet: Area of CH <sub>4</sub> , CO <sub>2</sub> , CO,	6852855, 84698, 257054,
C <sub>2</sub> H <sub>4</sub> , C <sub>2</sub> H <sub>6</sub> , C <sub>3</sub> H <sub>8</sub> , C <sub>4</sub> H <sub>10</sub>	18490, 44565, 15172, 2802
Calibration curve of C <sub>2</sub> H <sub>4</sub> (mole)	$6.75 \times 10^{-13}$ x area
Calibration curve of C <sub>2</sub> H <sub>6</sub> (mole)	$1.03 \times 10^{-12}$ x area
Calibration curve of C <sub>3</sub> H <sub>8</sub> (mole)	$4.34 \times 10^{-13}$ x area
Calibration curve of C <sub>4</sub> H <sub>10</sub> (mole)	$3.08 \times 10^{-13}$ x area
CH <sub>4</sub> amount	0.00001002 mol
C <sub>1</sub> hydrocarbon amount	0.00001927 mol ( 0.0001108 g)
CO <sub>2</sub> amount	0.00001082 mol
CO amount	0.00002513 mol ( 0.0007037 g)
C <sub>2</sub> H <sub>4</sub> hydrocarbon amount	0.00000001248 mol ( 0.00000035 g)
C <sub>2</sub> H <sub>6</sub> hydrocarbon amount	0.00000003023 mol ( 0.00000091 g)
C <sub>3</sub> H <sub>8</sub> hydrocarbon amount	0.00000000658 mol ( 0.00000029 g)
C <sub>4</sub> H <sub>10</sub> hydrocarbon amount	0.00000000086 mol ( 0.00000005 g)
Total hydrocarbon amount	0.00000927 g
CO conversion	2 %
CO effluent composition	86.2 %
Total hydrocarbon effluent composition	13.8 %
C <sub>1</sub> hydrocarbon selectivity	13.6 %
C <sub>2</sub> hydrocarbon selectivity	0.2 %
C <sub>3</sub> hydrocarbon selectivity	0.0 %
C <sub>4</sub> hydrocarbon selectivity	0.0 %

The conversion and selectivity results are shown in Appendix Tables B2-B9 as follows:

Appendix Table B2 Conversion of carbon dioxide and methane to synthesis gas: thermal reaction packed with sand<sup>1</sup>.

Sand	Temperature (°C)			
	500	600	700	750
CH <sub>4</sub> conversion (%)	0	0	1	5
CO <sub>2</sub> conversion (%)	1	1	4	11
Effluent composition (wt.%)				
CH <sub>4</sub>	43	43	43	42
CO <sub>2</sub>	57	57	55	53
CO	0	1	3	5

<sup>1</sup> The reaction conditions were as follows: CH<sub>4</sub>/CO<sub>2</sub> molar ratio of 1, total gas pressure of 10 atm, and total flow rate of 50 ml/min (NTP).



Appendix Table B3 Conversion of synthesis gas to hydrocarbon products: thermal reaction packed with sand<sup>1</sup>.

Sand	Temperature (°C)				
	200	220	240	260	280
CO conversion (%)	2	4	8	11	13
Effluent composition (wt.%)					
CO	86	85	84	83	82
Total hydrocarbon	14	15	16	17	18
Hydrocarbon selectivity (wt.%)					
C <sub>1</sub>	99	94	95	98	99
C <sub>2</sub>	1	3	2	1	1
C <sub>3</sub>	0	2	2	0	0
C <sub>4</sub>	0	2	1	0	0
C <sub>5+</sub>	0	0	0	0	0

<sup>1</sup> The reaction conditions were as follows: CH<sub>4</sub>/CO<sub>2</sub> molar ratio of 1, total gas pressure of 10 atm, and total flow rate of 50 ml/min (NTP); first-stage reforming reactor was packed with sand and operated at 750 °C.

Appendix Table B4 Conversion of carbon dioxide and methane to synthesis gas: catalytic reaction on  $\text{Al}_2\text{O}_3$  support<sup>1</sup>.

$\text{Al}_2\text{O}_3$	Temperature ( $^{\circ}\text{C}$ )			
	500	600	700	750
$\text{CH}_4$ conversion (%)	2	3	4	6
$\text{CO}_2$ conversion (%)	7	7	10	16
Effluent composition (wt.%)				
$\text{CH}_4$	44	44	44	43
$\text{CO}_2$	55	56	55	51
$\text{CO}$	0	0	1	7

<sup>1</sup> The reaction conditions were as follows:  $\text{CH}_4/\text{CO}_2$  molar ratio of 1, total gas pressure of 10 atm, and total flow rate of 50 ml/min (NTP).

Appendix Table B5 Conversion of carbon dioxide and methane to synthesis gas: catalytic reaction on  $5\text{Ni}/\text{Al}_2\text{O}_3$  catalyst<sup>1</sup>.

$5\text{Ni}/\text{Al}_2\text{O}_3$	Temperature ( $^{\circ}\text{C}$ )			
	500	600	700	750
$\text{CH}_4$ conversion (%)	61	69	74	75
$\text{CO}_2$ conversion (%)	13	31	58	75
Effluent composition (wt.%)				
$\text{CH}_4$	22	18	17	17
$\text{CO}_2$	64	55	37	24
$\text{CO}$	14	26	45	59

<sup>1</sup> The reaction conditions were as follows:  $\text{CH}_4/\text{CO}_2$  molar ratio of 1, total gas pressure of 10 atm, and total flow rate of 50 ml/min (NTP).

Appendix Table B6 Conversion of synthesis gas to hydrocarbon products: catalytic reaction on sand catalyst<sup>1</sup>.

Sand	Temperature (°C)				
	200	220	240	260	280
CO conversion (%)	2	4	8	11	13
Effluent composition (wt.%)					
CO	86	85	84	83	82
Total hydrocarbon	14	15	16	17	18
Hydrocarbon electivity (wt.%)					
C <sub>1</sub>	99	94	95	98	99
C <sub>2</sub>	1	3	2	1	1
C <sub>3</sub>	0	2	2	0	0
C <sub>4</sub>	0	2	1	0	0
C <sub>5+</sub>	0	0	0	0	0

<sup>1</sup> The reaction conditions were as follows: CH<sub>4</sub>/CO<sub>2</sub> molar ratio of 1, total gas pressure of 10 atm, and total flow rate of 50 ml/min (NTP); the first-stage reforming reactor was packed with 5Ni/Al<sub>2</sub>O<sub>3</sub> catalyst and operated at 750 °C.

Appendix Table B7 Conversion of synthesis gas to hydrocarbon products: catalytic reaction on SBA-15 support<sup>1</sup>.

SBA-15	Temperature (°C)				
	200	220	240	260	280
CO conversion (%)	11	13	16	18	21
Effluent composition (wt.%)					
CO	96	86	87	90	91
Total hydrocarbon	4	14	13	10	9
Hydrocarbon selectivity (wt.%)					
C <sub>1</sub>	92	90	90	95	95
C <sub>2</sub>	6	4	5	4	3
C <sub>3</sub>	1	3	3	1	1
C <sub>4</sub>	0	2	2	0	0
C <sub>5+</sub>	0	0	0	0	0

<sup>1</sup> The reaction conditions were as follows: CH<sub>4</sub>/CO<sub>2</sub> molar ratio of 1, total gas pressure of 10 atm, and total flow rate of 50 ml/min (NTP); the first-stage reforming reactor was packed with 5Ni/Al<sub>2</sub>O<sub>3</sub> catalyst and operated at 750 °C.

Appendix Table B8 Conversion of synthesis gas to hydrocarbon products: catalytic reaction on 10Co/SBA-15 catalyst<sup>1</sup>.

10Co/SBA-15	Temperature (°C)				
	200	220	240	260	280
CO conversion (%)	17	29	30	44	67
Hydrocarbon selectivity (wt.%)					
C <sub>1</sub>	79	83	77	86	81
C <sub>2</sub>	5	4	5	4	10
LPG	6	9	10	9	9
Naphtha	5	2	6	1	0
Gasoline	5	3	2	0	0
Diesel	0	0	0	0	0

<sup>1</sup> The reaction conditions were as follows: CH<sub>4</sub>/CO<sub>2</sub> molar ratio of 1, total gas pressure of 10 atm, and total flow rate of 50 ml/min (NTP); the first-stage reforming reactor was packed with 5Ni/Al<sub>2</sub>O<sub>3</sub> catalyst and operated at 750 °C.

Appendix Table B9 Conversion of synthesis gas to hydrocarbon products: catalytic reaction on 20Co/SBA-15 catalyst<sup>1</sup>.

20Co/SBA-15	Temperature (°C)				
	200	220	240	260	280
CO conversion (%)	46	52	61	58	68
Hydrocarbon selectivity (wt.%)					
C <sub>1</sub>	83	70	86	89	94
C <sub>2</sub>	1	4	5	3	2
LPG	4	11	7	8	4
Naphtha	4	4	0	0	0
Gasoline	7	11	1	0	0
Diesel	1	0	0	0	0

<sup>1</sup> The reaction conditions were as follows: CH<sub>4</sub>/CO<sub>2</sub> molar ratio of 1, total gas pressure of 10 atm, and total flow rate of 50 ml/min (NTP); the first-stage reforming reactor was packed with 5Ni/Al<sub>2</sub>O<sub>3</sub> catalyst and operated at 750 °C.

Appendix Table B10 Conversion of synthesis gas to hydrocarbon products: catalytic reaction on 30Co/SBA-15 catalyst<sup>1</sup>.

30Co/SBA-15	Temperature (°C)		
	200	220	240
CO conversion (%)	50	57	64
Hydrocarbon selectivity (wt.%)			
C <sub>1</sub>	76	84	75
C <sub>2</sub>	4	7	6
LPG	6	8	15
Naphtha	8	1	1
Gasoline	5	0	2
Diesel	1	0	0

<sup>1</sup> The reaction conditions were as follows: CH<sub>4</sub>/CO<sub>2</sub> molar ratio of 1, total gas pressure of 10 atm, and total flow rate of 50 ml/min (NTP); the first-stage reforming reactor was packed with 5Ni/Al<sub>2</sub>O<sub>3</sub> catalyst and operated at 750 °C.

Appendix Table B11 Conversion of synthesis gas to hydrocarbon products: catalytic reaction on 20Co/SBA-15 catalyst with metal promoters<sup>1</sup>.

	Amount of metal promoters		
	0.1 wt.%Li	0.3 wt.%Na	0.5 wt.%K
CO conversion (%)	3	8	10
Hydrocarbon selectivity (wt.%)			
C <sub>1</sub>	97	98	88
C <sub>2</sub>	2	1	10
LPG	1	1	2
Naphtha	0	0	0
Gasoline	0	0	0
Diesel	0	0	0

<sup>1</sup> The reaction conditions were as follows: CH<sub>4</sub>/CO<sub>2</sub> molar ratio of 1, total gas pressure of 10 atm, and total flow rate of 50 ml/min (NTP); the first-stage reforming reactor was packed with 5Ni/Al<sub>2</sub>O<sub>3</sub> catalyst and operated at 750 °C.



**CURRICULUM VITAE**

NAME : Mr. Yuttanawee Koontasang

BIRTH DATE : October 6, 1981

BIRTH PLACE : Ubon Ratchathani, Thailand

EDUCATION : YEAR      INSTITUTION      DEGREE/DIPLOMA  
2004      Srinakarinwirot U.      B.Eng. (ChE.)

SCHOLARSHIP : Teacher Assistant Scholarship from ADB Program of  
Department of Chemical Engineering, Kasetsart University  
2004-2005